

# FINAL REPORT

PROJECT G2

AUGUST 2022

Quantitatively Evaluate Work Zone Driver Behavior  
using 2D Imaging, 3-D Lidar & Artificial Intelligence  
in Support of Congestion Mitigation Model Calibration  
& Validation

---

**Yichang (James) Tsai, Ph.D.**, Georgia Institute of Technology  
**Rod Turochy, Ph.D.**, Auburn University  
**Nick Jehn, M.S.**, Auburn University  
**Cibi Pranav, Ph.D.**, Georgia Institute of Technology  
**Pingzhou (Lucas) Yu, M.S.**, Georgia Institute of Technology

# TECHNICAL REPORT DOCUMENTATION PAGE

<b>1. Report No.</b> Project G2	<b>2. Government Accession No.</b>		<b>3. Recipient's Catalog No.</b>	
<b>4. Title and Subtitle</b> Quantitatively Evaluate Work Zone Driver Behavior Using 2D Imaging, 3D LiDAR, and Artificial Intelligence in Support of Congestion Mitigation Model Calibration and Validation			<b>5. Report Date</b> 8/12/2022	
			<b>6. Performing Organization Code</b>	
<b>7. Author(s)</b> Yichang (James) Tsai, Ph.D., Georgia Institute of Technology Rod Turochy, Ph.D., Auburn University Nick Jehn, M.S., Auburn University Cibi Pranav, Ph.D., Georgia Institute of Technology PingZhou (Lucas) Yu, M.S., Georgia Institute of Technology			<b>8. Performing Organization Report No.</b> STRIDE Project G2	
<b>9. Performing Organization Name and Address</b> Samuel Ginn College of Engineering, Auburn University, 3101 Shelby Center, Auburn AL 36849 College of Engineering, Georgia Institute of Technology, 225 North Avenue, 3rd Floor Tech Tower, Atlanta, GA 30332			<b>10. Work Unit No.</b>	
			<b>11. Contract or Grant No.</b> Funding Agreement Number 69A3551747104	
<b>12. Sponsoring Agency Name and Address</b> University of Florida Transportation Institute/ Southeastern Transportation Research, Innovation, Development and Education Center (STRIDE) 365 Weil Hall, P.O. Box 116580 Gainesville, FL 32611 U.S Department of Transportation/Office of Research, Development & Tech 1200 New Jersey Avenue, SE Washington, DC 20590			<b>13. Type of Report and Period Covered</b> 8/15/2018 to 8/12/2022	
			<b>14. Sponsoring Agency Code</b>	
<b>15. Supplementary Notes</b> N/A				
<b>16. Abstract</b> - This project addressed the following: 1) a lack of a system to process raw traffic footage obtained from work zones to extract traffic and driver behavior information, especially systems that leverage recent advances in computer vision and artificial intelligence (machine learning), 2) a lack of understanding of the factors impacting the accuracy of the data extracted using an AI-system, and 3) a lack of quantitative analysis that presents the potential benefits of using the extracted real-world traffic and driver behavior information in the work zone traffic simulation models in comparison to default values. As a result, a preliminary version of an AI-based work zone traffic and driver behavior information extraction system using widely available 2D camera images, machine learning, and computer vision was developed to extract real-world traffic and driver behavior information, including vehicle count, vehicle classification, vehicle speed, time headway, and lane change location. A case study using the real-world videos collected on I-95 has demonstrated that the data extracted using the preliminary version of the developed AI-system is promising and can be analyzed to obtain accurate and refined real-world work zone traffic and driver information. It can provide valuable input that has previously not available to transportation agencies for developing appropriate traffic control strategies to manage and/or improve safety and mobility in work zones, and it can greatly help develop accurate and reliable traffic simulation models. This research focused on studying the feasibility of using AI technology to extract traffic information to enhance traffic simulation. A separate effort with a pilot study with a large diverse data set is recommended in the future to further validate, refine and implement the proposed method.				
<b>17. Key Words</b> automatic work zone traffic and driver behavior information extraction, artificial intelligence, camera images, traffic simulation, congestion mitigation			<b>18. Distribution Statement</b> No restrictions	
<b>19. Security Classif. (of this report)</b> N/A	<b>20. Security Classif. (of this page)</b> N/A	<b>21. No. of Pages</b> 143 pages	<b>22. Price</b> N/A	

## DISCLAIMER

The contents of this report reflect the views of the authors, who are responsible for the facts and the accuracy of the information presented herein. This document is disseminated in the interest of information exchange. The report is funded, partially or entirely, by a grant from the U.S. Department of Transportation's University Transportation Centers Program. However, the U.S. Government assumes no liability for the contents or use thereof.

## ACKNOWLEDGEMENT OF SPONSORSHIP AND STAKEHOLDERS

This work was sponsored by a contract from the Southeastern Transportation Research, Innovation, Development and Education Center (STRIDE), a Regional University Transportation Center sponsored by a grant from the U.S. Department of Transportation's University Transportation Centers Program.

The authors also want to express our special thanks to the Georgia Department of Transportation for helping the collection of work zone traffic videos, Marius Francois-Marchal for conducting literature review on error causing factors for traffic data extraction, and Paul Estano and Jack Gruendler for helping the development of the AI system.

Funding Agreement Number - 69A3551747104

## LIST OF AUTHORS

### Lead PI:

#### **Yichang (James) Tsai, Ph.D.**

Department of Civil & Environmental Engineering  
Georgia Institute of Technology  
Email: james.tsai@ce.gatech.edu

### Co-PI:

#### **Rod Turochy, Ph.D. | ORCID 0000-0003-2294-7388**

Department of Civil Engineering  
Auburn University  
Email: rodturochy@auburn.edu

### Additional Researchers:

#### **Nick Jehn, M.S.**

Department of Civil Engineering  
Auburn University  
Email: nzj0017@auburn.edu

#### **Cibi Pranav, Ph.D.**

Department of Civil & Environmental Engineering  
Georgia Institute of Technology  
Email: cibipranav@gatech.edu

#### **Pingzhou (Lucas) Yu, M.S.**

Department of Civil & Environmental Engineering  
Georgia Institute of Technology  
Email: pyu68@gatech.edu

## Chapter 1: TABLE OF CONTENTS

DISCLAIMER.....	ii
ACKNOWLEDGEMENT OF SPONSORSHIP AND STAKEHOLDERS.....	ii
LIST OF AUTHORS.....	iii
LIST OF FIGURES.....	vii
LIST OF TABLES.....	ix
ABSTRACT.....	x
EXECUTIVE SUMMARY .....	xi
Chapter 1: Introduction .....	13
Chapter 2: Literature Review .....	17
2.1 Work Zone Driver Merge Behavior Analysis.....	17
2.1.1 Factors impacting work zone driver merge behavior .....	17
2.1.2 Work zone driver merge behavior analysis applications and challenges.....	17
2.2 Review of Traffic and Driver Behavior (vehicle classification, count, speed, and lane change) Extraction Techniques Using Camera Images and AI.....	18
2.2.1. Vehicle Detection Using Computer Vision, Image Processing, and Traditional Machine Learning .....	18
2.2.2. Vehicle Detection and Classification Using Deep Learning (Yolo3) .....	23
2.3 Error Analysis and Identification of Factors Causing Errors in Traffic and Driver Behavior Information Extraction Using a Camera.....	24
2.3.1. Review of Error-Causing Factors in Traffic and Driver Behavior Information Extraction .....	24
2.3.2. Review of Methods to Improve Accuracy in Traffic and Driver Behavior Information Extraction and Needs to Further Improve Accuracy .....	29
2.4 Review of Microscopic Traffic Simulation Applications in Freeway Work Zones.....	32
2.5 Summary .....	33
Chapter 3: TRAFFIC AND DRIVER BEHAVIOR EXTRACTION SYSTEM USING 2D IMAGES AND AI (Yolo3) .....	35
3.1 Development of an AI system for Traffic and Driver Behavior Information Extraction .....	35
System inputs.....	36
Module 1. Pre-processing module.....	38
Module 2. Camera calibration .....	39
Module 3. Vehicle detection, classification, and re-identification module.....	41

Module 4. Data extraction module.....	43
Module 5. <i>Data aggregation module</i> .....	43
3.2 Vehicle Detection and Classification Using 2D Images and AI (Yolo3) .....	43
3.3 Vehicle Count and Speed Computation Methodology Using the Outcomes of AI-based Vehicle Detection and Classification.....	44
3.3.1 Data Extraction Component: Count.....	44
3.3.2 Data Extraction Component: Speed .....	47
3.3.3 Data extraction component: Time headway .....	50
3.3.4 Data extraction component: Lane change.....	51
Chapter 4: CASE STUDY OF THE AI-BASED SYSTEM AND DRIVER BEHAVIOR ANALYSIS .....	53
4.1 Case study data description.....	53
4.2 Use of the AI-system .....	54
4.4 Traffic and driver behavior analysis.....	55
Traffic count results .....	56
Traffic speed results.....	56
Traffic headway results.....	57
Work zone merge behavior analysis.....	60
Work zone driver merge behavior results .....	62
Chapter 5: ERROR ANALYSIS AND IDENTIFICATION OF FACTORS .....	64
5.1 Error Analysis Methodology.....	64
5.1.1 Design of Error Analysis .....	64
5.1.2 Ground Reference Data preparation (on I-95) .....	64
5.2 Error Analysis Findings, Interpretations, and Recommendations .....	68
5.2.1 Vehicle count error analysis results.....	68
5.2.2 Vehicle speed error analysis results .....	70
5.2.3 Pilot study of data cleaning and error case identification using statistical analysis ...	73
5.2.4 Interpretations and recommendations .....	76
Chapter 6: SENSITIVITY STUDY AND APPLICATIONS OF WORKZONE TRAFFIC SIMULATION USING EXTRACTED REAL-WORLD DRIVING BEHAVIOR AND TRAFFIC INFORMATION .....	78
6.1 Chapter Organization and Research Objectives .....	78
6.2 Vissim Model Development and Analysis Framework .....	79
6.2.1 Background .....	79



6.2.2 Base Model Development and Data Collection .....	81
6.2.3 Analysis Framework .....	91
6.3 Task 1 – Sensitivity Analysis .....	95
6.3.1 Introduction .....	95
6.3.2 Sensitivity Analysis Experiment Design .....	95
6.3.3 Sensitivity Analysis Results .....	99
6.4 Task 2 – Modeling Freeway Work Zone Traffic Operations at Sites With Varying Characteristics.....	112
6.4.1 Introduction .....	112
6.4.2 Experiment Design and Refinement .....	112
6.4.3 Factorial Experiment Results .....	115
6.5 Summary .....	126
Chapter 7: CONCLUSIONS AND RECOMMENDATIONS.....	128
REFERENCE LIST .....	133

## LIST OF FIGURES

Figure 2-1: Decision boundary of an SVM .....	21
Figure 2-2: YOLO object detection process (Redmon, 2016) .....	24
Figure 3-1: Architecture of AI-based driver behavior and traffic information extraction system	36
Figure 3-2: Example of lane marking labelling on a real image .....	37
Figure 3-3: Zone demarcation in a work zone .....	37
Figure 3-4: Example of zone labelling on a real image .....	37
Figure 3-5: Example of virtual speed loop labeling on real image .....	38
Figure 3-6: Camera calibration component design .....	41
Figure 3-7: Vehicle detection, classification and re-identification module along with the pre- processing module .....	42
Figure 3-8: Traffic Count Data Extraction Processing Flowchart .....	44
Figure 3-9: Short-Term Vehicle Tracking for Traffic Counting .....	45
Figure 3-10: Condition for Traffic Counting Using Bounding Boxes and Reference Lines .....	46
Figure 3-11: Traffic Speed Data Extraction Processing Flowchart .....	47
Figure 3-12: Long-Term vehicle tracking using OpenCV tracker .....	47
Figure 3-13: Vehicle Reference Point Estimation Using a Bounding Box .....	48
Figure 3-14: Sample Calculation of a Vehicle's Time Spent in the Virtual Loop .....	49
Figure 3-15: Compute time headway from vehicle count sequence .....	50
Figure 3-16: Estimating time gap from time headway .....	51
Figure 3-17 Illustration of data extraction steps .....	52
Figure 4-1: Camera mounting tower and work zone sites for collecting videos .....	54
Figure 4-2: Videos A and B with low and high traffic density condition in the work zone .....	54
Figure 4-3: User interface and required input for implementing AI-system .....	54
Figure 4-4: Vehicle counts over time aggregated into five-minute intervals .....	56
Figure 4-5 Traffic speed estimation in inner and outer lanes .....	57
Figure 4-6 Four zones defined in this study to group the merge locations (adopted from Tsai et al., 2011) [1 feet = 0.305 m] .....	60



Figure 4-7 Manual drawing of merge zones, virtual speed loop reference lines and the merge detection line in images collected from the GA I-95 work zone. ....	61
Figure 4-8 Comparison of the percentage of cars merging at different zones at low, and high-density traffic conditions .....	63
Figure 5-1: User interface of traffic annotator with reference lines .....	65
Figure 5-2: Traffic count by AI-System and manual count in inner and outer lanes.....	69
Figure 5-3: Traffic count error at different traffic speed and density .....	69
Figure 5-4: Example of false-positive detections and occlusion caused false-negatives .....	70
Figure 5-5: Traffic speed estimated (est.) by AI-System and manual method (GT) in one minute intervals.....	71
Figure 5-6: Traffic speed estimation errors at different ground reference traffic speed .....	71
Figure 5-7: Traffic speed computation errors introduced by high vehicle speed .....	72
Figure 5-8: Traffic speed distribution results of the same 15-minute period aggregated in different time intervals. ....	74
Figure 5-9: Traffic speed distribution extracted using AI-system (a) compared with ground truth distribution (b) .....	74
Figure 5-10: Procedure for identifying error cases.....	75

## LIST OF TABLES

Table 2-1: Methods to address factors impacting vehicle count and speed computation accuracy .....	25
Table 3-1 Zone-based vehicle merge count increment table along with vehicle type .....	52
Table 4-1 Sample vehicle detection results using Yolo3.....	55
Table 4-2 Lane-wise traffic count aggregated in five-minute intervals.....	56
Table 4-3 Statistics of extracted speed data in 5-minute intervals .....	56
Table 4-4 Statistical values of time-gap from video A and B .....	59
Table 5-1 Extracted lane-wise traffic data using AI-System and ground reference traffic data ..	66
Table 5-2: Impact of miscounting one frame to speed estimation .....	77

## ABSTRACT

Roadway work zones reduce road capacity, increase traffic delays, and create dangerous situations for drivers and construction workers. It is important to study real-world work zone traffic and driver behavior, including vehicle count, vehicle classification, driving speed, headway, lane changing, etc. to understand and analyze how they impact safety and mobility under different work zone scenarios (e.g., time periods, traffic conditions, roadway geometry, traffic control configurations, etc.). Work zone traffic simulation models have been developed to quantitatively evaluate work zone impacts by considering driving behavior (e.g., vehicle headway, speed profile, merging location and time, vehicle lateral offset, etc.) and work zone scenarios. However, to support simulation models, the real-world traffic and driver behavior information at a detailed level is currently lacking. Simulations have to rely on default behavior values, which hinders the reliability and accuracy of the results. Recently, widely available traffic camera images, together with artificial intelligence, provide a promising alternative for cost-effectively acquiring detailed real-world traffic and driver behavior information needed for analyzing work zone driver behavior and for developing accurate and reliable simulation models.

However, there is 1) a lack of a system to process raw traffic footage obtained from work zones to extract traffic and driver behavior information, especially systems that leverage recent advances in computer vision and artificial intelligence (machine learning), 2) a lack of understanding of the factors impacting the accuracy of the data extracted using an AI-system, and 3) a lack of quantitative analysis that presents the potential benefits of using the extracted real-world traffic and driver behavior information in the work zone traffic simulation models in comparison to default values. Therefore, a preliminary version of an AI-based work zone traffic and driver behavior information extraction system using widely available 2D camera images, machine learning, and computer vision has been proposed and developed to extract real-world traffic and driver behavior information, including vehicle count, vehicle classification, vehicle speed, time headway, and lane change location. A case study using the real-world videos collected on I-95 has demonstrated that the data extracted using the preliminary version of the developed AI-system is promising and can be analyzed to obtain accurate and refined real-world work zone traffic and driver information. It can provide valuable input that has previously not available to transportation agencies for developing appropriate traffic control strategies to manage and/or improve safety and mobility in work zones, and it can greatly help develop accurate and reliable traffic simulation models. This research focuses on studying the feasibility of using AI technology to extract traffic information to enhance traffic simulation. A separate effort with a pilot study with a large diverse data set is recommended in the future to further validate, refine and implement the proposed method.

*Keywords: Automatic Workzone traffic and driver behavior information extraction, artificial intelligence, camera images, traffic simulation, congestion mitigation*

## EXECUTIVE SUMMARY

Roadway work zones reduce road capacity, increase traffic delays, and create dangerous situations for drivers and construction workers. There is a need to study real-world work zone traffic and driver behavior in response to different work zone scenarios using widely available 2D camera footages a) to understand a work zone's impacts on traffic and driver behavior, and b) to develop appropriate traffic control strategies to manage and/or mitigate these impacts. Work zone traffic simulation models have been used to quantitatively evaluate the impacts of various work zone scenarios on traffic and driver behaviors. However, the lack of real-world traffic and driver behavior data is forcing simulations to use default parameter values, which may not be representative to the actual traffic and driver behavior, hindering the accuracy and reliability of traffic simulation results. Therefore, in this research project, a preliminary version of an AI-based work zone traffic and driver behavior information extraction system using widely available 2D camera footages, machine learning, and computer vision has been proposed and developed to extract real-world traffic and driver behavior information, including vehicle count, vehicle classification, vehicle speed, time headway, and lane change location.

In this report, a case study involving two 30-minute work zone videos was used to 1) demonstrate the use of the proposed AI-system, 2) present the benefits of analyzing the extracted information to obtain accurate and refined traffic and driver behavior information. The results show that the data extracted from 2D cameras can capture different traffic and driver behaviors in different traffic conditions. An error analysis was also performed to assess the accuracy of the proposed AI-system and identify the factors contributing to the errors. A manual data extraction method is proposed to obtain ground truth data used in error analysis, and by comparing accuracy in different scenarios, accuracy-impacting factors are identified based on three categories: a) sensor-related factors; b) traffic and environment-related factors; and c) algorithm-related factors. Based on the error analysis findings, it is recommended that the traffic camera be set at a high location (over 50 ft) to occlusion, high frame rate videos be used, and vehicle detection and re-identification algorithm be refined to improve the vehicle count and traffic speed accuracy of the preliminary version of the proposed AI-system.

Moreover, a work zone simulation model was developed to perform a study that explored the sensitivity of Vissim model outputs to changes in key input parameters, especially lane change distance, leveraging the extracted real-world traffic and driver behavior information instead of using typical "default" value found in the literature. The outcomes of this simulation study confirmed the utility of the extracted real-world traffic and driver behavior information. Therefore, when developing a more reliable work zone traffic simulation models, it is recommended that the work zone camera footages be used to provide data to calibrate and validate the traffic simulation models.

This research focuses on studying the feasibility of using AI technology to extract traffic information to enhance traffic simulation. A separate effort with a pilot study with a large diverse data set is recommended in the future to further validate, refine and implement the proposed method. Recommendations in this report include 1) further validating and refining

the AI-based work zone traffic and driver information extraction system with a large data set for implementation of the developed system, 2) enhancing the driver behavior study using the widely available read-world camera images, 3) extending the Vissim traffic simulation study presented in this report, and 4) scheduling work zone lane closures and designing work zone configuration to enhance safety and mobility.

## Chapter 1: Introduction

The presence of a work zone reduces road capacity and increases traffic delays, which causes twenty-four percent of non-recurring congestion (Chin et al., 2004). In addition, work zones also create dangerous situations for drivers and construction workers and have been involved in close to 800 fatalities (FARS, 2018) annually in the U.S. There is a need to study the real-world traffic (traffic volume, traffic speed, etc.) and driver behavior information (e.g., vehicle count, vehicle classification, driving speed, headway, lane changing, etc.) in response to different work zone scenarios (e.g., time periods, traffic conditions, roadway geometry, traffic control configurations, etc.) using the widely available 2D camera footage to a) understand the potential work zone impacts on traffic (e.g., traffic speed, delay/queue, and conflicts) and driver behavior (e.g., driving speed, merging location and time, vehicle headway, vehicle lateral offset, etc.), and b) develop appropriate traffic control strategies to manage and/or reduce these work zone impacts. The different work zone scenarios are comprised of 1) time periods, including but not limited to different times of the day in which driver behaviors are normal or rushed (8 AM going to work or 4 PM returning from work), etc., 2) traffic conditions, including but not limited to traffic speed, density, saturation condition, queue condition, etc., 3) roadway geometry information, including but not limited to curve/straight sections on/before a work zone, exit position, etc., and 4) traffic control configuration information, including but not limited to location of starting point of work zone taper, length of the work zone, type of work zone, number of lanes closed, setup of traffic merge locations, types of merge signals, etc.

Work zone traffic simulation models have been developed to quantitatively evaluate work zone impacts by considering driving behavior (e.g., vehicle headway, speed profile, merging location and time, vehicle lateral offset, etc.) and work zone scenarios. Microcosmic traffic simulation for work zones has been predominantly performed using VISSIM or CORSIM (Jehn & Turochy, 2019; Sun & Elefteriadou, 2010). Ideally, field data measured in a work zone would be used to calibrate VISSIM and CORSIM by providing actual data for obtaining reliable simulation results and ensuring the simulated scenarios comply with realistic representations. However, detailed and region-specific driver behavior data to support simulation models is currently lacking; this hinders the reliability and accuracy of simulation results.

Work zone traffic camera footage, together with artificial intelligence, provide a promising alternative that can cost-effectively acquire detailed real-world traffic information (e.g., traffic count, density, etc.) and driver behavior information (e.g., vehicle type, vehicle speed, merging location and time, vehicle lateral offset, vehicle headway, etc.). Previously, researchers have used video-based processing techniques to obtain detailed driver behavior data with a focus on collecting speed data (Boora & Ghosh, 2016; Fitzsimmons et al., 2012; Dey et al., 2006; Jacob & Anjaneyulu, 2012) and headway data (Sila & Maji, 2017). However, a system to process raw camera footage obtained from work zones to extract traffic and driver behavior information is lacking, especially a system that uses AI deep learning models (such as Yolo3). Consequently, there is a need to develop an AI-based work zone traffic and driver behavior information



extraction system (AI-system) using camera footage to obtain real-world work zone driver behavior and traffic information.

After developing such an AI-system, it is important to understand the performance of the system, including its accuracy and factors contributing to errors so that we are aware of the limitations of the data extracted by the system and can further refine the AI-system. Limited research, including Sil and Maji (2014) and Alkherret et al. (2017) studied the accuracy of vehicle speed extracted using traditional image-processing techniques and identified a) frame rate, b) camera resolution, c) camera angle of view (Sila & Maji, 2017), and d) pixel size of the vehicle in the video log images (Alkherret et al., 2017) as impacting the accuracy of speed extraction. However, there is a lack of comprehensive studies that assess the accuracy of the data extracted using AI-based video processing techniques and identify how various factors (e.g., camera configuration, including height, distance, angle, and resolution, frame rate, lighting conditions, vehicle occlusions, processing algorithms, etc.) impact the accuracy of the detected speed, count, headway, etc. Therefore, there is a need to assess the accuracy of the data extracted using an AI-based work zone traffic and driver behavior information extraction system and identify the factors contributing to errors in extracted errors.

Due to the lack of real-world work zone traffic and driver behavior information, default values are often used for the input parameters for the development of work zone traffic simulation models. Although the real-world work zone traffic and driver behaviors (such as merge location, driving speeds, etc.) vary in different time periods, different geometrical locations, and different traffic (saturation) conditions, the default values do not account for this variation. Therefore, the use of default values significantly hinders the accuracy and reliability of simulation outcomes, especially the inability to capture diverse real-world behaviors. The data extracted from the AI-based work zone driver behavior and traffic information extraction system provides real-world data to run the traffic simulation models. However, the benefit of using the real-world data compared to default values on simulation outcomes is not quantified. Therefore, there is a need to quantitatively assess the potential benefits of using the extracted real-world traffic and driver behavior information in comparison to default values used in work zone traffic simulation models.

In summary, the following are the research needs that must be addressed:

There is a need to develop an AI-based work zone traffic and driver behavior information extraction system using the camera footage widely available to obtain real-world driver behavior and traffic information.

There is also a need to assess the accuracy of the data extracted using the AI-based work zone traffic and driver behavior information extraction system and identify the factors contributing to the errors.

Finally, there is a need to quantitatively assess the potential benefits of using the extracted real-world traffic and driver behavior information in the work zone traffic simulation models in comparison to default values.

The following are the objectives of this research:

To develop an AI-based work zone traffic and driver behavior information extraction system using work zone camera footage to extract real-world traffic and driver behavior information, including vehicle count, vehicle classification, vehicle speed, time headway, and lane change location;

To assess the accuracy of the traffic and driver behavior information extracted (traffic count, vehicle classification, vehicle speed) using the AI-based system and identifying the factors contributing to the errors;

To develop a work zone simulation model and perform a sensitivity study to quantitatively assess the potential benefits of using the extracted real-world traffic and driver behavior information for comparison to default values in work zone traffic simulation models.

This report is organized as follows:

Chapter 1 introduces the background of the problem, research needs, and objectives.

Chapter 2 presents a four-part literature review studies related to work zone driver merge behavior analysis, techniques for driver behavior and traffic information extraction using camera footages and AI, the errors associated with these techniques, and microcosmic traffic simulation and parameters.

Chapter 3 presents a preliminary version of an AI-based traffic and driver behavior extraction system (AI-system) using widely available 2D camera footages and AI (Yolo3).

Chapter 4 presents a case study involving two 30-minute work zone videos collected on an I-95 work zone near Savannah, Georgia, to 1) demonstrate the use of the proposed AI-system to extract traffic and driver behavior information, and 2) present the benefits of analyzing the extracted information to obtain accurate and refined traffic and driver behavior information (called analyzed information), including traffic counts, traffic speeds, traffic headway, work zone driver merge behavior.

Chapter 5 presents an error analysis methodology, identifies and categorizes the factors impacting the performance of the proposed AI-system, and recommends the possible methods to remove bias and outliers for improving the accuracy and reliability of the extracted information.

Chapter 6 presents a work zone traffic simulation model developed using the extracted real-world work zone traffic and driver behavior information and quantitatively assesses the sensitivity of traffic simulation outcomes by comparing default values with the extracted real-world driver behavior and traffic information. The applications of the enhanced work zone traffic simulation models using the extracted real-world work zone traffic and driver behavior

information to improve transportation agencies' work zone traffic management are also presented.

Chapter 7 presents conclusions and recommendations.

## Chapter 2: Literature Review

This chapter reviews 1) studies related to work zone driver merge behavior, 2) techniques for vehicle detection and classification from camera footage and the use of AI to extract traffic and driver behavior (vehicle classification, count, speed), 3) error analysis in vehicle classification, count, speed estimation, and lane change, including the identification of error-causing factors, and 4) microscopic traffic simulation applications in freeway work zones. Finally, this chapter presents a summary of the literature review.

### 2.1 Work Zone Driver Merge Behavior Analysis

Unlike regular roadway conditions, work zones are associated with more frequent lane changing and merging due to mandatory and discretionary lane closures (He et al., 2016). Such lane closures increase the number of traffic conflicts and push drivers to change their behavior patterns, which lead to the potential risk for both driver safety and traffic mobility (Zhu & Saccomanno, 2004; Edara & Cottrell, 2007). Work zone statistics suggest that 26% of fatalities are caused by late merges (defined as changing lanes inside a work zone transition area where the lane is closed in a tapered form) in the work zone (Daniel et al., 2000). Therefore, there is an urgent need to improve our understanding of where drivers merge in a work zone, how drivers' merge location decisions vary with different vehicle types, and how the merge decision behaviors are affected by different roadway and traffic characteristics.

#### 2.1.1 Factors impacting work zone driver merge behavior

According to Hang et al. (2018), lane change behaviors during the merge at a work zone is a continuous process and can be impacted by the highway design elements, surrounding traffic conditions, and driver characteristics. The following is a list of comprehensive factors that can impact driver merge decisions, including 1) vehicle type (Li & Bai, 2009); 2) roadway geometries (Tsai et al., 2011); 3) environmental conditions, such as weather (Li & Bai, 2009), and lighting conditions (Ghasemzadeh & Ahmed, 2019); 4) traffic conditions, such as traffic density (Lou et al., 2015), traffic flow (Kockelman & Ma, 2007), and traffic speed (Ito & Kaneyasu, 2017); 5) time of the day (Li & Bai, 2009); and 6) work zone configuration, such as design (regular work zone, zipper work zone, etc.) (Weng & Meng, 2015), and the nature of the road closed (Sarasua et al., 2004).

#### 2.1.2 Work zone driver merge behavior analysis applications and challenges

In summary, several studies have investigated the impacts of different factors on work zone driver behaviors through simulated studies, surveys, and crash data analysis; however, study of the actual driver merge behaviors using real-world camera footage under different scenarios involving (but not restricted to) different roadway geometries, traffic densities, type of lane closed, etc., is still very limited, although there are many potential applications of the real-world driver merge behavior analysis, including 1) enhancement of the accuracy and reliability of work zone traffic calibration and simulation models so the work zone traffic patterns and queues can be predicted more

accurately, 2) optimization of work zone configurations and traffic control strategies to reduce conflicts (near-crashes and actual crashes) and improve work zone mobility, 3) enablement of transportation agencies to develop work zone hazard awareness systems to ensure the safety of workers in the work zone, 4) assistance to autonomous/connected vehicles so they can safely navigate through work zone areas, and 5) prediction of dangerous situations (actual crashes and near-crashes) in different roadway and traffic conditions.

The major challenge faced by researchers studying work zone driver merge behaviors is the lack of a) a system to extract real-world traffic and driver behavior information (vehicle classification, count, speed, and lane change) using widely available camera footages, and b) a methodology to analyze the extracted data. The following section (Section 2.2) reviews the traffic and driver behavior (vehicle classification, count, speed, and lane change) extraction techniques using camera footages and AI.

## 2.2 Review of Traffic and Driver Behavior (vehicle classification, count, speed, and lane change) Extraction Techniques Using Camera Images and AI

Conventional traffic detection technologies have the capabilities to detect basic traffic flow characteristics, such as the number of vehicles passing a detection site, the height of vehicles, and the speed of vehicles. Examples of such technology include inductive loops (Burnos et al., 2007; Hall, 1992; Ramachandran et al., 2002), microwave (Hall, 1992; Ho & Chung, 2016; Steux et al., 2002), infrared (Hall, 1992), etc. These technologies have been widely applied worldwide; however, they have been rarely used to detect vehicle trajectory and classification of the vehicles (Burnos et al., 2007; Hall, 1992; Kaempchen, 2007; Ramachandran et al., 2002; Steux et al., 2002). Consequently, it is difficult to evaluate some driver behaviors, such as change in speed over time, solely based on these technologies (Kaempchen, 2007; Ramachandran et al., 2002). Vision-based vehicle detection uses one or more cameras as the primary sensor suite and can obtain continuous trajectory data.

In this research project, we focus on reviewing the technologies and methods using widely available 2D camera footages to automatically detect and classify vehicles in support of subsequent traffic information extraction (e.g., vehicle counts, vehicle classification, speed, and lane change).

### 2.2.1. Vehicle Detection Using Computer Vision, Image Processing, and Traditional Machine Learning

This section presents algorithms and methods using computer vision, image processing, and machine learning to process single camera footage for automatic vehicle detection and classification. Recent major advances in monocular vision-based vehicle detection have mirrored advances in computer vision, machine learning, and pattern recognition. There have been immense improvements from template matching to sophisticated feature extraction and classification. Please note that a major portion of this review is

based on the paper by Sivaraman and Trivedi (2013). The vehicle detection algorithms and methods are categorized based on 1) feature-based vehicle detection and 2) vehicle detection using classifiers, including conventional machine learning and deep learning. They are presented below.

#### Feature-Based Vehicle Detection

In computer vision and image processing, a feature is a piece of information that helps solve a computational task. Features may be low-level representations, such as points, edges, or objects. Features may also be the result of a general neighborhood operation, such as convolution operations or feature detection algorithms, such as SIFT, SURF, etc., applied to the image. The idea of a feature is generic, but we might need to choose very specific types of features to solve the problem at hand.

A variety of appearance features have been used in the field to detect vehicles. Many prior studies used the principle of symmetry to identify vehicles. They created a vertical axis over image patches and checked for symmetry. The symmetry was often checked for after finding the edges of vehicles; this principle can be used to detect the rear and front of vehicles (Hoffmann, 2006; Hilario et al., 2005; Arrospide et al., 2008). Identifying edges helps detect the sides and shadows of vehicles based on the relative distance and angle between the edges. Blanc et al. (2007), Chan et al. (2007), Kim (2006), Nuevo et al. (2010), and Idler et al. (2006) used the concept of edge energy and symmetry to identify the headlights of vehicles during darkness. Chang et al. (2005) and Aytekin and Altug (2010) combined edges and symmetry with longitudinal distance and time to estimate collisions based on the width of vehicles.

Over the past two decades, work in this field has advanced to using a more robust set of features that have properties such as invariance to scale, angle, brightness, etc. These feature sets create vector-based representations of objects and can be used to train machine learning models to classify objects. Histograms of oriented gradient (HOG) features and Haar-like features are two very popular features that we will discuss in the next section.

#### *Histogram of Gradients*

HOG features (Dalal & Triggs, 2005) are extracted by running an edge detector, such as the Sobel Filter, over the image. This filter allows us to calculate the horizontal and vertical gradients; then, the magnitude and orientation of the gradients are computed and the values are discretized (ie., divided into intervals and binned to form a histogram). The histogram is then used as a feature vector. HOG features have proven to be very good descriptors and have been used in such things as pedestrian and vehicle detection. Teoh and Brunl (2012) and Sivaraman and Trivedi (2011) use HOG features. Machida and Naito (2011) used HOG to determine the vehicle pose. The main bottleneck of HOG is the amount of time it takes to compute the features; Machida and Naito (2011) propose a technique that extracts HOG features using GPU's.



### *Haar Features*

Haar-like features are sums and differences in intensities of rectangular regions in an image (Viola & Jones, 2001). In general, the intensities inside each rectangular region are summed, and the sums between adjacent regions are subtracted. They are computationally inexpensive and are sensitive to vertical and horizontal edges and to symmetry, making them ideal for vehicle detection. In the work by Liu et al. (2007), the front faces of vehicles following the vehicle with a rear-facing camera were detected using Haar-like features. Likewise, Haar-like features have been used to detect the rear faces of vehicles ahead using a forward-facing camera. Sivaraman and Trivedi (2011), Sun and Bebis (2006), Ponsa et al. (2005a), Ponsa et al. (2005b), Cui et al. (2010), Song et al. (2008), Withopf and Jahne (2006), Haselhoff et al. (2008); Haselhoff and Kummert (2009a), and Chang and Cho (2008) used Haar-like features to find the side profiles of vehicles by detecting the rear and front wheels. Haselhoff and Kummert (2009b) used Haar-like features to track vehicles. In the work by Sivaraman and Trivedi (2012), Haar features were used to find different parts of vehicles and localize the vehicle based on the parts.

### *Other Features*

Negri et al. (2008) combined HOG and Haar-like features to detect vehicles. Scale invariant feature transform (SIFT) features (Lowe, 1999) were used (Zhang et al., 2011) to find the rear faces of vehicles despite the presence of partial occlusions. Lin et al. (2012) used SURF (Bay et al., 2008) and edges to detect vehicles in the blind spot. Zhang et al. (2006) used Gabor and Haar features for vehicle detection. Principal component analysis and independent component analysis was used by Wang and Lien (2008) for detecting parked sedans in static images.

The major issue with feature-based detections is their limitation of what can be expressed; each type of feature, such as SIFT or ORB, has unique characteristics, but by using just one of them, the levels of expression are limited. Deep learning feature extraction is an inherent part of the algorithm that is learned through backpropagation, allowing the model to learn the features that best represent the object. Another issue is that pure, feature-based matching without using any classification model will not be robust to different conditions and different instances in the same class of objects.

### *Vehicle Detection Using Classifiers*

Classification is the process of assigning a discrete label to an entity. In machine learning, certain algorithms, such as SVM's, Decision Trees, etc., are trained based on feature vectors to correctly identify the class of a data point. Computer vision makes use of these classifiers that are trained on feature vectors, such as the ones mentioned in the previous section, to predict the class of an object in an image.

Classification models/algorithms can be broadly split into two categories: discriminative and generative. Discriminative classifiers model the posterior probability of a class given a label, whereas generative models model the joint probability of the data and label. Discriminative models have been used more widely than generative models for vehicle detection. In classifier-based techniques, it is common for features of the chosen kind to be extracted for each patch in an image, and the classifier would classify whether that patch contains the object the algorithm is searching for.

### *Support Vector Machines*

Support Vector Machines are binary classifiers that learn to draw a hyperplane that maintains the maximum margin between the two classes. An example of the boundary that an SVM can learn is shown in Figure 2-1. As can be observed, the boundary is placed so that the distance between the two classes is maximized. SVM's were very popular due to the fact that they were non-parametric and can learn non-linear decision boundaries using the "kernel trick." SVMs can be used for multi-class classification using the "one-versus-all" training paradigm. In this concept, if there are  $n$  different classes, we train each specialized SVM to predict whether the instance belongs to the class it is trained to recognize or not. The SVM with the highest confidence/score is deemed to be the winner, and the class that the SVM was trained to recognize is allotted as the class of that instance.

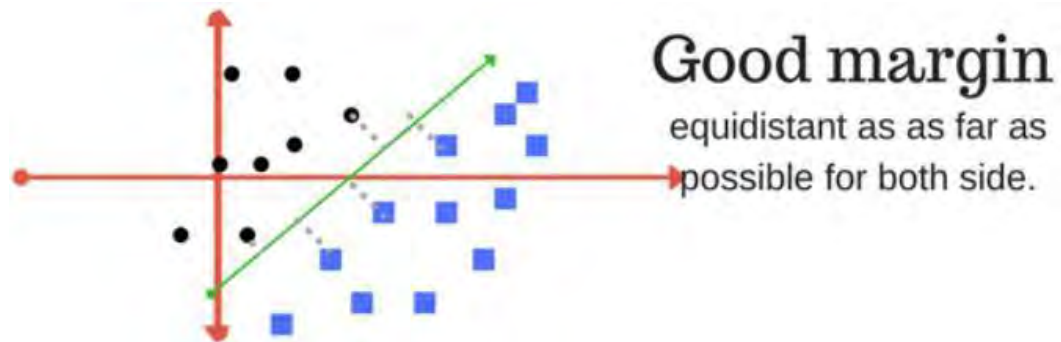


FIGURE 2-1: DECISION BOUNDARY OF AN SVM

SVMs have been widely used for vehicle detection. In the work done by Liu et al. (2007), Haar wavelet coefficients were used to train an SVM to detect vehicles. SVM classification trained on HOG features has been used in Teoh and Brunl (2012), Sivaraman and Trivedi (2011), and Sun and Bebis (2006). The HOG-SVM formulation was extended to detect and calculate vehicle orientation using multiplicative kernels in Yuan et al. (2010). SVMs trained on edge features were used in Blanc et al. (2007) and Kim (2006) to detect vehicles. Zhang et al. (2006) combined Haar and Gabor features with SVM classification.

### *Boosting*

Boosting is the concept of creating an ensemble of multiple weak classifiers that can form an extremely well-performing classifier when combined together.

AdaBoost (Freund & Schapire, 1999) has been also widely used for classification. Liu et al. (2005) used AdaBoost classification to detect vehicles based on symmetry feature scores. In Khammari et al. (2005), edge features were classified using AdaBoost. Haar-like feature extraction and AdaBoost classification were used to detect the rear faces of vehicles in Cui et al. (2010), Withopf and Jahne (2006), Kallenbach et al. (2006), Son and Mita (2009), and Acunzo et al. (2007). Chang and Cho (2008) detected the front and rear of vehicles from the side view using Haar features and AdaBoost classification. The combination of Haar features and AdaBoost classification was used to detect different parts of vehicles in Sivaraman and Trivedi (2012).

Identifying objects as a combination of their parts was one technique that has been extensively used for vehicle detection. This approach helps because we can exploit the spatial properties between parts to localize the entire object, as well as weed out false positives if objects do not contain all the required parts. In Blanc et al. (2007), a combination of SURF and edge features was used to detect vehicles with vehicle parts identified by key point detection. Zhang et al. (2006) used SIFT features and hidden conditional random fields to detect various parts of vehicles and then identify the vehicle. Takeuchi et al. (2010), Niknejad et al. (2011), and Niknejad et al. (2012) used the deformable parts model based on HOG and SVMs to identify vehicles. Sivaraman and Trivedi (2012) and Sivaraman and Trivedi (2013b) independently detected the front and rear parts of a vehicle encoded by an SVM.

Robert (2009) proposed a method that detects vehicles based on a hierarchy of features detection and fusion. The first layer of the hierarchy extracts image features. The next layer fuses image features to detect vehicle features, such as headlights, windshields, and vehicle appearance. The last layer fuses the vehicle features to train a classifier. From vehicle standards, the authors find the average size of a headlight and its average height (in meters). A headlight is modeled by a disk and is projected to all pixels of the camera image. Similarly, they find the average distance between the headlights of a vehicle (around 1m. for a car and 2m. for a heavy vehicle). They then use a homography matrix to convert the distances in meters to pixel distances for all pixels of interest in the camera image plane, creating two new 2D arrays of cars and heavy vehicles headlights' separation distance. They go on to find the windshield by estimating where it would be based on the presence of headlights. Then, they find the median value of the windshield to ascertain whether the confidence of their detection should increase or decrease. Their heuristic is that the windshield is usually dark. If the confidence is too low after the 2 stages mentioned above,

they extract features from the patch containing the headlights and windshield and use an SVM/ANN classifier to classify the patch.

The problem with parts-based detections lies with the fact that we have to customize/choose features that best identify the part; for example, in the paper mentioned above, the features methodology to identify headlights was different from that of the windshield. In case we need to identify more than one class of objects, such as vehicles and humans, we would need to customize parts-based models to detect humans. It is an idea that does not scale very well.

Deep learning modules have proven to learn lower-level features, such as edges, texture, etc. and gradually learn higher features, such as shapes; they also eventually learn to represent individual parts if they are distinct enough. This can be observed in the studies on scene recognition. All of these features/representations are learned automatically by the network through backpropagation if there are enough training examples. Therefore, using deep learning for multi-class detection would be much easier.

### 2.2.2. Vehicle Detection and Classification Using Deep Learning (Yolo3)

In recent years, increasing computer power has made it possible to build neural networks with a large number of hidden layers. Object recognition and detection have become an increasingly trivial task. There are 2 main kinds of deep learning architectures that are used to identify and detect vehicles/objects in images or videos:

1. Networks that use region proposal networks that predict if an object is present in a particular region of the image, such as the RCNN and Faster RCNN.
2. Networks that divide the entire image into segments/zones and predict if an object is present in those zones, such as SSD and YOLO.

Yolo (You Only Look Once) (Redmon, 2016) is an object detection model. This is a one-stage detection model, meaning all the outputs ([object-class-probabilities] [xcenter][ycenter] [width] [height] [confidence]) are computed at the same time.

Yolo (like other deep neural network-based object detection techniques) basically adapts historical detection algorithm ideas to a regression model using a deep neural network and vectorized computation. The YOLO object detection process is shown in Figure 2-2; the network first extracts features like we would first extract Haar features in Viola and Jones (2004), which are then used by the last layers of the network to regress bounding boxes' locations, dimensions, and class probabilities. Like in a classical sliding window algorithm, the image is divided into an SxS grid in which each cell contains B anchor boxes generating SxSxB bounding boxes. However, unlike a sliding window, the YOLO deep neural network processes all the image cells at the same time. Finally, non-maximal suppression over IoU values is used to avoid multiple detections of the same objects.

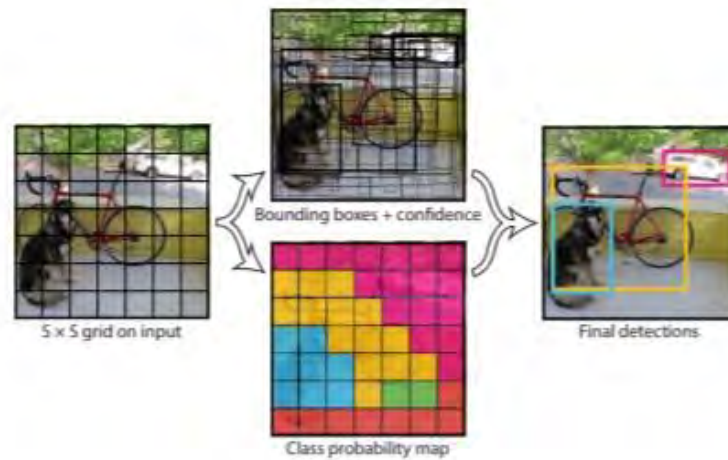


FIGURE 2-2: YOLO OBJECT DETECTION PROCESS (REDMON, 2016)

## 2.3 Error Analysis and Identification of Factors Causing Errors in Traffic and Driver Behavior Information Extraction Using a Camera

The purpose of this review is to 1) identify the errors, summarize the factors that impact the accuracy of driving behavior data extracted using AI-based image processing techniques at various stages of processing (image down sampling, resizing, vehicle detection, classification, tracking, count, and speed computation, etc.), and 2) identify the potential methods to reduce/manage the errors when extracting the traffic and driver behavior information. Although there are several image processing techniques to process and extract traffic and driver behavior information from camera footage, the focus of this literature review is on using AI-based image processing techniques such as Yolo, Faster-RCNN, etc. for vehicle detection and classification.

The outcomes of this review recommend best practices to 1) collect (e.g., camera setup (e.g., height, distance, angle, etc.), lighting, video resolution, and frequency), 2) process (vehicle detection, classification, and tracking technique, count computation, speed computation, etc.), and 3) manage the errors to reduce and/or manage their impact on the extracted traffic and driver behavior information using AI-based image processing techniques.

### 2.3.1. Review of Error-Causing Factors in Traffic and Driver Behavior Information Extraction

In this section, a review of error-causing factors in traffic and driver behavior information extraction is presented. The review focuses on errors that could occur in different stages of traffic and driver behavior information extraction and categorizes the errors based on the error-causing factors. A typical traffic and driver behavior information extraction using AI-based image processing techniques consists of the following stages:



**Stage 1:** Preprocessing the acquired camera video (images resized to the same size, extraction, and segmentation of the road surface before using it in the YOLO algorithm (Song et al., 2019); camera calibration to compute lane-mark equations (Liu et al., 2020)

**Stage 2:** Vehicle detection (computation of a bounding box)

**Stage 3:** Vehicle classification

**Stage 4:** Vehicle tracking

**Stage 5:** Vehicle count estimation (traffic density can then be deduced)

**Stage 6:** Vehicle speed estimation

**Stage 7:** Lane change location determination

The review showed three major categories of error-causing factors impacting the accuracy of the extracted traffic and driver behavior information. **Error! Reference source not found.** summarizes the methods developed to address the factors impacting the accuracy of extracted traffic information, and there are detailed factors under each of the three categories. As shown in **Error! Reference source not found.**, the factors related to camera height and angle, camera resolution, viewing location, camera speed, and traffic density (vehicle occlusions) have been addressed and improved by high position and definition cameras (the hardware improvement and camera setup). Many methods have been developed to improve the tracking algorithms, as shown in **Error! Reference source not found.**. Many methods have been developed to address the lighting and shadow issues. These improvements show the importance and interest in addressing these factors. Although improvement has been made, the lighting and shadow factors and roads that are especially busy still remain a challenge. There is a need for developing an enhanced method to improve robustness for complicated shadows (such as shadows from trees) (Liu et al., 2020).

**TABLE 2-1: METHODS TO ADDRESS FACTORS IMPACTING VEHICLE COUNT AND SPEED COMPUTATION ACCURACY**

			Methods									
			High position and definition camera	RSCH method	GMM	YOLO	Faster R-CNN	Pretraining data	Kalman filter	ORB algorithm	Virtual loops (15m)	UAV method
Factors	Sensor	Camera height and angle	×									
		Camera resolution	×									
		Viewing location	×									
		Camera movements										×
		Camera speed	×									
	Traffic and environment	Traffic density	×	×		×	×					×
		Vehicle type		×		×	×					
		Lightning and shadows		×	×	×			×			×



		Driver behavior		×		×						×
		Road shape									×	
	AI-system algorithm factors	Tracking algorithm		×		×			×	×	×	×
		Training data						×				

#### Sensor factors:

Five major sensor factors impact the accuracy of the extracted traffic and driver behavior information at various stages of the processing: 1) camera height and angle, 2) camera resolution, 3) viewing distance, 4) camera movements and 5) camera speed/frame rate.

##### 1. Camera height and angle:

When the camera height is low and the camera angle is weak relative to the horizontal, the chances of getting multiple vehicle occlusion situations increase (Buch et al., 2011). Therefore, vehicles cannot be detected accurately (i.e. the bounding box cannot be drawn correctly, or the vehicle detection is completely missed) and misclassification occurs. Even though solutions exist to tackle occlusions, it can lead to important estimation errors in case of total occlusion: the vehicle that is completely hidden behind another vehicle cannot be detected, tracked, classified, or counted.

##### 2. Camera resolution (Song et al., 2019; Liu et al., 2020; Maji, 2017; Buch et al., 2011)

A poor resolution video contains fewer vehicle feature points and, therefore, detection and classification using YOLO is affected because the algorithm extracts features from images to detect and classify vehicles. If detection is performed on a preprocessed image computed using foreground segmentation techniques, a poor camera resolution can reduce the accuracy of the segmentation because there are not sufficient pixels to segment a vehicle properly or because poor resolution adds noise to the video.

##### 3. Viewing distance (Song et al., 2019; Liu et al., 2020; Jamzad, 2005):

When vehicles are farther away, they have fewer pixels to be detected. This impacts classification, as well. Assuming the vehicle is correctly detected and classified at a longer distance from the camera, the speed computation at that location may be inaccurate because the actual distance travelled by the vehicle between two-time stamps is difficult to estimate because of the pixel vs. distance error. For example, 100 pixels may represent 1 m close to the camera, but only 10 pixels may represent 1 m farther away from the camera.

##### 4. Camera movements (Ke et al., 2016; Lam et al., 2004):

Since the camera is moving, it is difficult to estimate the distance a vehicle travels between frames; all methods using a reference line do not work because

the position of the reference line changes; therefore, counting and speed computation are impacted. NOTE: This is an issue if the camera is on a drone flying above the roads, but it can also be an issue if the camera is only mounted on a pole and is shaking. Detection techniques relying on foreground segmentation need the background to be stationary and fixed. Since both foreground and background are moving, detection is impacted.

5. Camera speed/frame rate (Maji, 2017):

When the camera's speed/frame rate is low, it is challenging to track a vehicle position because the time between two frames is too high. In that case, two consecutive bounding boxes do not overlap, or non-corresponding bounding boxes are detected as being the same. It also impacts counting and speed computation because if the time between frames is too high, it is possible that no frame containing the vehicle crossing the virtual line is recorded; on one frame, the vehicle bounding box is situated before the line, and on the next frame, the bounding box is situated after the line. Therefore, the vehicle's crossing of the reference line is not detected.

#### Traffic and environmental factors

Five major traffic and environmental factors impact the accuracy of the extracted traffic and driver behavior information at various stages of the processing: 1) traffic density, 2) vehicle type, 3) lighting and shadows, 4) driver behavior, and 5) road shape.

1. Traffic density:

In heavy traffic, vehicle occlusions happen frequently (Bharadwaj et al., 2016; Li et al., 2014; Buch et al., 2011; Sohn, 2018; Pang et al., 2004; Pang et al., 2007; Jamzad, 2005; Zhang et al., 2008). The impact is more important when the occlusion is severe; this can happen when many vehicles are involved or when vehicles are almost completely hidden, etc. Heavy traffic is often slow, which impacts preprocessing foreground segmentation; some vehicles are considered to belong to the background because their positions have not changed between consecutive frames (Buch et al., 2011).

2. Vehicle type:

Vehicle type can impact counting methods that use several virtual detection loops for each lane; some vehicles are very large and occupy almost two lanes and, therefore, are counted twice (Li et al., 2014). If a particular vehicle type is not represented enough in the training data, the classification of that vehicle type will be inaccurate. This point is also mentioned in AI-system algorithm factors below. A vehicle with a color similar to the background color cannot be segmented fully or extracted correctly, and its length and area are hard to obtain accurately. Therefore, this condition impacts detection and classification that is

based on vehicle length (Liu et al., 2020; Jamzad, 2005). Vehicle type impacts vehicle length-based classification because some large car dimensions are close to the dimensions of a bus or a truck (Song et al., 2019).

3. Lighting and shadows (Song et al., 2019; Liu et al., 2020; Bharadwaj et al., 2016; Li et al., 2014; Buch et al., 2011; Chang et al., 2018; Mousa et al., 2014; Pang et al., 2007; Jamzad, 2005; Ke et al., 2016; Lam et al., 2004):

For methods using interest points (a point with rich information around it, robust to perturbations such as those caused by various illuminations), more interest points are detected during the day than at night. Some of these points are inaccurate, leading to wrong detections and wrong tracking. At night, only accurate feature points are detected (such as vehicle lights), leading to accurate vehicle tracking (Ke et al., 2016). This means that at night, when using the interest point method (Ke et al., 2016) (the Kanade-Lucas-Tomasi tracker), tracking is more accurate than daytime tracking, but the classification would be poor (it is based on vehicle lengths). Lightning and shadows may affect classification (Liu et al., 2020) because they create “wrong” feature points; the algorithm considers the shadow as being part of the vehicle. The impact of this factor decreases if the neural network has been trained with several situations containing shadows and illuminations. When using foreground segmentation methods and when the illumination is insufficient, it is difficult to extract the edge of the vehicle or detect a moving vehicle because some parts of the vehicle may have different colors. Shadows or reflective regions affect foreground segmentation, and shadows are considered part of the vehicle, which leads to errors when extracting vehicle shapes and dimensions. Therefore, vehicle detection and classification are impacted (Buch et al., 2011; Lam et al., 2004; Li et al., 2014; Mousa et al., 2014; Rad and Jamzad, 2005; Song et al., 2019).

4. Driver behavior:

Non-lane-based movements of vehicles impact detection accuracy mostly because they lead to occlusion situations (Bharadwaj et al., 2016; Li et al., 2014; Mousa et al., 2014). Tracking accuracy is impacted because vehicles change lanes between two frames. Therefore, predictive trajectory algorithms can lose a vehicle. When the vehicle is detected again, it can be counted twice (Bharadwaj et al., 2016; Li et al., 2014; Buch et al., 2011; Pang et al., 2004; Jamzad, 2005). Speed computation is impacted because vehicles changing lanes do not follow a straight path; therefore, it is difficult to estimate the travelled distance. Algorithms using the bounding box approach may have tracking failures in high-speed traffic because of a lack of bounding box overlap when a vehicle has moved a longer distance.

5. Roadway geometry:

The virtual loop is placed on a slight slope, which is difficult to detect. Therefore, between the two lines of the loop, the road is not flat, and the estimated distance between the two reference lines is slightly wrong, which leads to speed computation errors (Liu et al., 2020).

#### AI-system algorithm factors

There are two major AI-system algorithm factors impacting the accuracy of vehicle count and speed estimation at various stages of the processing: 1) the tracking algorithm and 2) the training data.

1. Tracking algorithm:

Algorithms tracking a particular vehicle feature, such as a vehicle's head (front) may lead to tracking failure when there are two consecutive vehicles and one vehicle's feature point is hidden by the other vehicle; both vehicles are, consequently, considered to be one single vehicle (Jamzad, 2005). Tracking errors impact the algorithms that use tracking positions to count and compute speed (Bharadwaj et al., 2016; Jamzad, 2005). Tracking failures (i.e. vehicle tracking is lost and then recovered) lead to overcounting (the recovered vehicle is counted twice).

2. Training data:

When there is not sufficient training labelled data for a vehicle class, the class is poorly detected and classified (Buch et al., 2011; Chang et al., 2018; Sohn, 2018). If there is not sufficient data, including complicated situations containing shadows, varying illumination conditions, poor lightning, etc., vehicles will be poorly detected and classified.

#### 2.3.2. Review of Methods to Improve Accuracy in Traffic and Driver Behavior Information Extraction and Needs to Further Improve Accuracy

The following presents the methods adopted by the researchers to reduce and manage errors when detecting, classifying, tracking, and counting vehicles and when computing vehicles' speeds. They are categorized based on the different stages of a typical traffic and driver behavior information extracted using AI-based image processing techniques.

##### Detection

Many of the errors mentioned above are due to vehicle occlusions. Many documents propose methods to solve this problem. The methods giving the best results are presented below. They are classified as sensor-based solutions or algorithm-based solutions.

In sensor-based solutions, to reduce the number of occlusions, it is recommended to place a high-definition camera in a high position, close to the road and pointing to the

road to get a better viewing angle, which limits the occlusion (Buch et al. 2011). The camera speed should not be too low.

In algorithm-based solutions, there are two major algorithm-based solutions: 1) recursive segmentation and the convex hull method, and 2) YOLO and deep learning methods.

The method presented in Chang et al. (2018) seems to provide excellent results. It proposes a real-time video processing algorithm to segment multiple vehicles involved in an occlusion by analyzing the closure and convex hull of vehicles (recursive segmentation and convex hull methods).

To detect vehicles, as done in many papers, this method extracts the moving foreground. Many documents use the modified Gaussian mixture model (GMM) for this purpose instead of other less robust models. This model is robust to illumination changes but has a slightly higher computational complexity than other methods (Buch et al. 2011). Using the convex hull of the occluded vehicle region, occlusions are detected, and vehicles are segmented using recursive segmentation. If there is no occlusion, the vehicle is simply detected. This method outperformed other methods for detection and counting, but it needs good video resolution to obtain accurate foreground detection.

Other efficient methods use the YOLO3 algorithm to detect vehicles (Song et al. 2019; Liu et al. 2020). These methods use convolutional neural networks to extract the features of the input image. These algorithms are able to robustly detect vehicles and are immune to rainy conditions, night time, and complicated illumination conditions if correctly trained (Song et al. 2019; Liu et al. 2020). When the traffic is busy where vehicles occlude each other, the detector is still robust enough to get accurate bounding boxes of vehicles (Liu et al., 2020).

To reduce computation time, the method from Song et al. (2019) extracts and divides the road surface using a GMM-based model. Then, the YOLO3 algorithm is used only on the road, which achieves better detection results and reduces computation time because only the road zone containing vehicles is processed instead of the entire image. It is also possible to reduce the frame rate and, preferably, to use a GPU to train a deep CNN (Song et al., 2019; Sohn, 2018) to reduce computation time. However, a frame rate that is too low may also lead to more errors (frame rate is only mentioned without further details in most documents). If traffic is really busy, a faster R-CNN algorithm can be used to get slightly better performance, but the computational cost is higher (Song et al., 2019; Liu et al., 2020).

### Classification

Classification can be improved by training the classification algorithm with more diverse data, including different sizes and class objects (Song et al., 2019), occlusion situations (Sohn, 2018), rainy conditions, night times, and complicated illumination conditions (Liu et al., 2020)). However, such diverse labeled data is rare, and labeling its own data is



really time-consuming. To tackle this problem, documents (Sohn, 2018; Chang et al., 2018) propose pretraining strategies to improve classification performance when labeled data is limited and unlabeled data is used instead; for example, using unsupervised methods to pre-train the CNN before using supervised methods (Chang et al., 2018) using more or less accurate data (which is easily obtained) to pre-train the CNN in (Liu et al., 2020).

### Tracking

For tracking, most methods use bounding boxes computed from vehicle feature points. Many methods use a Kalman filter to predict the position of a vehicle bounding box on the next frame, which limits the loss of vehicles (Liu et al., 2020; Buch et al., 2011; Jamzad, 2005).

The ORB algorithm in Song et al. (2019) seems to provide accurate results. It uses the Features From Accelerated Segment Test (FAST) to detect feature points inside a predicted bounding box and to check if an object matches the feature points or not (Song et al., 2019). Detection of feature points is performed only in the bounding box instead of on the entire road surface, which improves computing time (Liu et al., 2020; Buch et al., 2011; Jamzad, 2005).

### Traffic and Driver Behavior Information Extraction

For traffic and driver behavior information extraction using 2D camera footage, two scenarios can be improved: one case occurs when the camera is stationary (not moving) and the second case occurs when the camera is moving.

When the camera is not moving, methods to count vehicles and compute speeds rely on accurate detection and tracking. If tracking is accurate, tracked vehicles can be counted. Methods using reference lines on images are accurate if the camera is not moving. In a similar way, if tracking is accurate and if the video has good resolution, consecutive vehicle tracked positions can be used to compute speeds. If the camera is not moving, using a virtual speed loop is accurate; Maji documents (2017) show that error is optimal for a speed loop length of 15 meters.

When the camera is moving (for example, in unmanned aerial vehicles with mounted cameras), different methods have to be used because both background and foreground are moving. Ke et al. (2016) provide a robust method to detect vehicles using Shi-Tomasi interest point tracking and motion-vector clustering (vehicles are detected and tracked thanks to their feature points' similar motion criteria and compared to the background feature points. Furthermore, interest points on the same vehicle share the same motion, so it can be determined if a group of interest points belongs to the same vehicle or not). Simple classification is performed based on the number of interest points of every vehicle. Counting is performed by counting the detected vehicles, and speed computation is performed by computing the average speed of all interests points of one vehicle. Even though this system classification method is a bit simple and sometimes



inaccurate, large errors occur when the image frames contain very few vehicles, it works well in both day and night settings (tracking is particularly efficient at night), and it is not sensitive to UAV movements. Furthermore, this type of system is not impacted by occlusions, since its camera flies (via a drone) right over the road; it can also deal with static backgrounds and has a high processing speed (real-time).

## 2.4 Review of Microscopic Traffic Simulation Applications in Freeway Work Zones

As highlighted in Chapter 1, the ever-increasing presence of work zones on our nation's highways has a profound impact on the mobility and safety of the traveling public. The Texas A&M Transportation Institute (TTI) estimates that drivers incurred 8.8 billion hours of delay in 2017, approximately 10% of which is attributable to work zones (Texas A&M Transportation Institute, 2019; FHWA, 2020). While the 762 fatal work zone crashes reported by the National Highway Traffic Safety Administration (NHTSA) in 2019 constitute a relatively minor proportion of the more than 33,000 fatal crashes occurring on all facilities, they represent a 13% increase from the 672 fatal work zone crashes reported in 2018. Moreover, these adverse safety impacts are magnified on freeways; Interstate highways accounted for only 13% of all fatal crashes but more than 38% of all fatal work zone crashes in 2019 (NHTSA, 2019).

To counteract these trends, researchers and practitioners have spent several decades studying the various factors that influence freeway work zone capacity in support of agency work zone scheduling and traffic control practices. A comprehensive literature search conducted in a 2013 study summarized these efforts, underscoring that a myriad of geometric, traffic stream, environmental, and work zone-specific characteristics have been found to influence work zone capacity (Weng and Meng, 2013). More recently, for example, a recent study focused on the impact of work activity types on the traffic conditions for freeway work zone based on the data from 10 reconstruction sites in Missouri (Bharadwaj et al., 2018). The researchers found that pavement-related activities have higher variation (1120 to 1728 vphpl) in capacity values compared to bridge-related activities (1488 to 1656 vphpl) for a 3-2 lane closure. The reason given for the discrepancy was that pavement-related work occurs frequently and covers a wide range of activities (pavement operation, pavement repair, and pavement resurfacing) than bridge-related works (bridge rehabilitation). An approach that combined geometric data generated by LiDAR with connected vehicle speed data at freeway work zone was used in another recent study to examine the influence of reconstruction area geometric features on traffic operations at two sites (Mekker et al., 2018). It was found that when lane width was reduced to 10-10.5 feet within a short segment and the merging taper was approximately 200 feet shorter than the standard, the work zone capacity decreased substantially and sooner led to congestion.

A more recent synthesis of work zone capacity models presents the factors considered as inputs to those models (Masshadi et al., 2021). That meta-analysis found that heavy vehicle percentage, number of open and closed lanes, and work zone intensity are the most commonly considered parameters among 40 selected studies. The next most frequently applied inputs to

capacity models were lane closure side and work zone length, found in almost half of the models reviewed.

Though the Highway Capacity Manual, 6th Edition includes a methodology for estimating freeway work zone capacity based on data from 90 archival literature sources and 12 field-collected datasets, the ability of this deterministic model to capture the full range of characteristics unique to specific sites across the southeastern United States is limited (TRB, 2016; Yeom et al., 2016). Furthermore, large-scale field data collection efforts are time and resource intensive. As a result, microsimulation has recently emerged as a valuable tool for assessing freeway work zone operations in a more comprehensive manner.

Recent applications of microsimulation to freeway work zones have varied in scope and purpose, from the development of analytical models for estimating capacity (Heaslip et al., 2009) to site-specific calibration and validation recommendations (Edara and Chatterjee, 2010; Kan et al., 2014; Yeom et al., 2016). Others have focused on guiding agency decision-making practices by assessing merge control strategies (Ramadan and Sisiopiku, 2016; Ren et al., 2021) or producing stochastic capacity estimates for use in risk tolerance-based work zone scheduling (Jehn and Turochy, 2020). Nonetheless, driving behavior at freeway work zones is still not fully understood. Microsimulation models developed as part of prior studies have typically lacked the field data necessary for informing the selection of input parameters capable of replicating the complexity of real-world traffic operations.

## 2.5 Summary

Review of methods for the use of AI in extracting traffic and driver behavior information:

- AI-based vehicle detection and classification is promising among the different techniques; Yolo is the most suitable algorithm for vehicle detection and classification.
- A virtual speed loop and a reference line are commonly used methods to compute speed and count in absence of robust tracking, and camera calibration and will be adopted in the AI-based traffic and driver behavior extraction system.

Review of error causing factors in traffic and driver behavior information extraction:

- Several factors, including sensors, traffic, environment, and the AI-system algorithm factors impact the accuracy of the AI and image-based vehicle count, classification, and speed computation.
- There is a lack of detailed (vehicle level, time interval) and comprehensive evaluation (different stages of data extraction) studies to identify the various factors (such as algorithm used, frame rate, traffic speed, traffic volume, lightning conditions, viewing location) that can have an impact on the accuracy of vehicle detection, classification, tracking, count, and speed computation, especially in work zones. The quantitative analysis of the impact of different factors (such as the impact of traffic speed on count accuracy) on the results is lacking.

Review of microscopic traffic simulation applications in freeway work zones showed that prior studies have lacked the field data necessary for informing the selection of input parameters capable of replicating the complexity of real-world traffic operations.

## Chapter 3: TRAFFIC AND DRIVER BEHAVIOR EXTRACTION SYSTEM USING 2D IMAGES AND AI (Yolo3)

An AI-based traffic and driver behavior information extraction system is developed to study real-world traffic and driver behavior information. This chapter presents the development of a traffic and driver behavior information extraction system that uses 2D images and AI. The extracted information focuses on vehicle classification, vehicle count, and vehicle speed. This chapter is organized into the following three parts:

- Part 1: Development of AI system for Traffic and Driver Behavior Information Extraction
- Part 2: Vehicle Detection and Classification Using 2D Images and AI (Yolo3)
- Part 3: Vehicle Count and Speed Computation Methodology Using the Outcomes of AI-based Vehicle Detections and Classification

### 3.1 Development of an AI system for Traffic and Driver Behavior Information Extraction

In this section, the outline of the data extraction procedure is presented. We designed an AI-based system to extract vehicle type, vehicle speed, lane change counts and location, and the traffic volume and flow using widely available camera footages. We combined the different steps involved in driver behavior and traffic information extraction into six operating modules as follows:

1. Pre-processing module that involves preparation of video data for downstream processing;
2. Camera calibration module that involves extraction of camera parameters for converting the image pixel coordinates to real-world coordinates;
3. Vehicle detection, classification, and re-identification module that involves detection and classification of vehicles by type (trucks, cars, etc.) and extraction of vehicle trajectories from the image sequences;
4. Data extraction module that involves computation of vehicle speed, count, and lane change based on the data extraction inputs, camera parameters, and trajectories;
5. Data aggregation module that involves post-processing data and infers useful information, such as time series, statistical distribution, etc., from raw measurements;
6. Data storage module that corresponds to the memory system where the collected data is stored.

Figure 3-1 illustrates the architecture of the AI-based system and the inputs that are associated with each module. In the next section, we discuss the three system inputs and details of the six modules, including the purposes, subcomponents, inputs, and outputs.

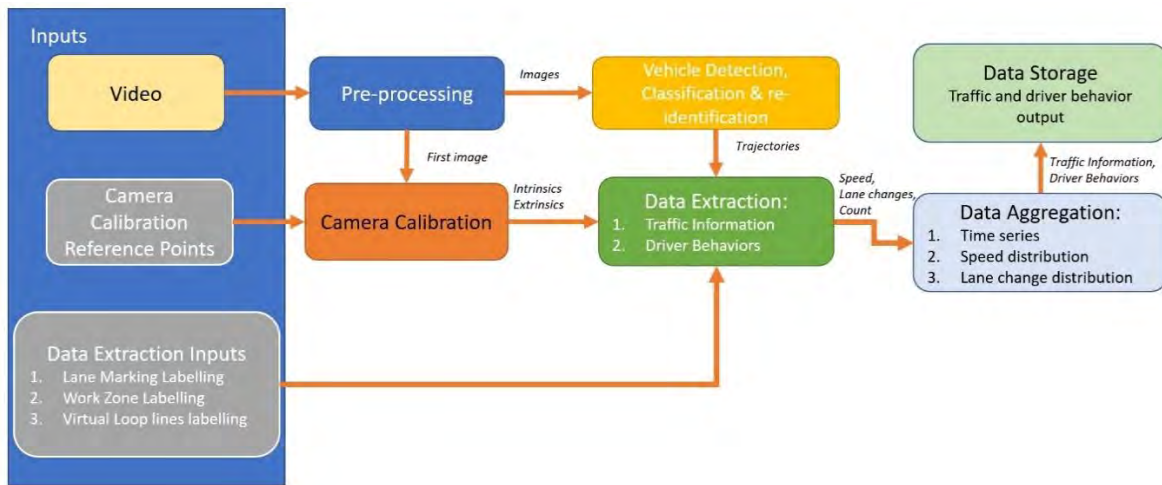


FIGURE 3-1: ARCHITECTURE OF AI-BASED DRIVER BEHAVIOR AND TRAFFIC INFORMATION EXTRACTION SYSTEM

### System inputs

System inputs can be divided into 2 different types: data inputs and user inputs. Data input is the traffic video the user wishes to extract and analyze. User inputs include labeling required by the modules of the system, such as the data extraction module and the camera calibration module. Some of the examples of user inputs include lane marking labeling to perform lane-based data aggregation, zone labeling to perform zones-based data aggregation, virtual speed loop labeling to compute speed and count vehicles at a specific location on the road, and camera calibration reference points. These user inputs are discussed below.

#### Lane Marking Labelling

To aggregate traffic and driver behavior information in each lane, the system requires information about where the lanes are located. Therefore, the lane markings need to be labelled on the image to demarcate the lanes. The lane markings may be labelled either manually or automatically. Figure 3-2 shows an example of lane marking labelling on a real image.

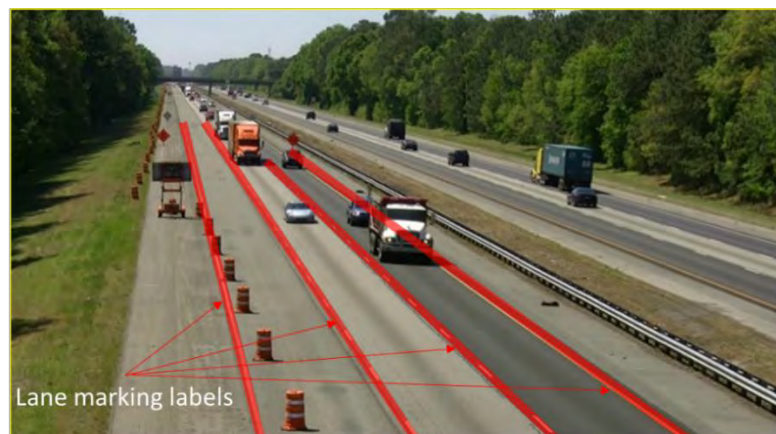




FIGURE 3-2: EXAMPLE OF LANE MARKING LABELLING ON A REAL IMAGE

### Zone Labelling

To aggregate traffic and driver behavior information in each zone upstream of the camera, the system requires information about where the zones are located. Therefore, the zones need to be labelled on the image to demarcate the lanes. The following example illustrates the zone labelling in a work zone area. To aggregate the lane change counts in each zone within a work zone area, the upstream roadway is demarcated into four zones, as shown in Figure 3-3. Figure 3-4 shows an example of zone labeling in a real image.

- Zone 1: Covers the transition area
- Zone 2: 500 ft. upstream from the beginning of transition area
- Zone 3: 500 ft. to 1000 ft. upstream from the beginning of transition area
- Zone 4: 1000 ft. and beyond upstream from the beginning of transition area

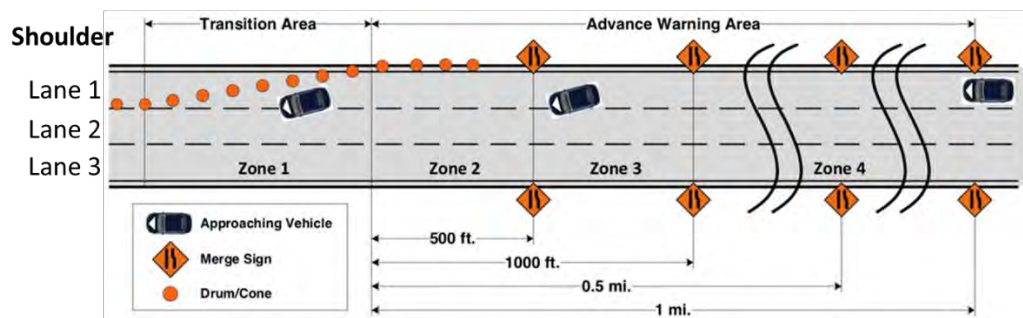


FIGURE 3-3: ZONE DEMARCATION IN A WORK ZONE

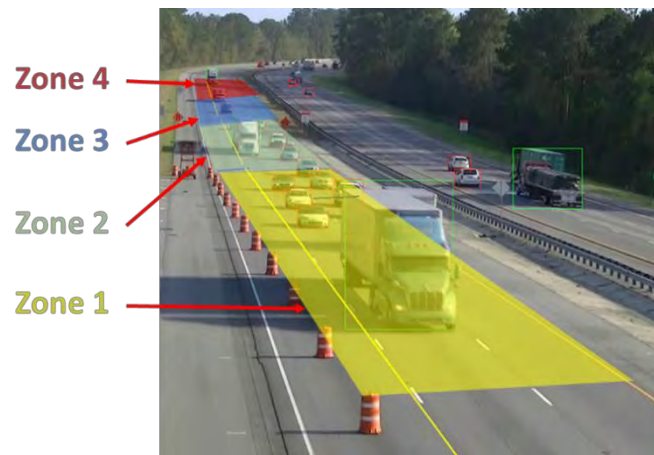


FIGURE 3-4: EXAMPLE OF ZONE LABELLING ON A REAL IMAGE

### Virtual Speed Loop Labelling

To compute speed and count vehicles at a specific location on the road using the system, it is required that users indicate the location of the vehicle whose speed needs



to be computed, and the vehicle count needs to be recorded. Like a loop detector used in the vehicle speed computation and counting the vehicles on the actual roadway, this system relies on a virtual loop detector to do the same. Therefore, the user needs to label the entry and exit points of the virtual speed loop on the image. An example of virtual speed loop labeling is shown in Figure 3-5. Here, the virtual speed loop entry and exit are marked at 40 feet from each other, and this distance is based on the standard lane marking design.



**FIGURE 3-5: EXAMPLE OF VIRTUAL SPEED LOOP LABELING ON REAL IMAGE**

#### Camera calibration reference points

To obtain the camera intrinsic and extrinsic parameters to be able to back project 2D image points to the 3D real-world points and access the real-world physical distances from the image, a few calibration reference points (pairs of 2D image coordinates and real-world 3D coordinates) are required. These reference points help obtain the camera's intrinsic and extrinsic parameters directly from the images. These reference point inputs can be avoided if the camera's intrinsic and extrinsic parameters are already available.

Finally, it is noted that the system is completely oblivious to the way these inputs are collected. Hence, some inputs, such as lane marking labels or camera calibration reference points, might be retrieved automatically via algorithms, while some others, like work zone labels, may require a user's manual intervention. In the next few sections, the six system modules are presented.

#### Module 1. Pre-processing module

Pre-processing is required to down sample the number of images from the video camera and prepare the down-sampled images to run AI-based vehicle detection, classification, and re-identification algorithms. The input for this module is the raw video feed from the camera. This module involves two steps: image extraction and image resizing.

### Image extraction

Most modern traffic video uses a 30-frame-per-second frame rate. Given the computation time required to run tracking, an AI-based vehicle detection algorithm, and the data extraction modules, processing 30 image frames will take an enormous amount of time. Therefore, we need to down sample the number of images and extract them. However, the down sampling frame rate must be chosen so that the traffic and driver behavior information can be efficiently extracted by the system without compromising the quality of the data. For example, the down sampling frame rate must be selected so that the tracking algorithm can precisely re-identify the vehicles in each subsequent frame. If the down-sampled frame rate is low (e.g., 5 fps), the vehicle would have moved a significant distance so that the tracking algorithm would fail to re-identify the vehicle in the subsequent frame, thereby losing that vehicle's position data and, subsequently, its speed data. Therefore, the final down sampling frame rate must be chosen depending on the vehicle detection and tracking algorithms chosen, acceptable processing time, and the availability of computation resources (GPU, CPU).

### Image resizing

In this step, the extracted images are resized to a smaller image size (e.g., 1080x1080 pixels to 700x700 pixels) to optimize the vehicle detection and classification algorithm's computation time.

The down sampled and resized images are fed as inputs into the vehicle detection, classification, and re-identification module. One image, typically the first image, is fed as input to the camera calibration module.

## Module 2. Camera calibration

The purpose of this module is to calibrate the camera that captures the input video; that is, we need to compute camera intrinsic and extrinsic parameters to be able to back project 2D points (point coordinates in the image plane) to the 3D world points (latitude, longitude) and access the physical measurements from the image. Intrinsic parameters correspond to parameters of the camera; extrinsic parameters are directly linked to camera orientation and location in the 3D world.

Calibrations of cameras usually use algorithms allowing the retrieval of the camera Matrix  $M$ , as defined in Equation 1 and 2, from the 2D coordinates and 3D coordinates of 6 known camera calibration points (Tsai, 1987). However, some methods (Criminisi, Reid, & Zisserman 2000; Sinha, Steedly, Szeliski et al., 2008) allow the use of geometrical properties of vanishing points along with several constraints on camera intrinsic parameters to retrieve several camera parameters. It is recommended to combine these 2 types of methods using an optimization program to relax constraints on the intrinsic parameters and obtain an accurate camera calibration algorithm like in Tang et al. (2018).

$$\mathbf{X} = \begin{bmatrix} sx \\ sy \\ s \end{bmatrix} = \begin{bmatrix} * & * & * & * \\ * & * & * & * \\ * & * & * & * \end{bmatrix} \begin{bmatrix} X \\ Y \\ Z \\ 1 \end{bmatrix} = \mathbf{M}\mathbf{X}$$

**Equation 1.** Camera calibration equation with  $(x)$  point coordinates in the image plane,  $(XYZ)$  point coordinates in the 3D world and  $\mathbf{M}$  as defined in Equation 2.

$$\mathbf{M} = \underbrace{\begin{bmatrix} f & s & x'_c \\ 0 & af & y'_c \\ 0 & 0 & 1 \end{bmatrix}}_{\text{intrinsic}} \underbrace{\begin{bmatrix} 1 & 0 & 0 & 0 \\ 0 & 1 & 0 & 0 \\ 0 & 0 & 1 & 0 \end{bmatrix}}_{\text{projection}} \underbrace{\begin{bmatrix} \mathbf{R}_{3 \times 3} & \mathbf{0}_{3 \times 1} \\ \mathbf{0}_{1 \times 3} & 1 \end{bmatrix}}_{\text{rotation}} \underbrace{\begin{bmatrix} \mathbf{I}_{3 \times 3} & \mathbf{T}_{3 \times 1} \\ \mathbf{0}_{1 \times 3} & 1 \end{bmatrix}}_{\text{translation}}$$

**Equation 2.** Calibration parameters: intrinsic and extrinsic parameters.  $\mathbf{R}$  and  $\mathbf{T}$  matrices correspond to the camera extrinsic parameters.

Therefore, our camera calibration module is primarily made of two main components, as shown in Figure 3-6:

1. A vanishing point detection module. This module will be used to retrieve vanishing points in the image. Once again, the system will be oblivious to the way these points are detected. Indeed, this task can typically be automated (Criminisi, 2002; Kong, 2013) or semi-automated (Tang, 2018).
2. An optimization problem solved using an algorithm like EDA (Larranaga et al., 2002)

The module is fed 2 types of inputs:

1. one of the video images.
2. a few calibration reference points (pairs of 3D world points and 2D image coordinates) were used to solve the optimization problem.

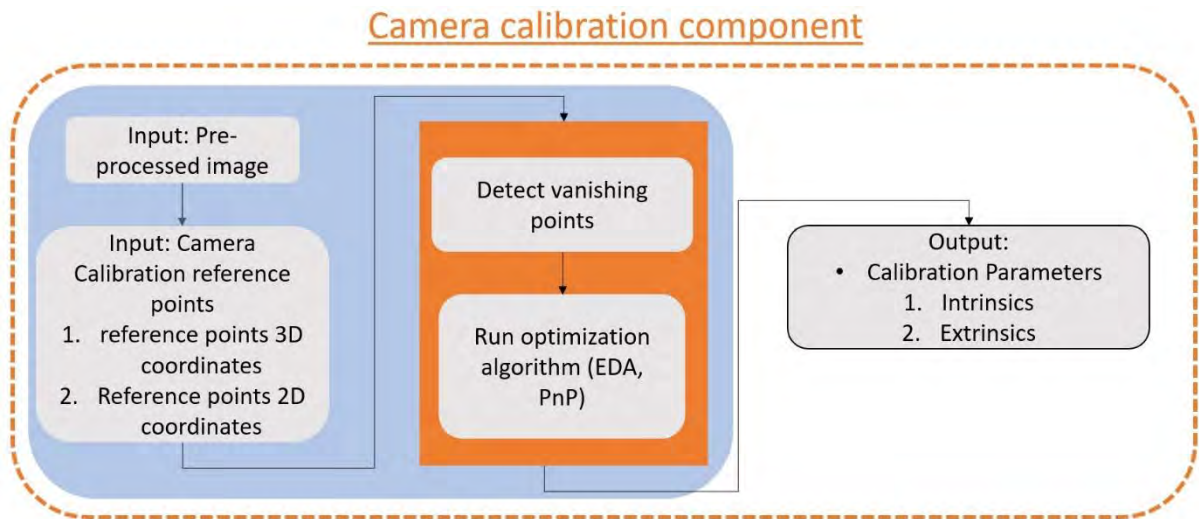


**FIGURE 3-6: CAMERA CALIBRATION COMPONENT DESIGN**

Our investigation revealed that the vanishing-points-based methods, although theoretically possible, can be challenging when obtaining reliable results in certain cases. As the method requires two vanishing points using parallel lines from the scene and even though the pavement markings provide a very good reference to find parallel lines that are parallel to the travel lanes, it can be difficult to find accurate parallel lines that are perpendicular to the travel lanes in certain scenes. It is recommended to refine the current method or use more robust methods for vanishing point detection in the camera calibration module.

However, when reliable camera calibration can not be obtained, the virtual speed loop labeling can still be used as a fallback method for extracting traffic speed. Since not all videos used in this project were able to obtain reliable camera calibration results, to minimize the impact of unreliable camera calibration on some videos, the traffic speed results presented in this report were not obtained through camera calibration but virtual speed loops with a bounding box- based method.

### Module 3. Vehicle detection, classification, and re-identification module

The purpose of this module is to detect, classify, and extract 2D trajectories of the vehicle crossing the camera's field of view. These trajectories are needed to extract any traffic information or driver behavior from the video. The idea is to be able to detect and classify vehicles entering the camera's field of view using a deep learning-based detection algorithm like Yolo (Redmon, 2016) or Faster RCNN (Ren, 2015), which have proven to achieve high performances in detection tasks (Everingham, 2015). The vehicle trajectory is then extracted using a tracking algorithm like a Kalman Filter or a particle filter.

Our vehicle detection, classification, and re-identification module is composed of two algorithms: 1. An AI-based vehicle detection and classification algorithm allowing us to



detect vehicles appearing in the image, and 2. a tracking algorithm allowing re-identification of vehicles along several consecutive video images. Figure 3-7 shows the design of this module along with its relationship to the pre-processing module. The input for this module is the down-sampled and resized images (about 18,000 images) from the video data (e.g., 30-minute video) that are sequentially indexed with an image number (1 to 18,000).

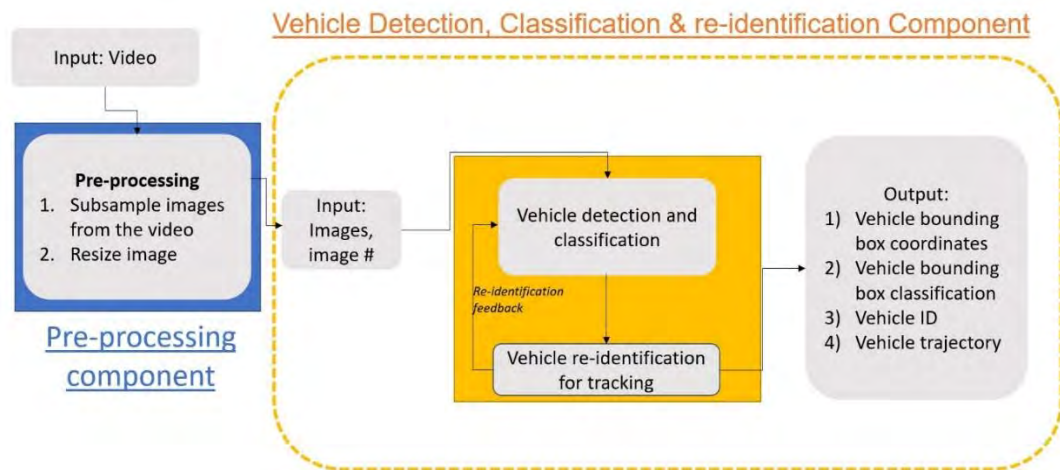


**FIGURE 3-7: VEHICLE DETECTION, CLASSIFICATION AND RE-IDENTIFICATION MODULE ALONG WITH THE PRE-PROCESSING MODULE**

These images are processed by the detection algorithm, which will output bounding box detections of the vehicles in every image. The tracking algorithm is then fed with these detections and the images. For each image, the tracking algorithm will track previously detected vehicles and match these vehicles with the bounding boxes provided by the detection model for the image. Unmatched tracked vehicles are considered "lost" and deleted when they are not matched with any detection for multiple consecutive images. This approach is very similar to SORT (Bewley, 2016). Ultimately, this module outputs four items:

1. vehicle bounding box coordinates: the locations and dimensions of boxes containing the vehicles in each image;
2. vehicle bounding boxes classification: every detected bounding box is categorized (truck or car) by the vehicle within it;
3. vehicle identifier: every vehicle detected in the video is given a unique identifier; this identifier is used to re-identify the vehicle along with the images it appears in.
4. vehicle trajectory: the location of every uniquely identified vehicle is appended together to generate the vehicle trajectory.

#### Module 4. Data extraction module

The purpose of this module is to compute traffic information, such as lane-based traffic volume, driver behavior measurements, vehicle speeds, zone-based lane change locations, and counts. The inputs for this module come from the trajectories extracted from the vehicle detection, classification, and re-identification module; camera parameters are obtained from the camera calibration module, and the user inputs, such as the virtual speed loop labels, lane marking labels, and the zone labels, are input. This module is composed of 3 sub-modules:

1. **Lane-based vehicle count** is a sub-module allowing extraction of the number of vehicles appearing in the camera's field of view for each lane.
2. **Vehicle speed computation** is a sub-module allowing extraction of speed measurements for every detected vehicle.
3. **Zone-based lane change counting** is a sub-module allowing detection and counting of the lane changes with their corresponding zone (as defined in the earlier "system inputs" section).

#### Module 5. Data aggregation module

The purpose of this module is to aggregate data collected from the data extraction module for representing the data in time series or computing traffic statistics so it can be used to study driver behavior and to plan traffic management strategies. For example, a time series for traffic flow at 5-minute intervals can be generated by aggregating lane-based vehicle counts into 5-minute bins. Another example is to aggregate the lane-based vehicle speeds into 5-minute bins and analyze the speed distribution statistics, including the mean, standard distribution, etc. The users can decide the granularity of the aggregated data depending on their needs (such as 5-minute aggregation for advanced warnings of traffic slowdown, hourly aggregation for traffic control planning, etc.).

The following sections will discuss specific methods to be used in Modules 3 and 4. Section 3.2 discusses the Vehicle Detection and Classification Using 2D Images and AI, and Section 3.3 describes the Vehicle Count and Speed Computation methodology using the outcomes of AI-based vehicle detections and classification.

### 3.2 Vehicle Detection and Classification Using 2D Images and AI (Yolo3)

This section presents the development of automatic vehicle detection and classification using a single camera. In this project, YoloV3 deep neural network (Joseph Redmon, 2018) with weights pre-trained on a COCO dataset was used. YOLOv3 was chosen because it processes frames in a reasonable amount of time and has very good performance in terms of mean average accuracy and precision.

As described in Chapter 2, YoloV3 is the third iteration of YOLO (You Only Look Once) (Redmon, 2016), an object detection model. This is a one-stage detection model, meaning all the detection and classification outputs, including the bounding box locations and dimensions on



the image, classification of the bounding box, and the classification confidence score, are computed at the same time. The output format from YOLOv3 is shown as the following:

<image-id>, <x-left>, <y-up>, <x-right>, <y-down>, <confidence>, <label>

Where:

- image-id corresponds to the image number
- x-left is the smallest horizontal coordinate of the bounding box
- x-right is the greatest horizontal coordinate of the bounding box
- y-up is the highest vertical coordinate of the bounding box
- y-down is the lowest vertical coordinate of the bounding box
- confidence corresponds to the confidence of the model that the detection is a true positive
- label corresponds to the type of vehicle (car or truck)

### 3.3 Vehicle Count and Speed Computation Methodology Using the Outcomes of AI-based Vehicle Detection and Classification

This section details the engineering approach of using the AI-based vehicle detection and classification results for determining traffic and driver behavior information. The extracted information includes traffic count, traffic speed, time headway between vehicles and lane change behavior. The proposed AI-system uses separate components for extracting the information. The following subsections detail the processing steps involved in each data extraction component.

#### 3.3.1 Data Extraction Component: Count

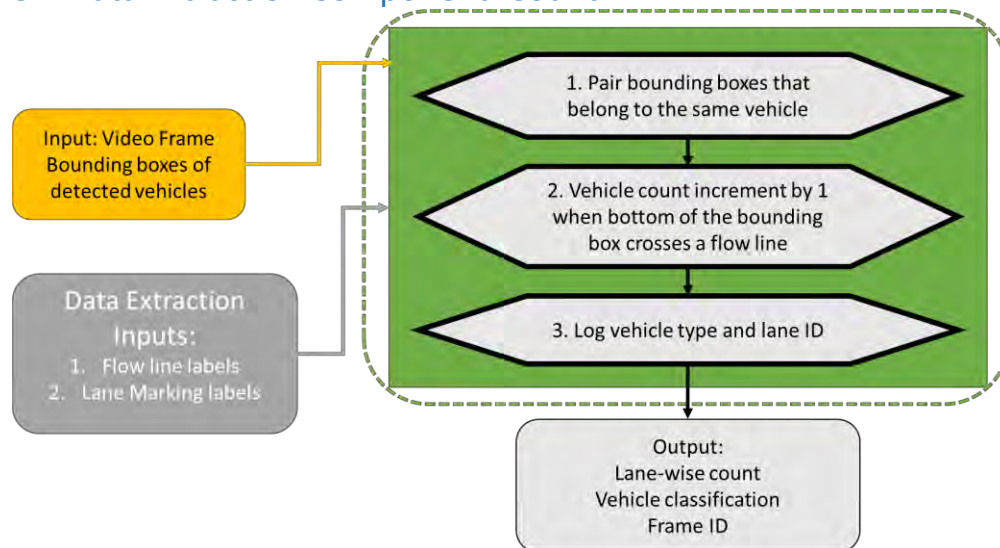


FIGURE 3-8: TRAFFIC COUNT DATA EXTRACTION PROCESSING FLOWCHART

The objective of this component is to determine lane-wise traffic count using vehicle detection bounding boxes. The core of the proposed method is to use a reference location, and whenever a vehicle (bounding box) moves past the reference location, we will include that vehicle in the count.

1. Establish short-term vehicle tracking from bounding boxes of detected vehicles.

Vehicle tracking using bounding boxes is performed by comparing the bounding boxes in two consecutive frames and linking the bounding boxes with the largest IOU as the bounding boxes from the same vehicle.

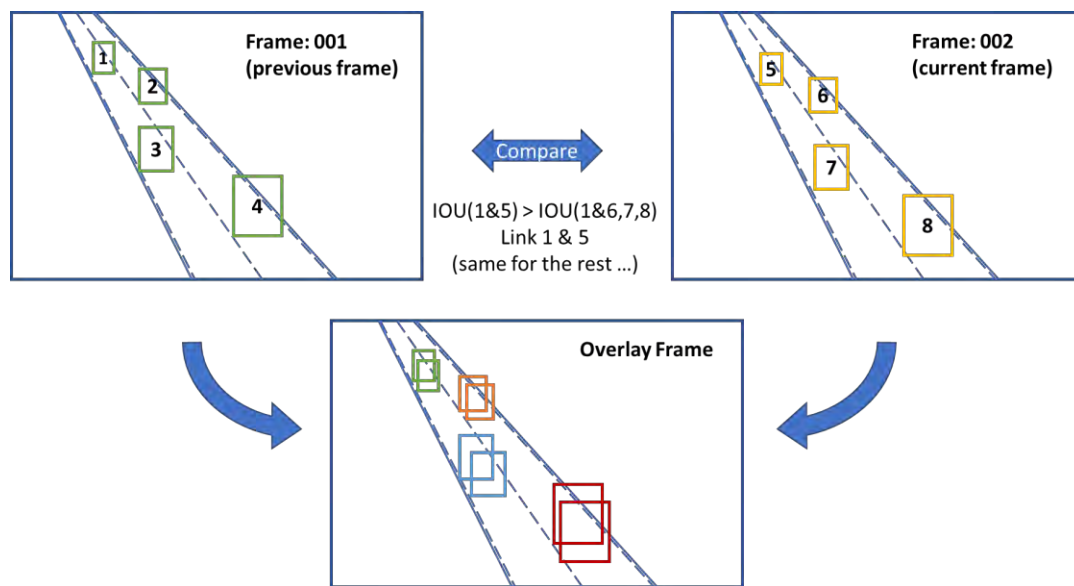
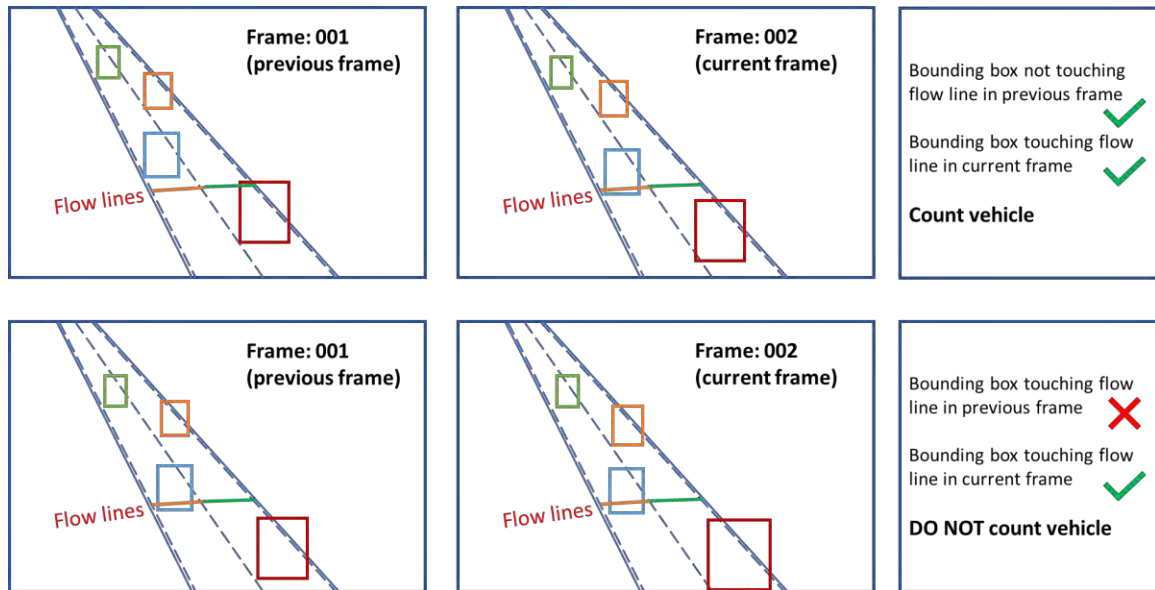


FIGURE 3-9: SHORT-TERM VEHICLE TRACKING FOR TRAFFIC COUNTING

- Inputs: Bounding boxes from two consecutive video frames.
- Outputs: Information about which two bounding boxes in the different frames belong to the same vehicle or are not a good candidate for a tracked bounding box (this could be due to detection being lost or a false detection in one frame).

2. Identify the frame in which a vehicle's bounding box FIRST crosses the reference line.

The purpose of this step is to identify the frame in which the vehicle's bounding box first crosses the reference line; it may take a vehicle's bounding box multiple frames to cross the reference line (used for counting). If the count goes up by one every time a bounding box touches the reference line, the final count results will be massively over-estimated. Therefore, it is important not to count bounding boxes from the same vehicle twice.



**FIGURE 3-10: CONDITION FOR TRAFFIC COUNTING USING BOUNDING BOXES AND REFERENCE LINES**

- Inputs: 1) bounding boxes from two consecutive frames, 2) information about which two bounding boxes belong to the same vehicle, and 3) position of each reference line in different travel lane.
- Outputs: The frame ID that a vehicle's bounding box first touches the reference line.

### 3. Log counted vehicle base on its class and lane.

To provide detailed lane-wise traffic count information, this data extraction component needs to log counted vehicles to produce a total traffic count, lane-wise traffic count, and vehicle-class-based traffic count. The frame ID of each vehicle passing the reference line can provide information regarding the time between the leading and following cars.

- Inputs: 1) detection results, 2) frame of the bounding box that first touches the referent line, and 3) which reference line the bounding box passed.
- Outputs: A csv file recording all input information.

### 3.3.2 Data Extraction Component: Speed

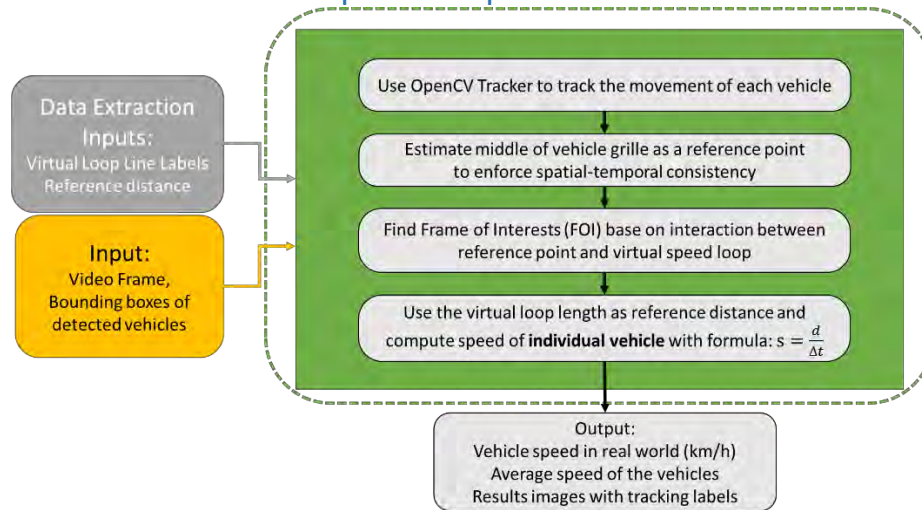


FIGURE 3-11: TRAFFIC SPEED DATA EXTRACTION PROCESSING FLOWCHART

The objective of this component is to determine vehicle traffic speed using the vehicle detection bounding boxes. The core of the proposed method is to use two reference locations with known distances to form a virtual speed loop; based on the time it takes for a vehicle to travel through the speed loop (extrapolated from frame ID), the speed of the vehicle can be computed. The following steps describe the method:

1. Establish vehicle tracking from bounding boxes using OpenCV tracker

The step is performed using OpenCV Tracker with the “CSRT” algorithm. Establishing tracking enables us to identify the frames when the vehicle of interest enters and exits the virtual speed loop and to estimate its traveling speed. Without tracking, it would be impossible to know if the bounding box interacting with the virtual speed loop belongs to the same vehicle or not.

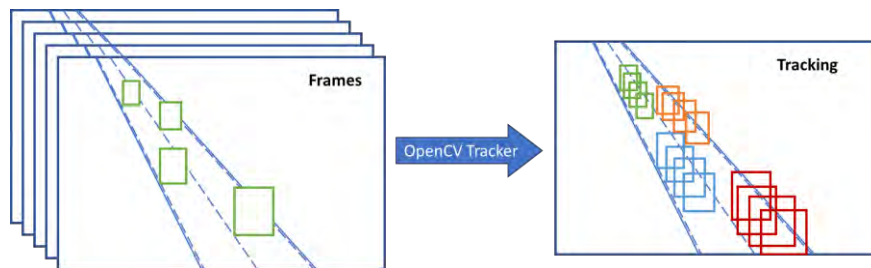


FIGURE 3-12: LONG-TERM VEHICLE TRACKING USING OPENCV TRACKER

- Inputs: Detection file with bounding box information in each frame
- Outputs: Established tracking information with a unique ID is assigned to each successfully tracked vehicle.

2. Estimate a consistent reference point from the vehicle to enforce spatial-temporal consistency

Using a consistent reference point on the vehicle when checking whether the vehicle has passed each reference speed line ensures the consistency and reliability of the computed traffic speed. One way to keep this consistency is to always use the center of the front grille as the reference point. The reference point estimation assumes the relative position of the reference point stays relatively the same in different vehicles at different distances.

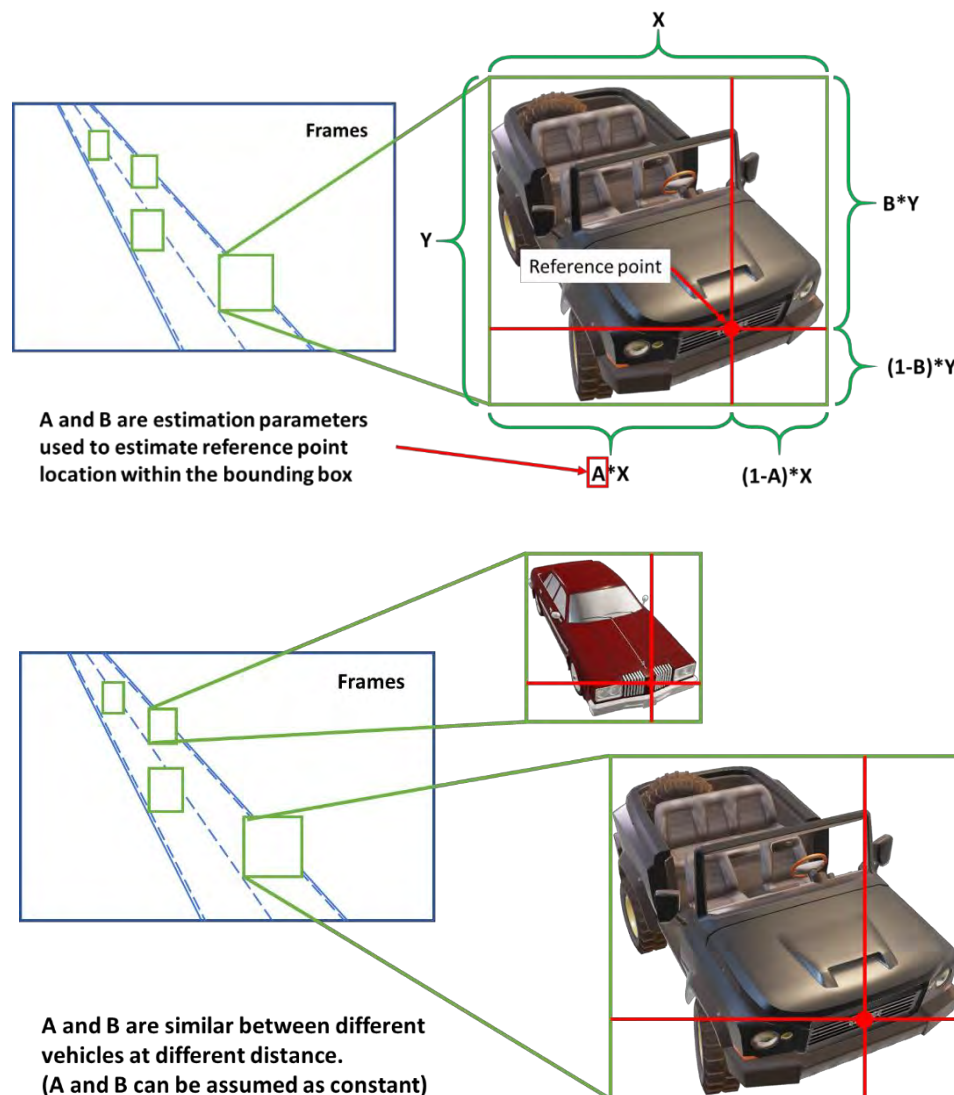


FIGURE 3-13: VEHICLE REFERENCE POINT ESTIMATION USING A BOUNDING BOX



- Inputs: 1) estimation parameters, which indicate the relative position of the reference point within the bounding box; 2) bounding boxes from the detection file.
  - Outputs: Location of reference point within each bounding box.
3. Find frames of interest (FOI) when the vehicle first enters and exits the virtual speed loop.

Identifying the frames that a vehicle first enters and exits the virtual speed loop can help us extrapolate the time it takes for a vehicle to travel through the speed loop. The time information is one of the key inputs for computing vehicle speed.

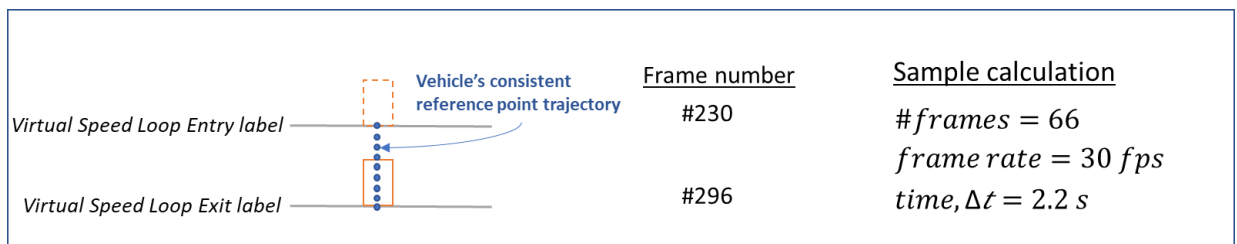


FIGURE 3-14: SAMPLE CALCULATION OF A VEHICLE'S TIME SPENT IN THE VIRTUAL LOOP

- Inputs: 1) bounding boxes with tracking labels (bounding boxes from the same vehicle would have same tracking labels), 2) the reference point position in each frame, and 3) the location of virtual speed lines.
  - Outputs: 1) for each vehicle, the frame IDs of when it first enters and exits the virtual speed loop. 2) the time it took for the vehicle to travel through the speed loop.
4. Compute individual vehicle speed using FOI

Once the time for a vehicle to cross the virtual loop is calculated, the speed of the vehicle can be computed using the distances  $d$  traveled by the vehicle and the time it takes for the reference point to intersect the entry and exit labels,  $\Delta t$ .

$$s = \frac{d}{\Delta t}$$

- Inputs:** 1) tracking ID of the vehicle, 2) the time it takes the vehicle to pass through the speed loop; and 3) the length of the speed loop.
- Outputs:** individual vehicle speed computed from  $V = \frac{ds}{dt}$ . This is shown as a csv file that logs tracking ID, FOI, and vehicle speed.



### 3.3.3 Data extraction component: Time headway

Desired time headway, as a required input in traffic simulation model, is an important information of driver behavior. The objective of this component is to derive traffic headway information from traffic count and the timestamp when each count occurs.

As described in traffic count data extraction component section, for each counted vehicle, the AI-system records the frame id when the vehicle crosses the reference line. Using this information, the time difference between two consecutive counts can be inferred base on the difference in frame id. Since the vehicles are being counted when their bounding boxes initially cross the reference line, the time difference between two counts can be effectively used as the time headway between a leading and following vehicle. Figure 3-15 illustrates how time headways are computed from the vehicle count sequence.

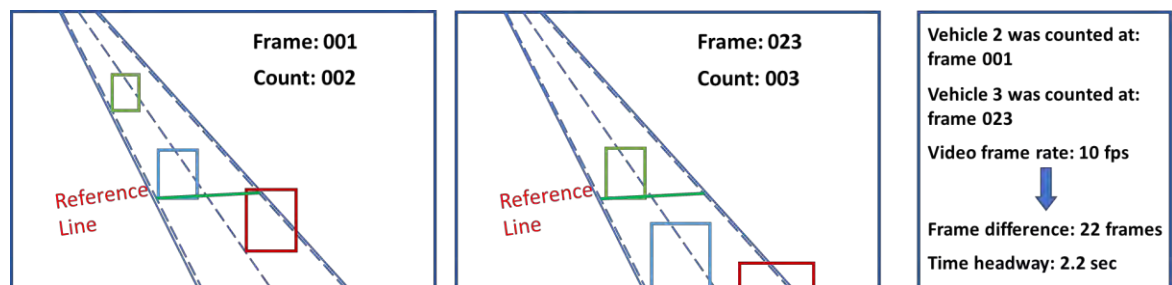


**FIGURE 3-15: COMPUTE TIME HEADWAY FROM VEHICLE COUNT SEQUENCE**

Certain traffic simulation software, such as Vissim, uses time gap parameters to describe driver following behavior. The difference between time headway and time gap is that time headway is based on the time difference between two vehicle's front bumpers crossing the same reference point, while time gap is the time difference between the leading vehicle's rear bumper and the following vehicle's front bumper. Although the current version of the AI-system does not record the time a vehicle's rear bumper crosses the reference line, the AI-system does provide enough information for the time gap between vehicles to be estimated. As shown in Figure 3-16, the time gap can be calculated by subtracting the time for the leading vehicle to travel its car length from the time headway. As previous data extraction component records the speed and vehicle type of each counted vehicle, self-time, and by extension time gap, can be estimated by assuming a typical vehicle length for each vehicle type.

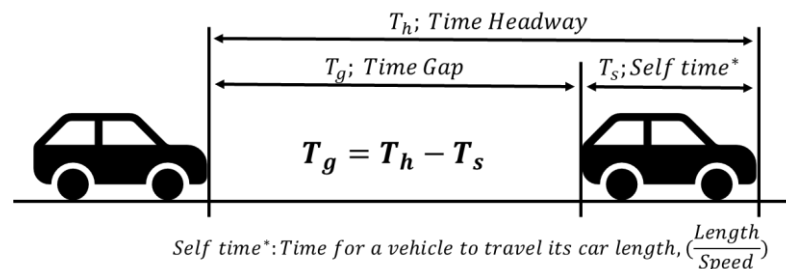


**FIGURE 3-16: ESTIMATING TIME GAP FROM TIME HEADWAY**

### 3.3.4 Data extraction component: Lane change

Extracting driver merge decision data (consisting of vehicle type and merging zone) involves the following three major steps:

- 1) Detecting individual vehicles and their positions in the image,
- 2) Classifying the detected vehicles (cars or trucks) in the image, and
- 3) Determining the merge location (the change lane decision) for each vehicle from the image sequence (frames) and classifying its corresponding zone (Zones1 to 4) and vehicle type.

Figure 3-17 illustrates the data extraction procedure. Each image is given a frame number to keep track of the sequence of the images, as shown in Figure 3-17(a). Figure 3-17(a) also illustrates Steps 1 and 2 for vehicle detection and vehicle classification in each image. The two vehicle-classification categories are cars and trucks; the “cars” class (represented by orange boxes in Figure 3-17(a)) includes passenger vehicles (sedans, SUVs, and small cars), and the “trucks” class (represented by green boxes in Figure 3-17(a)) includes pickup trucks, buses, and trailers. The position of each detected vehicle and the class of each vehicle in the image is recorded. Figure 3-17(b) illustrates how to determine the merge location. When the position of a detected vehicle in the image sequence crosses the pavement marking line separating the closed lane from the open lane, we determine the merge location and record its corresponding zone number.

Table 3-1 shows an example of how zone-based vehicle merge count is recorded. As graphically illustrated in Figure 3-17 (b), at frame #57, the car’s position changes from the closed lane to the open lane in Zone 2. Hence, in Table 3-1, a new record (57) is added under Frame # and the merge count in the corresponding zone (Zone 2) and vehicle type (Cars) is incremented by 1. Similarly, the first truck’s merge zone was recorded at Frame #47 in Zone 3, and the second truck merge location is recorded at Frame #97 in Zone 4. When the next car merges lanes in Zone 2, the count will be incremented to 2 at the corresponding frame number. The total number of vehicles that merged lanes at the end of 97 frames is 3. From Table 3-1, we can infer when (frame #) and where (zone #) each class of vehicle changes lanes for merging.

The lane-change location can be identified in this study. With the location reference, we can compute the location based on the distance to the work zone taper or different zones of the work zone, which is the one we used in our study. In addition, the speed during the lane change can also be computed in the future.

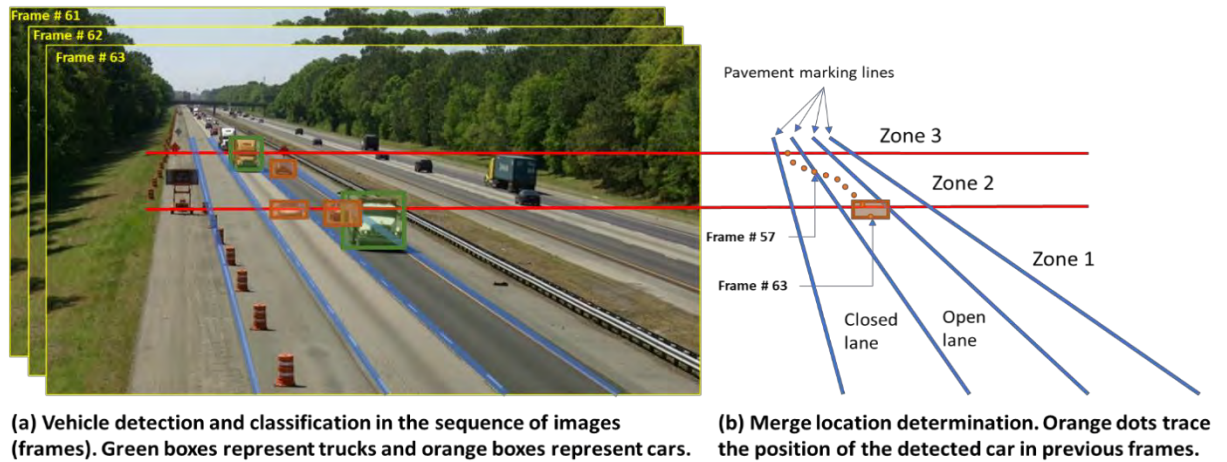


**FIGURE 3-17 ILLUSTRATION OF DATA EXTRACTION STEPS**

**TABLE 3-1 ZONE-BASED VEHICLE MERGE COUNT INCREMENT TABLE ALONG WITH VEHICLE TYPE**

	Zone 1		Zone 2		Zone 3		Zone 4	
Frame #	Cars	Trucks	Cars	Trucks	Cars	Trucks	Cars	Trucks
47	0	0	0	0	0	1	0	0
57	0	0	1	0	0	1	0	0
97	0	0	1	0	0	1	0	1

We demonstrate the implementation of the system through a case study on work zone traffic videos collected from Georgia Interstate-95 (I-95), in the following chapter.

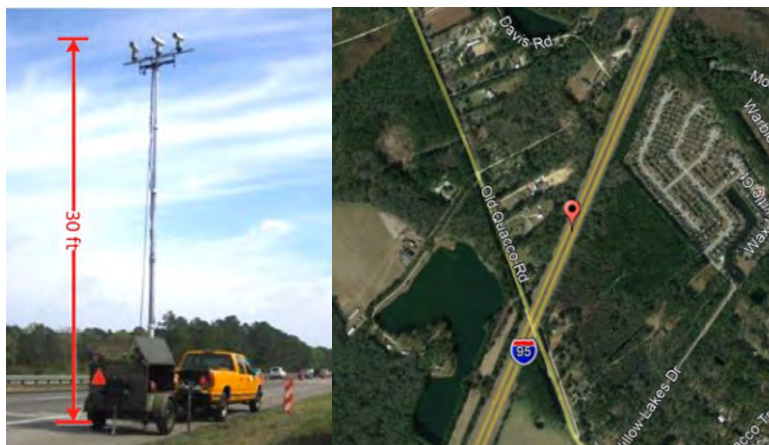
## Chapter 4: CASE STUDY OF THE AI-BASED SYSTEM AND DRIVER BEHAVIOR ANALYSIS

In this chapter, a case study presents the use of the proposed AI-system to extract traffic and driver behavior information from two 30-minute traffic footages using the proposed AI-system. In addition, this chapter also presents the benefits of analyzing the extracted information to obtain accurate and refined traffic and driver behavior information. The analyzed traffic and driver behavior information includes vehicle counts, vehicle types, driver behaviors, individual vehicle speeds, individual time headways/gaps, and lane change locations.

The case study involves two 30-minute work zone videos collected in a work zone on I-95 near Savannah, Georgia; the videos were chosen by design to analyze the impact of traffic density and vehicle type on work zone driver merge behaviors. First, we show the implementation of the proposed AI-system and the results of traffic count and speed aggregated into 3-minute intervals. Second, we demonstrate the application of using the extracted data for driver behavior study at the work zone with a) high traffic density conditions and b) low traffic density conditions.

### 4.1 Case study data description.

In this case study, we use two 30-minute-long work zone videos that were taken on I-95 with a camera mounted on a tower, as shown in Figure 4-1: Camera mounting tower and work zone sites for collecting videos. The work zone is in a straight section of the interstate with a right-lane closure. The videos were collected during clear weather conditions from 3:00 PM to 3:30 PM (video A) and 2:30 PM to 3:00 PM (video B). The two videos were chosen because of the difference in their traffic conditions. Video A shows dynamic traffic conditions in which the traffic evolves from slow-moving, high-density conditions to nearly free-flowing, low-density conditions. Video B shows a more static traffic condition in which traffic is constantly slow-moving, as shown in Figure 4-2. In Video A, the transition from congested traffic conditions to non-congested traffic occurred around the 9 to 10-minute mark.



(a) camera mounting tower

(b) work zone sites



FIGURE 4-1: CAMERA MOUNTING TOWER AND WORK ZONE SITES FOR COLLECTING VIDEOS



(a) low traffic density condition



(b) high traffic density condition

FIGURE 4-2: VIDEOS A AND B WITH LOW AND HIGH TRAFFIC DENSITY CONDITION IN THE WORK ZONE

## 4.2 Use of the AI-system

The user interface of the AI-system provides an interactive way for the user to set up the AI-system and visualize vehicle detection and reference lines on the original traffic video frames, as shown in the left part of Figure 4.3. Interactive functions of the interface are shown in the right part of Figure 4.3, including loading data, drawing of reference lines, defining reference distance, cycling through video frames, etc. Using this user interface, the user can complete the setup of the AI-system by drawing the boundaries of each lane and drawing two reference lines across the entire roadway with a known real-world distance. To control the real-world distance of the two reference lines, pavement striping is typically used as a visual aid, as the pavement striping has fixed 10-ft lengths and 30-ft gaps.

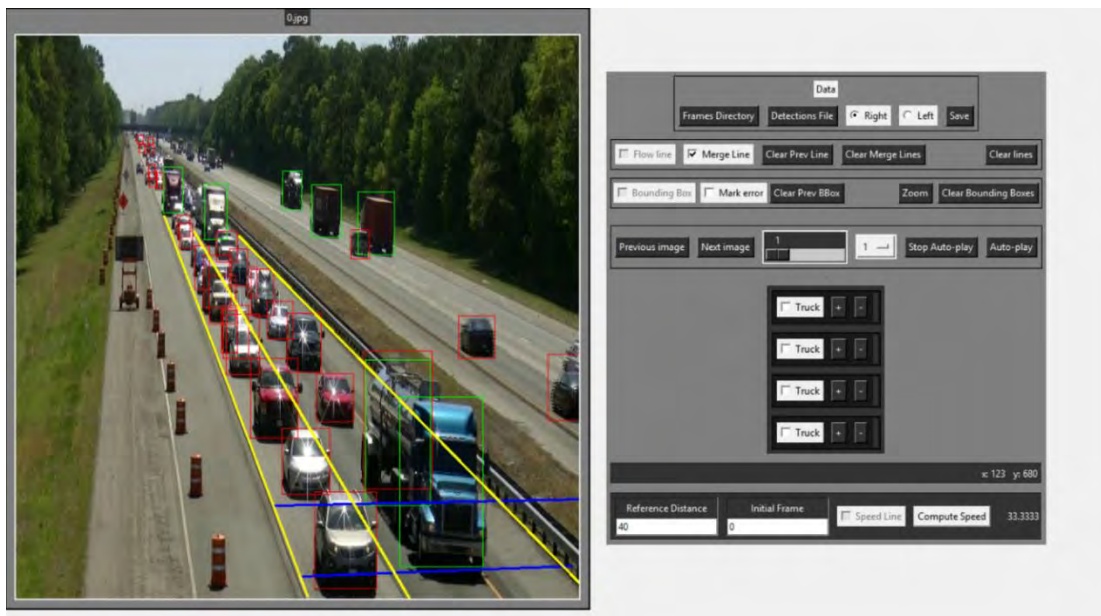


FIGURE 4-3: USER INTERFACE AND REQUIRED INPUT FOR IMPLEMENTING AI-SYSTEM

By performing vehicle detection and classification using the Yolo3 deep-learning model, detection and classification results are obtained; a portion of the results are shown in Table 4-1. Each entry in the table represents one instance of detection; the information regarding that detection is also recorded. Information includes the frame index of the detection, bounding box location within that frame (x, y, width, height), the confidence level of the detection, and the classification of the detection.

**TABLE 4-1 SAMPLE VEHICLE DETECTION RESULTS USING YOLO3**

Frame Index	X	y	width	height	confidence	label
4438	1021	846	210.6931	158.1098	0.999565	car
4435	992	815	209.3338	155.1874	0.999516	car
2078	986	856	213.1085	155.4163	0.999494	truck
6267	944	831	196.1606	137.9711	0.99949	car
4434	982	800	215.4278	160.2763	0.999476	car
6266	923	811	199.7261	142.763	0.999459	car
4436	997	827	211.4515	155.8624	0.999434	car
12610	984	851	208.1568	149.3467	0.999421	truck
4443	1059	882	226.681	180.8946	0.999411	truck
4867	1198	823	212.9472	135.7052	0.9994	car
1387	996	864	194.5786	143.9435	0.999399	car
4442	1051	871	222.3091	182.1582	0.999386	car
...	...	...	...	...	...	...

The 30-minute videos each contain 17962 frames (downsampled from 30 frames per second to 10 frames per second). Among these frames, the Yolo3 vehicle detection yielded more than 443,000 detection instances with an average detection confidence of 0.657. The classification results show about 24.4% of detections are classified as “trucks,” and the rest are classified as “cars.” These vehicle detection results are then used by the data extraction components described in Chapter 3 to extract traffic and driver behavior information.

#### 4.4 Traffic and driver behavior analysis

This section presents the benefits of obtaining the traffic and driver behavior information by conducting traffic and driver behavior analysis. The analysis uses information that can be extracted using widely available 2D cameras, the information extracted includes vehicle counts, vehicle types, driver behaviors, individual vehicle speeds, individual time headways/gaps, and lane change locations. Although the preliminary version of the proposed AI-System produces a promising outcome, there is still a discrepancy between the AI extracted data and the ground reference data (manually extracted data). To better demonstrate the use of the data extracted using widely available 2D camera images, we used the ground reference in the subsequent sections in this chapter to better present the traffic and driver behavior study that can be performed using the extracted data.



### Traffic count results

Table 4-2 and Figure 4-4 show the traffic count results obtained from the case study videos; the traffic count results are aggregated into five-minute intervals. The results generally show a higher proportion of vehicles traveling in the inner lane than in the outer lane, but the difference in traffic count number is reduced in high traffic density conditions.

**TABLE 4-2 LANE-WISE TRAFFIC COUNT AGGREGATED IN FIVE-MINUTE INTERVALS**

Time interval	Video A			Video B		
	Inner Lane	Outer Lane	Both Lane	Inner Lane	Outer Lane	Both Lane
1-5 min	92	76	168	48	56	104
6-10 min	93	64	157	70	51	121
11-15 min	90	70	160	88	85	173
16-20 min	83	59	142	67	69	136
21-25 min	92	62	154	98	88	186
26-30 min	96	66	162	101	103	204
Total	546	397	943	472	452	924

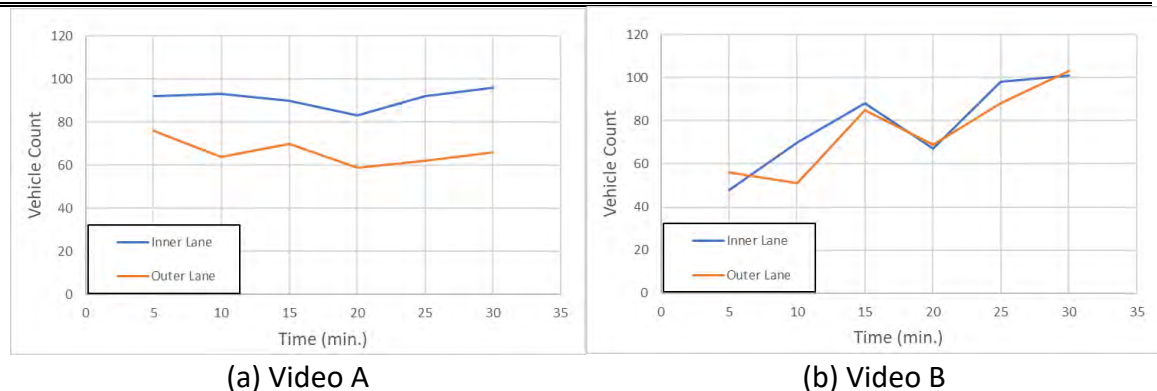


**FIGURE 4-4: VEHICLE COUNTS OVER TIME AGGREGATED INTO FIVE-MINUTE INTERVALS**

### Traffic speed results

The traffic speed information obtained from the case study videos is shown in Table 4-3. In this table, the speed is reported for each travel lane, and the statistical values, such as minimum, maximum, mean, median, and standard deviation, are used to describe the distribution of the traffic speed. This level of detail can be expected from the AI-system, as the system estimated speed at the individual vehicle level; thus, the system enables users to obtain speed information statistics that describe the distribution of traffic overall speed.

**TABLE 4-3 STATISTICS OF EXTRACTED SPEED DATA IN 5-MINUTE INTERVALS**

Video A											
Bins Minutes	Inner Lane Speed (MPH)					Outer Lane Speed (MPH)					
	Min	Mean	Max	Median	SD	Min	Mean	Max	Median	SD	

0-5	7.5	21.9	35.4	22.5	6.7	7.5	19.8	30.9	19.1	6.1
5-10	19.1	26.1	41.3	24.8	5.0	15.4	20.2	41.3	19.1	3.9
10-15	30.9	47.7	82.5	49.5	10.7	27.5	45.5	82.5	41.3	11.0
15-20	41.3	56.3	82.5	61.9	7.8	41.3	53.3	61.9	49.5	7.2
20-25	24.8	54.9	82.5	49.5	10.2	41.3	50.9	61.9	49.5	6.6
25-30	41.3	56.2	82.5	61.9	8.8	41.3	53.5	82.5	49.5	7.6

**Video B**

Bins Minutes	Inner Lane Speed (MPH)					Outer Lane Speed (MPH)				
	Min	Mean	Max	Median	SD	Min	Mean	Max	Median	SD
0-5	1.1	12.3	22.5	12.4	4.4	2.8	11.1	17.7	11.3	3.5
5-10	2.6	15.4	22.5	16.5	4.3	8.8	13.2	19.1	13.8	2.5
10-15	7.5	20.9	35.4	20.6	5.2	6.7	16.5	27.5	16.5	4.4
15-20	3.8	14.3	22.5	14.6	3.6	2.4	13.2	22.5	13.0	4.1
20-25	14.6	23.4	35.4	22.5	4.8	5.6	21.9	30.9	22.5	6.4
25-30	15.4	27.6	35.4	27.5	4.8	15.4	27.8	35.4	27.5	4.3

Figure 4-5 shows the average traffic speed in each lane. The results show a similar speed trend is being followed by traffic in both lanes, but a higher average speed can be found in the inner lane than in the outer lane; this result is reflective of typical traffic conditions. The traffic speed also captured the lower traffic speed in high-density conditions ( in Video B and in the beginning of Video A) and the transition from a congested to a non-congested condition in Video A.

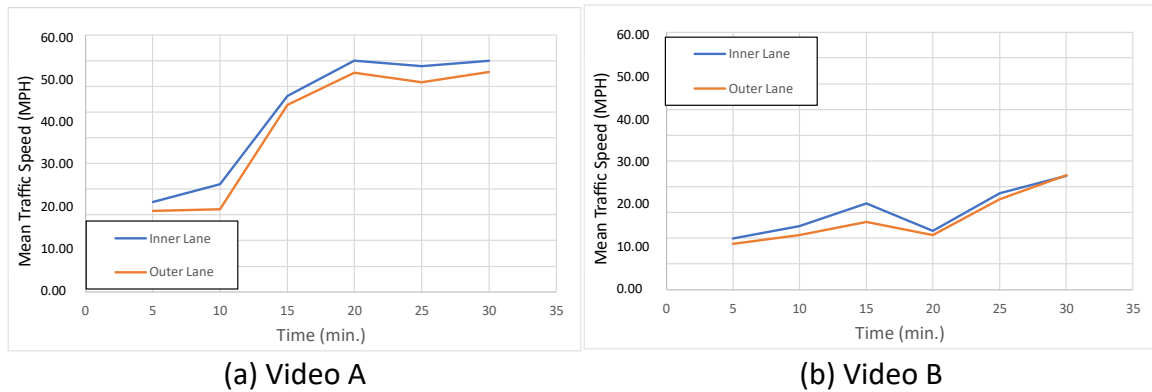


**FIGURE 4-5 TRAFFIC SPEED ESTIMATION IN INNER AND OUTER LANES**

### Traffic headway results

The preliminary version of the AI-system enables the extraction of time headway information at the individual vehicle level. Since the information about the drivers' following behaviors can be used in traffic simulation software like Vissim, the time gap information (as shown in Figure 3-16 of Chapter 3, time gap,  $T_g = T_h - T_s$ ) is estimated from the extracted time headway. Table 4-4 shows the time gap results. One advantage of having time headway information at the vehicle-level is the ability to filter the dataset

to suit the needs of the analysis. As an example, Table 4-4 also shows the time gap results where time gaps larger than 4-sec were removed to mitigate the impact of results from the random arrival of vehicles; this improves the reliability of the inferred driver following behavior using the filtered time gap results.

**TABLE 4-4 STATISTICAL VALUES OF TIME-GAP FROM VIDEO A AND B**

<b>Video A (inner lane)</b>										
Bins	Time Gap (sec)					Time Gap under 4-sec (sec)				
Minutes	Min	Mean	Max	Median	SD	Min	Mean	Max	Median	SD
0-5	0.550	2.297	8.525	1.850	1.484	0.550	1.959	3.975	1.825	0.891
5-10	0.450	2.424	13.375	1.775	2.093	0.450	1.821	3.900	1.625	0.817
10-15	0.400	2.621	14.650	1.800	2.477	0.400	1.534	3.900	1.350	0.816
15-20	0.350	2.499	17.825	1.500	2.917	0.350	1.566	3.975	1.350	0.944
20-25	0.200	2.618	30.675	1.450	3.781	0.200	1.549	3.800	1.300	0.913
25-30	0.350	2.594	12.000	1.650	2.534	0.350	1.506	3.900	1.250	0.822
<b>Video A (outer lane)</b>										
Bins	Time Gap (sec)					Time Gap under 4-sec (sec)				
Minutes	Min	Mean	Max	Median	SD	Min	Mean	Max	Median	SD
0-5	0.550	2.760	10.750	2.100	2.027	0.550	2.015	3.950	1.900	0.931
5-10	0.575	3.233	15.200	2.225	2.673	0.575	2.016	3.975	1.825	0.894
10-15	0.400	2.976	8.600	2.050	2.014	0.400	1.857	4.000	1.613	0.940
15-20	0.250	3.796	15.850	2.588	3.629	0.250	1.851	4.000	1.650	0.993
20-25	0.600	3.230	14.000	1.850	3.260	0.600	1.672	3.500	1.550	0.814
25-30	0.425	4.016	31.000	2.600	4.575	0.425	1.961	3.700	1.925	0.949
<b>Video B (inner lane)</b>										
Bins	Time Gap (sec)					Time Gap under 4-sec (sec)				
Minutes	Min	Mean	Max	Median	SD	Min	Mean	Max	Median	SD
0-5	0.675	3.481	15.300	2.300	3.253	0.675	2.070	3.625	2.000	0.765
5-10	0.450	2.790	13.900	2.150	2.281	0.450	1.814	3.150	1.850	0.787
10-15	0.500	2.268	6.825	1.850	1.329	0.500	1.871	3.600	1.750	0.752
15-20	0.750	2.792	9.550	2.388	1.760	0.750	2.230	3.950	2.250	0.803
20-25	0.450	2.061	5.600	1.875	1.167	0.450	1.859	3.725	1.750	0.896
25-30	0.400	2.144	8.200	1.775	1.422	0.400	1.828	4.000	1.700	0.864
<b>Video B (outer lane)</b>										
Bins	Time Gap (sec)					Time Gap under 4-sec (sec)				
Minutes	Min	Mean	Max	Median	SD	Min	Mean	Max	Median	SD
0-5	1.000	2.966	9.650	2.650	1.640	1.000	2.380	4.000	2.425	0.838
5-10	0.500	3.507	10.750	3.200	2.192	0.500	2.200	3.850	1.925	0.936
10-15	0.400	2.320	12.225	2.075	1.701	0.400	1.957	3.800	1.875	0.822
15-20	0.750	2.624	7.050	2.288	1.325	0.750	2.290	4.000	2.100	0.878
20-25	0.350	2.229	8.050	1.950	1.358	0.350	1.852	3.800	1.750	0.760
25-30	0.400	1.868	8.750	1.625	1.270	0.400	1.651	3.450	1.500	0.780

Based on the time-gap results obtained from the videos, we have observed that the drivers typically follow each other with a time-gap in the range between 1.5 sec to 2.5 sec. In different traffic conditions, speed does not significantly change the following behavior of outer lane vehicles, while the inner lane drivers follow each other closer at higher speeds (1.5 sec compared to 1.9 sec). Also, the following behavior shows a slightly smaller variation (standard deviation) in high traffic density conditions.

### Work zone merge behavior analysis

In this section, we analyze the impact of traffic density on the work zone driver merge behavior using the two highway work zone scenarios consisting of a) high traffic density conditions and b) low traffic density conditions. We grouped the lane change positions of each vehicle merging from the closed lane to the adjacent open lane into four zones, plotted the percentage of vehicles merging in each zone, and analyzed the merge location distribution to classify work zone driver merge behavior (by each vehicle type) as 1) late or early merges, and 2) dangerously late merges. We then compared the work zone driver merge behaviors for the two scenarios with high and low traffic density conditions to determine the impact of traffic density on the work zone driver merge behaviors.

### Zones for grouping driver merge locations

To group the different drivers' merge locations in a work zone and analyze drivers' merge location distribution, we defined four zones. Accordingly, we divided the work zone transition area and the advance warning area into four zones, as illustrated in Figure 4-6. Zone 1 represents the transition area, which consists of traffic control barriers (such as cones or cylinders) placed on the travel lane arranged in a tapering manner, gradually decreasing lane width. Zone 2, Zone 3, and Zone 4 cover the advance warning areas; they are 0 ft. to 500 ft. (152 m), 500 ft. (152 m) to 1000 ft. (304 m), and 1000 ft. (304 m) to 1500 ft. (458 m), measured upstream from the beginning of the transition area (the work zone taper), respectively.

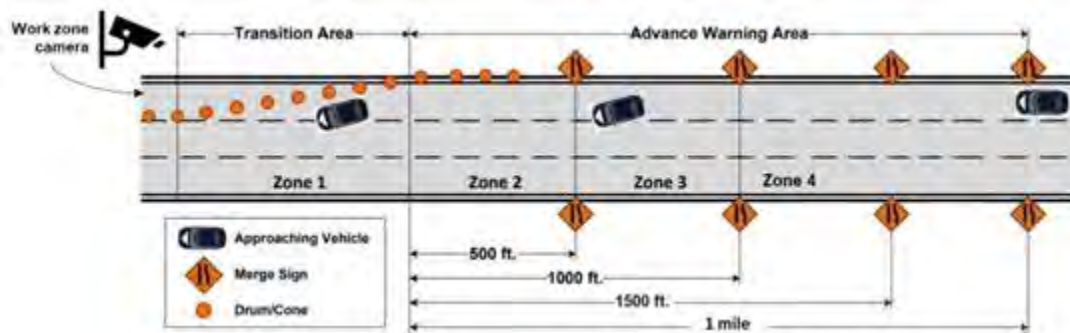
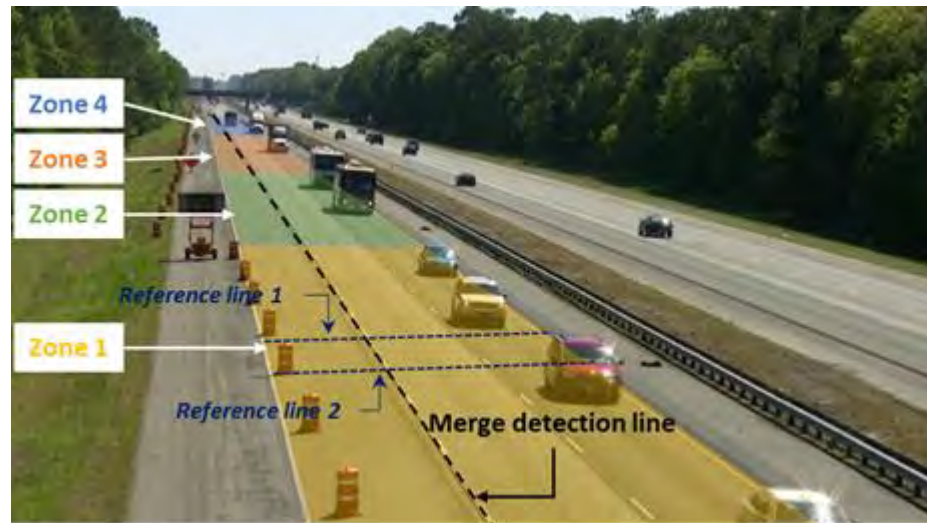


FIGURE 4-6 FOUR ZONES DEFINED IN THIS STUDY TO GROUP THE MERGE LOCATIONS (ADOPTED FROM TSAI ET AL., 2011) [1 FEET = 0.305 M]



### Data Processing

The four zone boundaries, the two reference lines for the virtual speed loop, and the merge detection line (based on the pavement marking between the closed lane and adjacent open lane) were manually drawn on the images, as shown in Figure 4-7. In both scenarios, the merge locations, along with vehicle type, frame #, and zone, were recorded visually.



**FIGURE 4-7** MANUAL DRAWING OF MERGE ZONES, VIRTUAL SPEED LOOP REFERENCE LINES AND THE MERGE DETECTION LINE IN IMAGES COLLECTED FROM THE GA I-95 WORK ZONE.

Using the traffic speed and the traffic flow extracted from the proposed AI-system, the traffic density was calculated. For example, traffic and merge data extracted from the scenario with low traffic density condition is summarized below:

Traffic Flow	= 1034 vehicles/0.5 hours
Traffic Speed	= 43.5 mph
Traffic Density	= 29.5 vehicles/mile
Number of merges	= 32 (17 cars, 15 trucks)

Similarly, traffic and merge data extracted from the scenario with high traffic density condition is summarized below:

Traffic Flow	= 1170 vehicles/0.5 hours
Traffic Speed	= 20 mph
Traffic Density	= 117 vehicles/mile
Number of merges	= 85 (81 cars, 4 trucks)

### Work zone driver merge behavior data analysis

After the data is extracted and processed for the two scenarios, there are three steps in work zone driver merge behavior data analysis:

Step 1: Determining the percentage of drivers merging in each zone by dividing the number of merges in each zone by the total number of merges. The percentages are computed separately for cars and trucks.

Step 2: Plotting the percentage of merges in each zone as a histogram separately for each vehicle type. This histogram produces a statistical distribution of the drivers' merging locations in different zones.

Step 3: Analyzing the impact of traffic density on driver merge location based on work zone driver merge behavior classifications, including 1) late or early driver merge behaviors, and 2) dangerously late merge behaviors. The details of each behavior are discussed below.

#### ***Analysis 1: Late or early driver merge behavior.***

Earlier driver merge behavior will result in a higher percentage of drivers perform merge maneuver in Zone 1 and Zone 2, while later driver merge behavior will result in a higher percentage of drivers perform merge maneuver in Zone 3 and Zone 4. Therefore, based on the distribution of merge locations among Zone 1 to Zone 4, the driver merge behavior can be evaluated across different traffic scenarios.

#### ***Analysis 2: Dangerously late merge behavior.***

In addition, if the percentage of vehicles in Zone 1 are higher in one scenario than in others, it indicates that the dangerous late driver merge behavior in this scenario is higher in than in other scenarios. Dangerous late merge occurs when a vehicle merges inside the transition zone (Zone 1) and is likely to impact the safety and mobility in the work zone. Merging in Zone 1 is dangerous because the pavement width continuously reduces, and the driver is at risk of crashing into the traffic control cones or, even, at risk of crashing with adjacent lane vehicles or causing congestion.

### Work zone driver merge behavior results

This section presents the analysis results of the work zone driver merge behavior for the two scenarios – low and high traffic density condition. The analysis was performed using the steps discussed in the data analysis section above. The analysis data for this case study is shown in Figure 4-8. It is observed that at low traffic density, the majority of car drivers tend to merge early (88% in Zone 3 and 4). However, in high traffic density, nearly half the car drivers merge late (53% in Zone 1 and 2). Comparing the two traffic conditions (low, and high traffic density) for dangerous late merges, it is clearly seen (in Figure 4-8) that car drivers merge later in high traffic density conditions than in low traffic density conditions (the percentage of dangerous late merges increases from 6% in low traffic density to 28% in high traffic density conditions for Zone 1). This late merge

behavior could be attributed to 1) drivers' tendency to merge early to avoid changing (reducing) speed, 2) drivers' feeling safer to merge late at slow speeds than at high speeds, 3) drivers' seeing the work zone earlier in low traffic density than in high traffic density, or 4) drivers being eager to get home at 5 pm and behaving aggressively (especially in the high traffic density scenario).

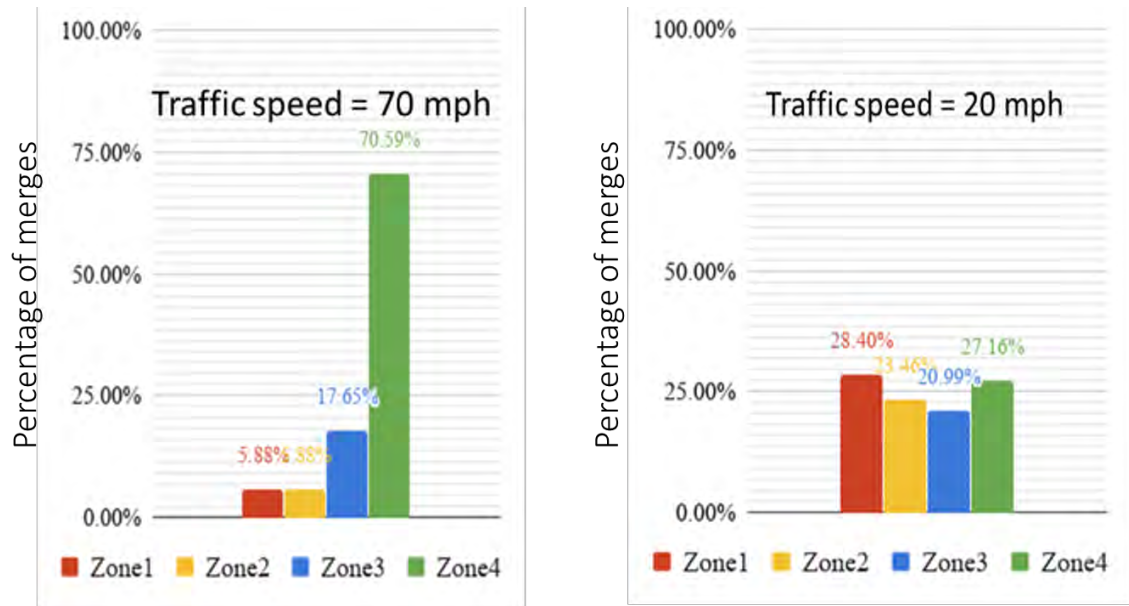


FIGURE 4-8 COMPARISON OF THE PERCENTAGE OF CARS MERGING AT DIFFERENT ZONES AT LOW, AND HIGH-DENSITY TRAFFIC CONDITIONS

## Chapter 5: ERROR ANALYSIS AND IDENTIFICATION OF FACTORS

A preliminary version of the AI-system has been developed in this research, and improvements of this preliminary AI-system are required. To further improve the developed AI-system, it is important to identify the errors and analyze the detailed causal factors and reasons of the errors (error analysis) so improvements can be made. The error analysis is an essential but complicated procedure for establishing a refined, robust, and sustainable AI-system. This chapter presents an error analysis methodology 1) by comparing the results obtained from the AI system with manually collected ground reference data and 2) by identifying the factors and reasons that impact the accuracy of the extracted traffic and driver behavior information (e.g. vehicle count and vehicle speed) using the developed AI-system. These factors and reasons are grouped based on three categories of factors (a. sensor, b. traffic and environment, and c. algorithm) presented in Table 2-1. Finally, this chapter also recommends the possible methods, including statistical methods and multi-interval aggregation methods, etc., to remove bias and outliers for improving the accuracy and reliability of the extracted information (e.g., vehicle count and vehicle speed).

### 5.1 Error Analysis Methodology

This section presents the error analysis methodology. The purpose of the error analysis is to study the accuracy of real-world driver behavior extracted using the AI-system and to identify the factors impacting the accuracy and to quantitatively analyze the impact of the factors causing the errors. This section presents the design of error analysis and the data preparation of the ground reference traffic data.

#### 5.1.1 Design of Error Analysis

The design of error analysis is to compare the performance of automatically extracted traffic information with ground reference data for a 30-minute long work zone traffic video a) to study the statistical distribution and signature of errors/differences, b) to identify the factors causing the errors, c) to qualitatively show the impact of different levels of error-causing factors, d) to recommend the statistical method, like median and standard deviation to eliminate the outliers/bias caused by error-causing factors, and e) to quantify/categorize the automatically extracted and refined traffic and driver behavior information.

#### 5.1.2 Ground Reference Data preparation (on I-95)

Figure 5-1 shows the traffic annotation tool used to manually extract traffic count and speed information. Using this traffic annotation tool, the ground reference is obtained by manually triggering the tool to log the frame ID every time a vehicle crosses the reference lines. The reference lines were drawn using the pavement markings as references, which ensures an estimated distance of 40 ft (10-ft long striping with 30-ft gaps) between the two reference lines.

Quantitatively Evaluate Work Zone Driver Behavior using 2D Imaging,  
3D LiDAR, & Artificial Intelligence in Support of Congestion Mitigation  
Model Calibration & Validation (Project G2)

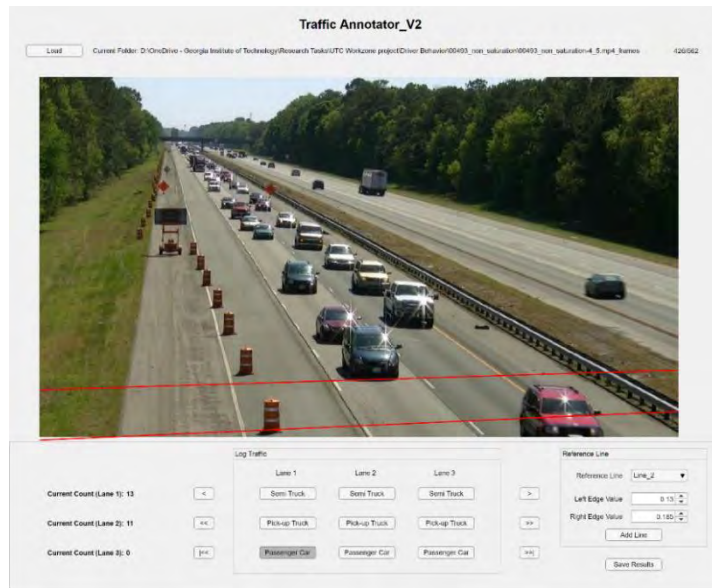


**FIGURE 5-1: USER INTERFACE OF TRAFFIC ANNOTATOR WITH REFERENCE LINES**

Using the traffic annotation tool, ground reference data obtained includes the lane that a vehicle is traveling in, the frame IDs of a vehicle entering and exiting the virtual speed loop, and vehicle class categorized by length (passenger car, pickup truck, and semi-truck). The traffic count is obtained based on the number of vehicles that enter the virtual speed loop and the time of occurrence of a count is obtained from the number of vehicles that enter the virtual speed loop. The time spent in the virtual speed loop is calculated based on the time difference between the frames in which the same vehicle enters the loop and exits the loop. Since the real-world length of the speed loop is known (about 40-ft), the estimated vehicle speed can be calculated.



**TABLE 5-1 EXTRACTED LANE-WISE TRAFFIC DATA USING AI-SYSTEM AND GROUND REFERENCE TRAFFIC DATA**

Time (minute)	Inner Lane				Outer Lane				Both Lanes			
	Estimated Speed (MPH)	GT Speed (MPH)	Estimated Count	GT Count	Estimated Speed (MPH)	GT Speed (MPH)	Estimated Count	GT Count	Estimated Speed (MPH)	GT Speed (MPH)	Estimated Count	GT Count
1	22.60	20.49	1	20	18.61	18.53	19	15	18.81	19.65	20	35
2	-	11.27	0	12	12.34	11.09	12	12	12.34	11.18	12	24
3	21.99	17.87	2	17	16.84	15.74	16	13	17.42	16.94	18	30
4	19.28	25.01	7	25	23.31	23.58	26	17	22.45	24.43	33	42
5	28.41	29.67	12	18	24.38	26.10	29	19	25.56	27.84	41	37
6	23.21	22.90	4	20	18.59	19.83	22	15	19.30	21.59	26	35
7	24.45	25.07	7	20	20.42	21.20	14	10	21.76	23.78	21	30
8	24.21	23.23	7	16	20.48	20.49	21	13	21.41	22.00	28	29
9	25.60	27.45	7	19	18.65	19.53	22	13	20.33	24.23	29	32
10	28.84	32.26	11	18	23.64	20.14	18	13	25.61	27.18	29	31
11	37.02	38.26	17	22	35.85	38.59	36	15	36.22	38.40	53	37
12	40.86	43.13	22	19	34.04	39.26	36	10	36.63	41.80	58	29
13	40.99	46.75	16	21	36.29	38.11	31	14	37.89	43.29	47	35
14	54.55	57.00	19	17	47.72	53.81	45	20	49.75	55.28	64	37
15	53.48	61.48	17	11	49.34	54.73	31	11	50.81	58.11	48	22
16	48.93	52.99	17	20	45.53	50.23	34	12	46.67	51.96	51	32
17	49.21	57.47	20	16	47.65	56.91	39	15	48.18	57.20	59	31
18	51.65	57.73	16	15	49.46	55.19	31	13	50.21	56.55	47	28
19	50.35	55.13	23	19	46.27	48.66	29	10	48.08	52.90	52	29
20	47.53	59.64	17	13	48.84	53.61	28	9	48.35	57.17	45	22
21	51.13	57.73	21	24	44.79	51.55	33	16	47.26	55.26	54	40
22	44.06	57.27	22	27	48.46	53.84	36	18	46.79	55.90	58	45
23	52.20	56.76	15	17	46.24	51.70	33	13	48.11	54.57	48	30
24	45.24	48.45	17	8	37.92	41.24	17	2	41.58	47.01	34	10
25	48.77	47.30	14	16	42.54	46.95	35	13	44.32	47.14	49	29
26	46.09	48.18	17	19	41.07	50.44	39	13	42.60	49.10	56	32
27	50.77	59.48	22	26	51.39	56.15	36	13	51.16	58.37	58	39
28	47.87	55.34	19	20	45.22	53.20	27	10	46.31	54.63	46	30
29	50.47	56.76	18	17	46.09	51.70	36	13	47.55	54.57	54	30

Quantitatively Evaluate Work Zone Driver Behavior using 2D Imaging,  
3D LiDAR, & Artificial Intelligence in Support of Congestion Mitigation  
Model Calibration & Validation (Project G2)

30	64.60	61.56	6	14	53.34	55.31	23	17	55.67	58.13	29	31
<b>Total</b>	<b>45.02</b>	<b>43.76</b>	<b>413</b>	<b>546</b>	<b>39.17</b>	<b>40.03</b>	<b>854</b>	<b>397</b>	<b>41.07</b>	<b>41.62</b>	<b>1267</b>	<b>943</b>

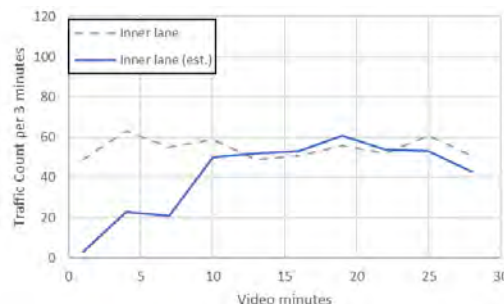
## 5.2 Error Analysis Findings, Interpretations, and Recommendations

This section presents the findings and analysis made by comparing the results obtained from the AI-system and the ground reference data. Although time headway is one of the pieces of information extracted by the AI-system, the accuracy of obtained headway information heavily depends on the traffic count accuracy. Therefore, the error analysis was performed with the main focuses on identifying factors that impact the accuracy in 1) vehicle count estimation and 2) vehicle speed estimation. Also, a pilot study is presented to 1) investigate the impact of different analysis periods/intervals, 2) experiment with different data cleaning methods, and 3) establish a framework to identify error cases and correct atypical cases (speeding or slow traffic). Finally, recommendations are made that could improve the accuracy of the extracted data.

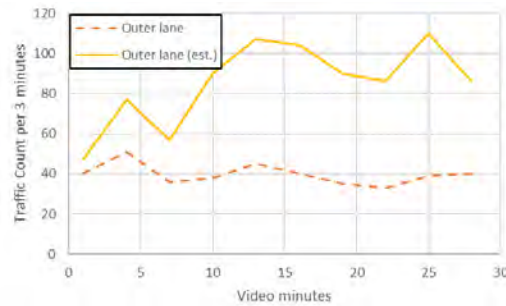
Table 5-1 shows the aggregated 1-minute traffic speed and count results from the manually obtained ground reference and the results estimated by the AI-system. The results show a 34.4% overestimation in total traffic count; the majority of overestimation cases occur in the outer lane, while the inner lane shows a closer traffic count to the ground reference. On the other hand, vehicle traffic speed results show very minimal error compared to the ground reference; the 30-minute average speed shows less than 2 MPH difference to the ground reference. Error analysis performed in the following sections show, in vehicle traffic count, the primary error causing factors are traffic and environment related. In low speed conditions, errors in count are caused by sensor-related factors, and in higher speed conditions, errors in count are caused by algorithm-related factors. The primary error-causing factor in traffic speed estimation is algorithm-related.

### 5.2.1 Vehicle count error analysis results

Figure 5-2 shows the lane-wise traffic count in each 3-minute interval of the video. We can see at the beginning of the video that the inner lane suffered significant undercounting before the 10-minute mark from Figure 5-2a. On the other hand, the outer lane shows overestimation of the traffic count, and this is most obvious after the 10-minute mark.



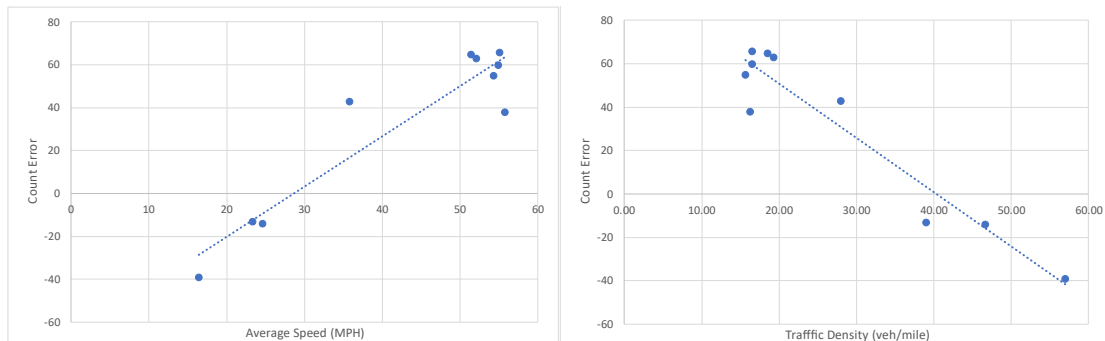
(a) manual traffic count and AI-system traffic count (est.) for the inner lane



(b) manual traffic count and AI-system traffic count (est.) for the outer lane

**FIGURE 5-2: TRAFFIC COUNT BY AI-SYSTEM AND MANUAL COUNT IN INNER AND OUTER LANES**

Since the traffic speed starts to increase at around the 9 to 10-minute mark, this observation suggests that the traffic speed could be an important factor impacting the performance of the vehicle traffic count. Upon further investigation, Figure 5-3 shows the relationship between traffic count error and traffic speed and traffic density; the positive count error indicates over-counting, and the negative count error indicates undercounting. The results show a positive relationship between count error and traffic speed and a negative relationship between count error and traffic density.



(a) count error at different traffic speed

(b) count error at different traffic density

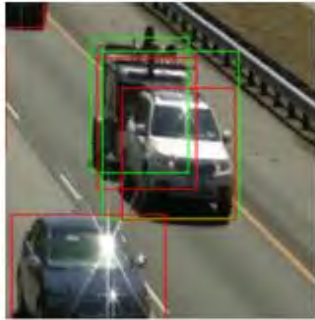
**FIGURE 5-3: TRAFFIC COUNT ERROR AT DIFFERENT TRAFFIC SPEED AND DENSITY**

Although the relationships between count errors, traffic speed, and traffic density are observed, the causes of these errors at different speeds and densities are different. At low traffic speed, typically caused by high traffic density, we observed undercounting is most obvious in the inner lane. Such errors are likely caused by the high traffic density in the outer lane blocking the view of the camera to the inner lane and leads to false-negative detection by Yolo3. This is a sensor-related error, as it is due to the height and angle of the camera.

On the other end of the spectrum, we observed a higher rate of overcounting at higher traffic speeds. As described in Chapter 3, vehicle counting relies on short-term vehicle tracking near the reference line; this tracking uses the intersection over union (IOU) area between bounding boxes in the consecutive frames. At high traffic speeds,

bounding boxes of the same vehicle may move significant distances in consecutive frames, which may cause short-term tracking to fail and recognize bounding boxes from the same vehicle in different frames as separate instances for counting, thus, leading to overcounting. This is an algorithm-related error, since it is caused by short-term tracking failure.

In addition to traffic speed, vehicle detection results from Yolo3 are another source of error. Figure 5-4 shows examples of false-positive and false-negative vehicle detections by Yolo3. As mentioned, high traffic density conditions are more likely to cause false-negative detections due to occlusion. False-positive detections were also observed for some vehicles, especially for vehicles with a trailer, causing Yolo3 to detect both the vehicle and the trailer as separate vehicles. Overall, since these types of vehicles do not make up a large portion of the traffic, the impact of this algorithm-related factor is not as obvious as the impact of traffic speed.



(a) false-positive detection



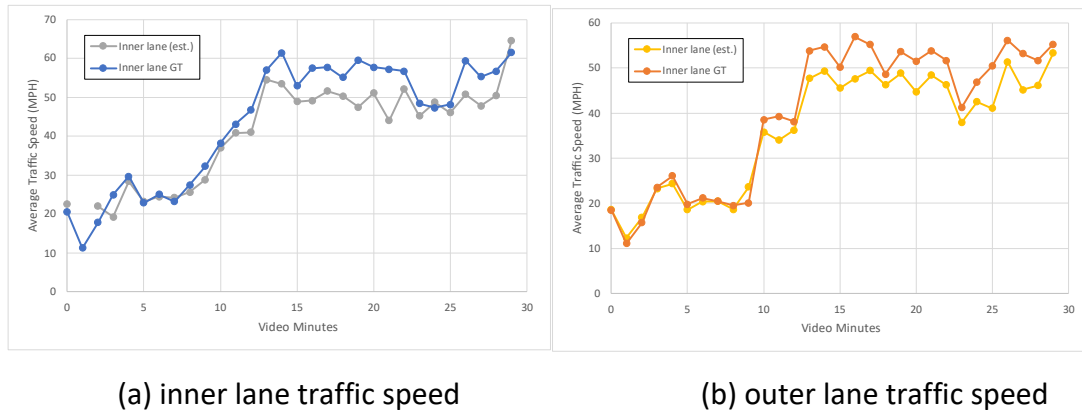
(b) false-negative detections

**FIGURE 5-4: EXAMPLE OF FALSE-POSITIVE DETECTIONS AND OCCLUSION CAUSED FALSE-NEGATIVES**

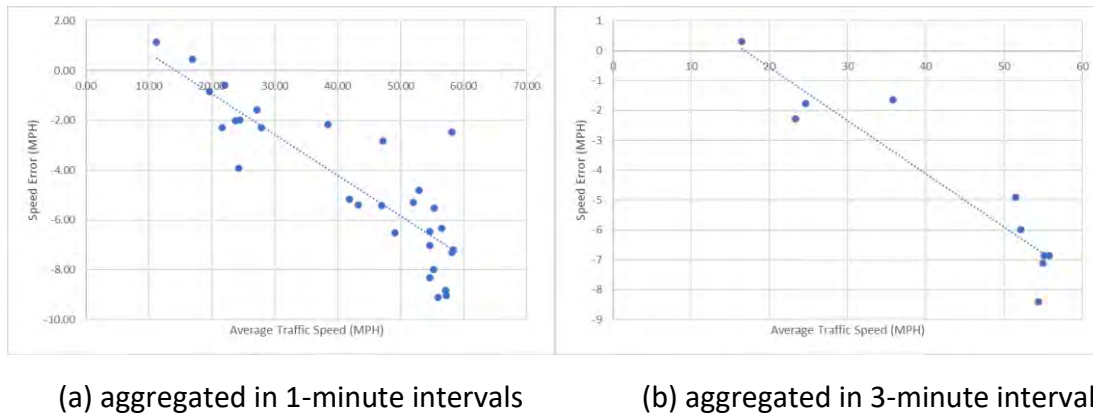
### 5.2.2 Vehicle speed error analysis results

Figure 5-5 shows the lane-wise traffic speed in each 1-minute interval of the video. From the figures, we can see in both traffic lanes that the AI-system captured traffic speed very accurately at the conditions in which traffic speed is below 40 MPH, while showing slight underestimation at a higher speed. The max error in average speed observed was around 10 MPH.





**FIGURE 5-5: TRAFFIC SPEED ESTIMATED (EST.) BY AI-SYSTEM AND MANUAL METHOD (GT) IN ONE MINUTE INTERVALS**



**FIGURE 5-6: TRAFFIC SPEED ESTIMATION ERRORS AT DIFFERENT GROUND REFERENCE TRAFFIC SPEED**

By plotting the traffic speed error against ground reference speed, as can be observed in Figure 5-6, the AI-system tends to underestimate speed in faster traffic than slower traffic. The error is likely caused by the fact that when the AI-system determines the time a vehicle exits the virtual speed loop, it only records the frame when the reference point of the vehicle has moved past the reference line. Since the frame rate of video used is at 10 fps, this means the AI-system is effectively rounding up the time a vehicle spends in the virtual loop to the nearest 0.1 seconds. This rounding error in travel time will cause a lower estimated speed, and, as the vehicle travels faster, the effect of rounding becomes more significant, thus causing a larger underestimation of speed at higher traffic speeds. This effect is illustrated in Figure 5-7. Since this error is introduced because of how speed is estimated, this is an algorithm-related error.

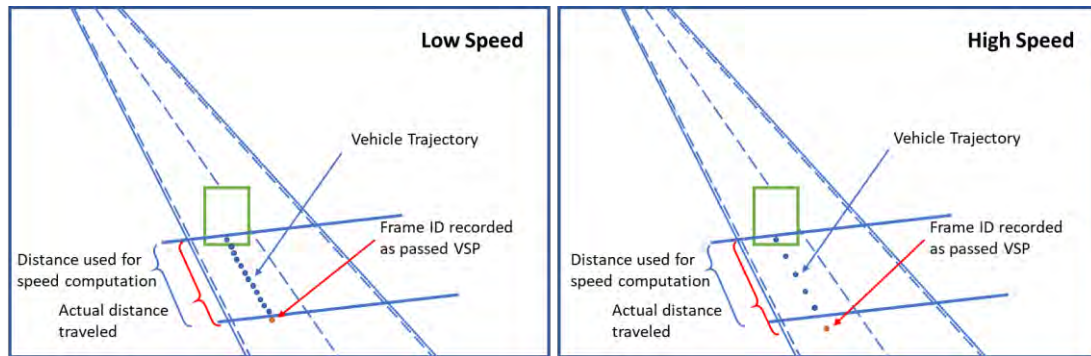


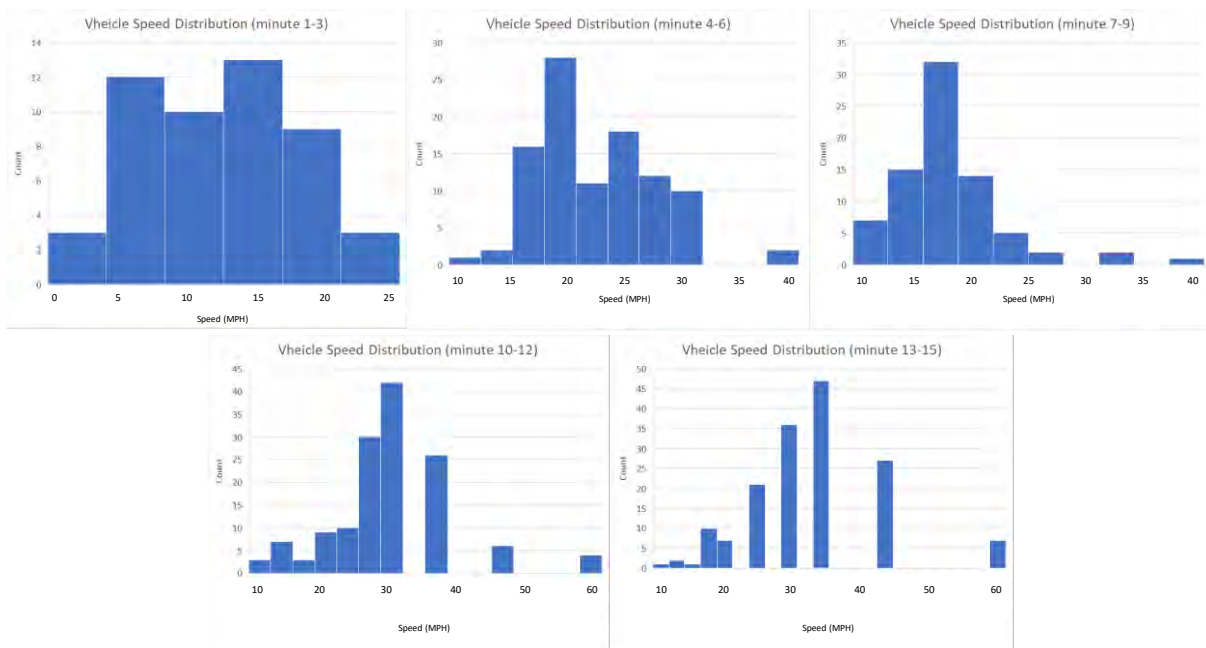
**FIGURE 5-7: TRAFFIC SPEED COMPUTATION ERRORS INTRODUCED BY HIGH VEHICLE SPEED**

### 5.2.3 Pilot study of data cleaning and error case identification using statistical analysis

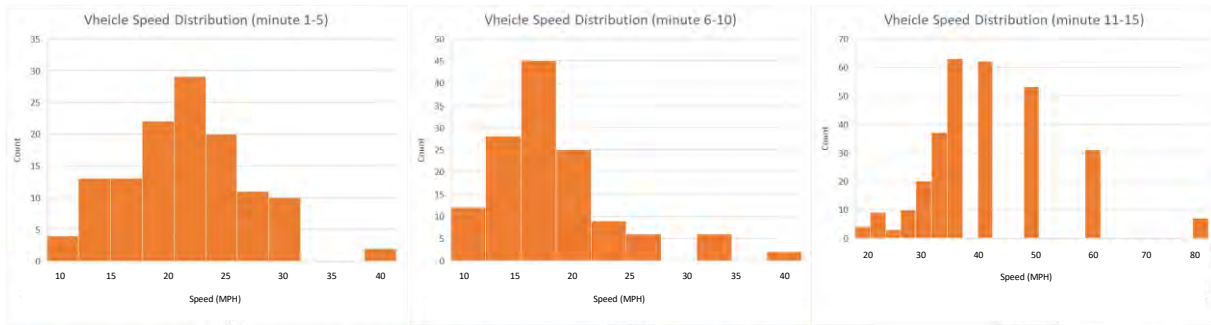
As part of error analysis in this section, a pilot study is presented 1) to explore the smallest temporal resolution required to identify atypical traffic and error cases produced by the AI-system, 2) to propose methods to identify atypical traffic and error cases, and 3) to propose methods to remove the bias in traffic speed computation.

Using the first 15 minutes of traffic video, Figure 5-8 represents the traffic speed distribution aggregated in 3-minute, 5-minute, and 15-minute intervals. From the distribution of traffic speeds, we can see the traffic distribution is a normal-distribution-like distribution. Thus, by assuming a normal distribution, we can identify outliers in the distribution and investigate further and verify if it is atypical traffic that is driving too fast or too slow or if it is an error case produced by the AI-system.

With the assumption that traffic speed distribution follows normal distribution, we can observe that when traffic is analyzed at 3-minute intervals, such distributions can be easily observed; at 5-minute intervals, the normal distribution shape is still very noticeable but may present skewness during the transition of traffic speed condition change. Figure 5-8 also shows that when traffic speed data is aggregated at 15-minute intervals, identifying outlier cases is difficult, as the traffic condition changes during the 15-minute period and makes it so that the distribution no longer follows normal distribution.



(a) traffic speed distribution results aggregated in 3-minute intervals



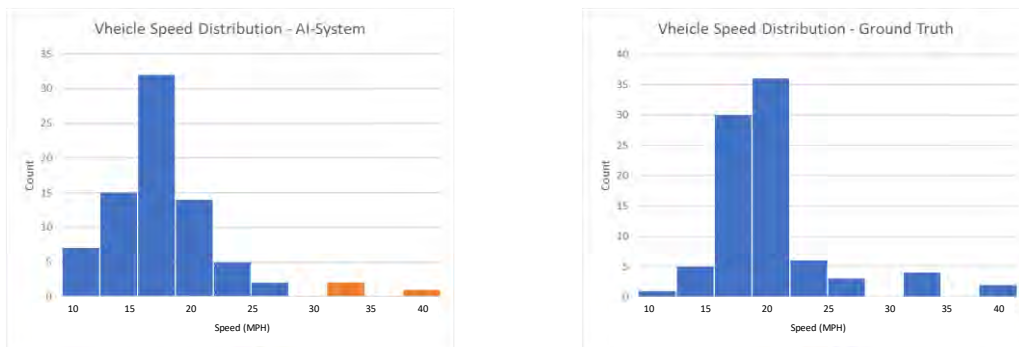
(b) traffic speed distribution results aggregated in 5-minute intervals



(c) traffic speed distribution results aggregated in 15-minute intervals

**FIGURE 5-8: TRAFFIC SPEED DISTRIBUTION RESULTS OF THE SAME 15-MINUTE PERIOD AGGREGATED IN DIFFERENT TIME INTERVALS.**

As a method to identify outliers in the distribution, we marked instances with more than two times the standard deviation from the mean as potential atypical traffic cases. However, these cases are not necessarily caused by errors in the AI-system. As shown in Figure 5-9, by comparing the distribution between AI-system results and ground truth, we can see cases marked as outliers by the standard deviation threshold method are not error results but some atypical vehicles traveling faster than other vehicles . Therefore, further investigation is needed for these cases before deciding which instances should be removed.



(a) estimated speed distribution

(b) ground truth distribution

**FIGURE 5-9: TRAFFIC SPEED DISTRIBUTION EXTRACTED USING AI-SYSTEM (A) COMPARED WITH GROUND TRUTH DISTRIBUTION (B)**

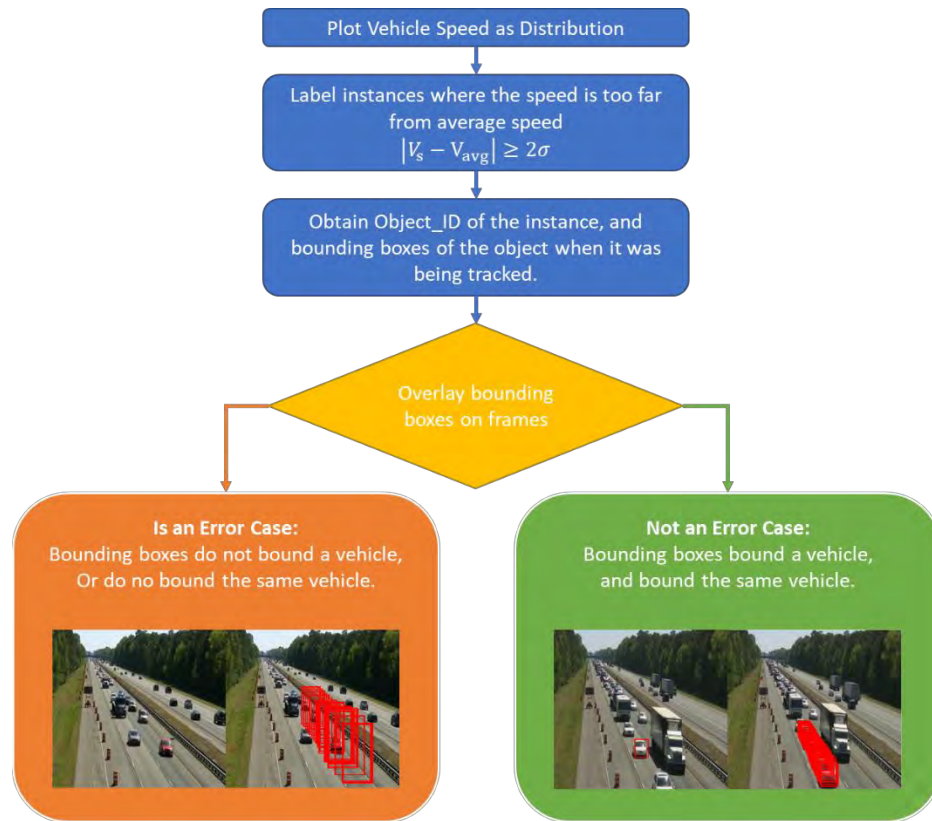


FIGURE 5-10: PROCEDURE FOR IDENTIFYING ERROR CASES

Although simply using the standard deviation method cannot guarantee identification of error-cases produced by the AI-system, this method does help identify potential error cases for further investigation. Using the “object\_id” recorded by the AI-system, the results can be traced back to the frames and bounding boxes used to compute the traffic speed. Figure 5-10 shows two cases where potential cases are traced back to the video frames in which Case (a) shows the trajectory of the bounding boxes and frames where the bounding boxes were obtained. We can see the bounding boxes belong to the same vehicle in all frames, indicating this instance is not an error case. In Case (b), the bounding box does not belong to any vehicle visible in the frame, indicating an error; the exact cause of this case has yet to be determined. It might be caused by incorrect vehicle detection or mismatching of vehicle detection and video frame.

The procedure presented in this section is mostly a manual analysis to demonstrate the process of identifying error cases; a more robust and automatic method should be explored for large-scale implementation.





(a) correct vehicle trajectory tracking case



(b) incorrect vehicle trajectory tracking case

FIGURE 5.10 CORRECT AND INCORRECT VEHICLE TRAJECTORY TRACKING CASES

#### 5.2.4 Interpretations and recommendations

The results presented in this chapter show that traffic speed and occlusion are the main impacting factors in vehicle traffic count errors. In this analysis, we found higher traffic speed generally leads to higher traffic over-counting due to short-term vehicle tracking failure (algorithm-related factor), and in congested conditions, occlusion, sensor-related factors also cause undercounting, especially for inner-lane traffic. This shows traffic conditions would impact the traffic count accuracy and algorithm and sensor-related factors also impact the accuracy in high and low traffic speed conditions, respectively. The AI-system generally produces accurate traffic speed results, but we observed a

larger amount of underestimation at higher traffic speeds than at lower traffic speeds. We found that traffic speed and video frame rate impact the accuracy in speed results, and the errors are caused by algorithm-related factors.

As a recommendation, we believe that increasing the frame rate of videos would help improve the performance of the AI-system. From the standpoint of vehicle counting, when using a higher frame rate, the AI-system would have more frames to track the vehicle; thus, we can expect an improvement in higher speed conditions. The increasing frame rate of the video would also help improve speed estimation, as illustrated in Figure 5-7. The reason for speed error at high speeds is caused by trajectory data points being too far apart from frame to frame, and the time spent in the virtual speed loop is always rounded up to the nearest 0.1 seconds. Table 5-2 shows the error when one more frame was counted as the vehicle spent in the virtual speed loop due to rounding; the error is computed by adding the frame time of one frame to the time spent in the speed loop and compared to the re-estimated speed to the actual speed. Since the error in the time spent in the speed loop equals one frame time, the speed error represents the maximum speed error that can be introduced by the frame rate; we can see the error is reduced significantly when increasing the frame rate from 10 fps to 30 fps.

**TABLE 5-2: IMPACT OF MISCOUNTING ONE FRAME TO SPEED ESTIMATION**

Actual Speed (MPH)	Time Spent in Speed Loop (40-ft)	Speed Error when over-count one frame (@ 10fps)	Speed Error when over-count one frame (@ 30fps)
10	2.73 sec	-0.2 MPH	-0.1 MPH
20	1.36 sec	-0.8 MPH	-0.4 MPH
30	0.91 sec	-1.6 MPH	-0.9 MPH
40	0.68 sec	-2.8 MPH	-1.5 MPH
50	0.55 sec	-4.3 MPH	-2.3 MPH
60	0.45 sec	-5.9 MPH	-3.3 MPH
70	0.39 sec	-7.9 MPH	-4.4 MPH
80	0.34 sec	-10.0 MPH	-5.6 MPH

## Chapter 6: SENSITIVITY STUDY AND APPLICATIONS OF WORKZONE TRAFFIC SIMULATION USING EXTRACTED REAL- WORLD DRIVING BEHAVIOR AND TRAFFIC INFORMATION

### 6.1 Chapter Organization and Research Objectives

This chapter presents a methodology for developing freeway work zone simulation models in PTV Vissim using data from the AI-based traffic and driving behavior extraction system (herein referred to as the “AI-based extraction system”) summarized in Chapters 3-5 of this report. The Vissim model development effort and analysis framework are detailed in **Section 6.2**. The outcomes of two subtasks are then presented in the sections that follow:

- **Task 1 – Sensitivity Analysis (Section 6.3).** The purpose of this initial task is to determine the sensitivity of model outputs to changes in key input parameters. The outcomes of this task answer two critical questions. First, how can one translate data from the AI-based extraction system to Vissim model inputs? The lane-changing observations collected as part of the case study in Chapter 4 and additional scenarios may be used to *inform* Vissim model inputs and *validate* model outputs but cannot be replicated without adjusting multiple parameters in the software. A full factorial experiment is conducted to identify an optimum parameter set for use in Task 2.

Second, how do model outputs generated under typical default parameter values differ from those under the optimum parameter set selected previously? The results of this sensitivity analysis are used to evaluate the reliability and utility of the semi-automatically extracted traffic data and provide recommendations for modelers.

- **Task 2 – Modeling Freeway Work Zone Traffic Operations at Sites With Varying Characteristics (Section 6.4).** The purpose of this task is to determine how traffic measures of effectiveness (MOEs) of interest to agencies and practitioners (e.g., throughput, speed, travel time, and queue length) vary at three-to-two freeway lane closures with different prevailing characteristics. The outcomes of this task are used to provide recommendations supporting agency work zone scheduling and traffic control decisions and allude to opportunities for future research.

Key findings are summarized in **Section 6.5** at the conclusion of this chapter. Recommendations for further extending the simulation study and recommendations for the practitioners are presented in **Chapter 7**.



## 6.2 Vissim Model Development and Analysis Framework

### 6.2.1 Background

An abundance of microsimulation software packages are currently available to researchers and practitioners, each with strengths and weaknesses dependent on the purpose of a given analysis. In response to the increased use of microsimulation as an analysis tool for transportation projects, many state departments of transportation (DOTs) have published guidelines in recent years. Though some DOTs maintain a broader set of traffic analysis and microsimulation guidelines—such as those published by the Florida (FDOT, 2014), Colorado (CDOT, 2018), Virginia (VDOT, 2020), and Wisconsin (WISDOT, 2019) DOTs—others provide guidance specific to PTV Vissim (Iowa DOT, 2017; MDOT, 2016; WSDOT, 2016). Based on a review of agency guidelines, familiarity with pertinent literature, and experience among project team members, PTV Vissim was selected as the preferred analysis tool for use in this research. Given its widespread use in practice, the Vissim-specific freeway work zone simulation guidance produced as part of this research is expected to serve the largest audience of modelers.

PTV Vissim is a stochastic, behavior-based microsimulation software package with wide-ranging applications. Given its ability to model the acceleration, deceleration, car-following, and lane-changing behavior of individual vehicles under nearly unlimited combinations of input parameters, Vissim is well-suited for use in analyzing the complexity traffic flow at freeway work zones. However, developing and calibrating a model capable of producing robust outputs is often an arduous task. Previous sensitivity analyses in the literature have attempted to simplify this process and found the Vissim input parameters summarized in **Table 6-1** to be most critical to modeling traffic conditions at freeway work zones (Jehn and Turochy, 2019).

**Table 6-1: Key Vissim Calibration Parameters for Modeling Freeway Work Zones**

Category	Parameter	Description	Default Value	Literature-Recommended Range <sup>1</sup>
Car-Following	CC0	Standstill distance (ft)	4.92 ft	4.92 – 20 ft
	CC1	Desired following headway (s)	0.9 s	0.9 – 2.7 s
	CC2	Following Distance Oscillation (ft)	13.12 ft	13.12 – 55 ft
Lane-Changing	SDRF	Safety Distance Reduction Factor	0.6	0.1 – 0.6
	Lane Change Distance	Lane Change Distance (ft)	656.2 ft	≥ 2500 ft

<sup>1</sup>Ranges represent the minimum and maximum values explored in freeway work zone-specific literature

The importance of other input parameters to modeling freeway work zones—such as the maximum deceleration for cooperative braking ( $\text{ft/s}^2$ ), desired acceleration for heavy trucks ( $\text{ft/s}^2$ ), and deceleration per distance for necessary lane changes ( $-1 \text{ ft/s}^2$ )—have also been explored in the literature and will be discussed further in subsequent sections of this chapter. The reader may refer to the PTV Vissim User Manual for

additional detail regarding the full set of car-following and lane-changing parameters included in the software (PTV Group, 2020). However, the following brief descriptions are offered here:

#### Car-Following Parameters

**CC0 (Standstill Distance, ft)** – The CC0 parameter is the first of 10 parameters that comprise the Wiedemann 99 car-following model used in Vissim. This parameter has no variation and defines the desired distance between a trailing and lead vehicle when both are stopped.

**CC1 (Gap Time Distribution, s)** – The multiplicative component of the desired safety distance between a trailing and lead vehicle is defined by the CC1 parameter. This desired safety distance is calculated at each simulation time step as:

$$\text{Desired Safety Distance} = CC1 * \text{speed} + CC0 \quad (6-1)$$

The desired safety distance directly influences the time gap (i.e., front bumper to rear bumper) between vehicles in a following pair. As a result, the CC1 parameter has been found to have the greatest influence on simulated capacity (Lownes and Machemehl, 2006). As of the release of PTV Vissim 9 in 2016, CC1 may be coded as a static value or as a vehicle class-specific distribution.

**CC2 (Following Distance Oscillation)** – The CC2 parameter defines the maximum additional distance beyond the desired safety distance that a trailing vehicle will allow before intentionally moving closer to the lead vehicle.

#### Lane-Changing Parameters

**SDRF (Safety Distance Reduction Factor)** – This unitless parameter is used to calculate the maximum reduction in the desired safety distance allowed by a vehicle when selecting an acceptable gap for changing lanes. At the default value of 0.6, a vehicle will accept a gap in the adjacent lane equivalent to 60% of its desired safety distance.

**LCD (Lane Change Distance, ft)** – For each connector in a Vissim network, the lane change distance defines the distance upstream of a necessary lane change (e.g., turn bay, off-ramp, or lane closure) at which a vehicle will begin to look for opportunities to merge. As of PTV Vissim 2020, this parameter can be coded as a static value or as a vehicle class-specific distribution.

The purpose of calibration is to establish confidence in a model's ability to replicate a known base condition, thereby maximizing the validity of model outputs under a theoretical condition (e.g., existing versus future conditions on a given roadway segment of interest). Recent study of typical practice highlights the need to limit ambiguity in the model calibration process to improve model robustness and transferability (VDOT, 2020). If a modeler were to test just three levels of each of the five parameters listed in **Table 6-1** as part of the calibration process, the result would be a total of 243 unique simulation runs. When additional parameters are considered, the



size of a given calibration experiment quickly balloons, and any number of parameter sets may produce a reasonable match to the base condition. Consequently, there is still an evident need to limit the number of “unknowns” in calibrating freeway work zone simulation models to increase consistency in methods and resultant outputs.

Past research has aimed to address this need by providing recommended default values or regression equations for estimating specific parameter values based on expected lane utilization, capacity, and queue length at a given freeway lane closure (Chatterjee et al., 2009; Edara and Chatterjee, 2010; Yeom et al., 2016). However, none of these studies considered differences in driving behavior by vehicle class, and each were conducted in legacy versions of Vissim not equipped with features included in more recent releases of the software. Specifically, past literature has demonstrated the value of modeling the CC1 parameter as a distribution (Jehn and Turochy, 2020) in producing robust outputs when modeling freeway lane closures. Similarly, the use of vehicle class-specific lane change distance distributions—defined by the data summarized in Chapters 3-5 of this report—is expected to have a noteworthy influence on the capability of freeway work zone simulation models to capture differences in traffic operations at sites with varying geometric and traffic stream characteristics.

The remainder of this section is organized as follows. First, the critical components of base Vissim model development are described in detail. Next, a methodology is offered for translating data collected from the AI-based extraction system to Vissim model inputs. Where applicable, publicly available traffic data and pertinent literature are referenced as supplemental data sources used in model development. Finally, a framework for the sensitivity analysis and factorial experiment conducted as part of Task 1 and Task 2 is presented.

## 6.2.2 Base Model Development and Data Collection

### 6.2.2.1 Base Vissim Model Geometry and Network Objects

Vissim 2021 (Build 2021.00-03) was selected for use in this study, as this version of the software was the latest released by PTV at the time of this writing and includes each of the advantageous features highlighted in Section 6.2.1. A core purpose of this research is to develop generalized recommendations for modelers and agencies. Accordingly, key model inputs were carefully selected to be representative of typical rural and urban six-lane freeways across the southeastern United States. While a baseline model was developed and outputs were validated against the field data from the AI-based extraction system described earlier in this report, model development and calibration were primarily informed by other data sources. These sources included recommendations from the literature, data from previous work by the research team, and publicly available traffic data from continuous count stations (CCSs) maintained by the Georgia Department of Transportation (GDOT). This broad-based modeling approach was intended to minimize the risk of “over-calibrating” to site-specific data while allowing for a wide range of traffic conditions to be captured.

Two freeway work zones on I-95 near Savannah, GA, were used for calibrating the Vissim model. Characteristics of each site are summarized below:

- Northbound I-95 milepost 86 in Richmond Hill, GA (herein referred to as “Site A”)
  - 2019 Annual Average Daily Traffic (AADT) = 57,900 vehicles per day (GDOT Count Station 029-0194)
  - 2019 Daily Truck Percentage = 23% (GDOT Count Station 191-0187)
  - Six-lane Cross Section
  - Curved roadway geometry upstream of the lane closure taper
- Northbound I-95 milepost 97 in Pooler, GA (herein referred to as “Site B”)
  - 2019 AADT = 85,300 vehicles per day (GDOT Count Station 051-0381)
  - 2019 Daily Truck Percentage = 14% (GDOT Count Station 051-0383)
  - Six-lane Cross Section
  - Straight roadway geometry upstream of the lane closure taper

In each case above, three northbound through lanes were reduced to two open lanes through the work zone (herein referred to as a “3-2 lane closure”). The base Vissim model included the following elements, as depicted in **Figure 6-1**.

#### Network Geometry

A total of five three-lane links and one two-lane link were coded upstream and downstream of the modeled lane closures, respectively. The portion of the network upstream of the modeled lane closure was extended to six miles to allow adequate distance for queues to propagate and dissipate during the simulation period and for discretionary lane changes to occur prior to the advance warning area. This six-mile segment was subdivided to represent each of five zones:

- Zone 1: Transition Area
- Zone 2: 0-500 feet upstream of the Transition Area
- Zone 3: 500-1000 feet upstream of the Transition Area
- Zone 4: 1000-5280 feet upstream of the Transition Area
- Zone 5: 0-5 miles upstream of the Advance Warning Area

Zones 1-4 were coded based on the field data collection effort detailed in Chapter 4 of this report and informed by the work zone traffic control guidance prescribed in Part 6 of the *Manual on Uniform Traffic Control Devices* (MUTCD; FHWA, 2012). At a posted speed limit of 70 miles per hour (mph) and lane width of 12 feet, the MUTCD recommends a minimum merging taper length of 840 feet. As such, Zone 1 was coded to extend 840 feet, with approximately one-half of this distance assumed wide enough to accommodate a typical passenger vehicle. To capture partial use of the merging taper

as a travel lane in Vissim, the emergency stop distance associated with the two-lane connector joining the three- and two-lane links was set to 420 feet. The emergency stop distance parameter defines the distance upstream of a necessary lane change that a simulated vehicle will come to a complete stop and wait for an acceptable gap to merge. Visual observations of the simulation confirmed that this setting functioned as intended.

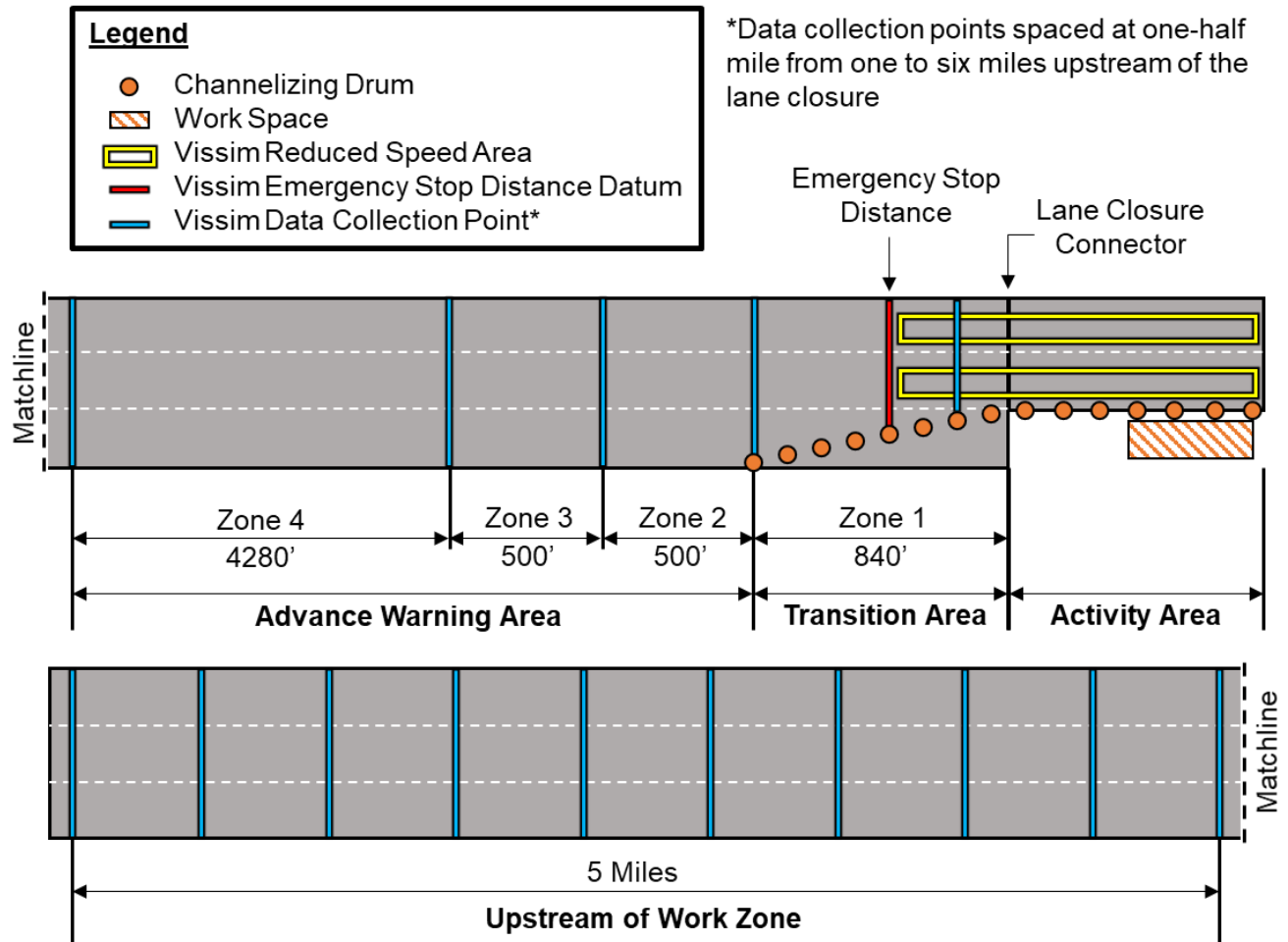


**FIGURE 6-1: DIAGRAM OF BASE VISSIM MODEL (NOT TO SCALE)**

### Network Objects

Network objects in Vissim are comprised of lines and polygons coded to control vehicle behavior and collect data during the simulation. Given the simplicity of the modeled network, only desired speed decisions, reduced speed areas, data collection points, and travel time measurements were necessary in this case. For further background regarding the mechanics of each of these network objects, the reader is referred to the PTV Vissim User Manual (PTV Group, 2020).

### *Desired Speed Decisions and Reduced Speed Areas*

Desired free flow speed within Zones 2-4 and upstream of the advance warning area was governed by a set of lane-wise desired speed decisions placed at the entry point to the Vissim network. Typical mean free flow speed by lane and vehicle class was extracted from GDOT CCS data at Site A and Site B from September 2019. However, speed data was only available as an average for a given lane and vehicle class aggregated in one-hour intervals. Consequently, prior study of freeway work zones by Jehn and Turochy (2019) was referenced to develop full desired speed distributions for use as inputs in Vissim. Free flow speed data from this study exhibited a standard deviation of 9 mph (passenger cars) and 7 mph (heavy trucks) upstream of the advance warning area. These values were combined with known mean free flow speeds from GDOT CCS data to form the desired speed distributions summarized in **Table 6-2**.

**Table 6-2: Vissim Desired Speed Distributions (Upstream of Work Zone)**

Lane	Observed Average Speed <sup>1</sup>	Desired Speed Distribution (Percentile) <sup>2</sup>				
		10th	25th	50th	75th	90th
All Vehicles						
Right	69	57	63	69	75	81
Center	77	65	71	77	83	88
Left	79	67	73	79	85	91
Passenger Cars						
Right	70	58	64	70	76	81
Center	78	66	72	78	84	89
Left	80	68	74	80	86	92
Heavy Trucks						
Right	65	53	58	65	71	76
Center	72	60	66	72	78	83
Left	74	62	68	74	80	85

<sup>1</sup>Observed average speed from GDOT CCS 191-0187 in September 2019

<sup>2</sup>Estimated desired speed distributions used as Vissim inputs

Similarly, free flow speeds within and downstream of the transition area were defined based on a combination of guidance from HCM6 and the literature (TRB, 2016; Jehn and Turochy, 2019). Speed data within the transition area at Site B was available from trajectory data collected through the AI-based extraction system during the one-hour period from 2:30PM – 3:30PM on April 6, 2011. However, since free flow conditions were not observed during these periods, this data could not be utilized to develop Vissim desired speed distributions. Furthermore, additional components of the work zones studied as part of this research were unknown, including the posted speed limit during construction. Part 6 of the MUTCD states that the posted speed limit within a freeway work zone should represent a reduction of no more than 10 mph from the

typical posted speed limit. Therefore, since the studied segments of I-95 have a normal posted speed limit of 70 mph, it was assumed that the speed limit was posted at 60 mph during construction.

Mean free flow speed through the work zone was then estimated based on Equation 10-10 in HCM6 Volume 2:

$$FFS_{WZ} = 9.95 + 33.49 \times f_{Sr} + 0.53 \times SL_{WZ} - 5.60 \times LCSI - 3.84 \times f_{Br} - 1.71 \times f_{DN} - 8.7 \times TRD \quad (6-2)$$

Where:

$FFS_{WZ}$  = work zone free flow speed (mph)

$f_{Sr}$  = ratio of non-work zone speed limit (mph) to work zone speed limit (mph)

$SL_{WZ}$  = work zone speed limit (mph)

$LCSI$  = lane closure severity index

$f_{Br}$  = indicator variable for barrier type (0 for rigid barrier, 1 for soft barrier)

$f_{DN}$  = indicator variable for daylight or night (0 for daylight, 1 for night)

$TRD$  = total ramp density along the facility (ramps/mile)

The reader is referred to Chapter 10 in HCM6 for the full definition of each of the variables listed in the equation above. When each variable is defined based on the characteristics of the studied 3-2 lane closures, a work zone free flow speed of 61 mph is calculated. Since this free flow speed only represents a mean for all lanes and vehicle classes, full desired speed distributions were constructed based on data from prior work by Jehn and Turochy (2019). Free flow speed data from this study exhibited a standard deviation of 7 mph (passenger cars) and 5 mph (heavy trucks) within and downstream of the transition area. These values were combined with the mean free flow speed estimated from HCM6 methodology to form the desired speed distributions summarized in **Table 6-3** for a right-side lane closure. For the left-side lane closure to be studied as part of Task 2, data for the “Center” and “Left” lane below was used to define free flow speeds for the “Right” and “Center” lane, respectively. Desired speed distributions were coded by vehicle class and lane by way of reduced speed areas, as shown in **Figure 6-1**. Reduced speed areas were used in lieu of desired speed decisions so that simulated vehicles would begin to decelerate upstream of the transition area.



**Table 6-3: Vissim Desired Speed Distributions (Work Zone)**

Lane	Calculated Average Speed <sup>1</sup>	Desired Speed Distribution (Percentile) <sup>2</sup>				
		10th	25th	50th	75th	90th
All Vehicles						
Center	56	47	51	56	61	65
Left	65	56	60	65	70	74
Passenger Cars						
Center	58	49	54	58	63	67
Left	68	59	63	68	72	77
Heavy Trucks						
Center	54	47	50	54	57	60
Left	62	56	59	62	66	69

<sup>1</sup>Estimated average speed from HCM6 Equation 10-10

<sup>2</sup>Estimated desired speed distributions used as Vissim inputs

#### *Data Collection Points and Travel Time Measurements*

A total of 44 data collection points were coded in the base Vissim model to measure lane utilization, volume, speed, and queue propagation at each of the locations noted in **Figure 6-1** and **Table 6-4**. The purpose of each of these data collection points falls into one of three categories. First, two data collection points were placed 200 feet downstream of the emergency stop distance location in Vissim to extract measures of capacity (i.e., speed and flow rate versus time in each lane). Next, four sets of data collection points were placed in each lane at the beginning of Zones 1-4 to measure speed, flow, and lane utilization for the purposes of model validation against lane change observations from the AI-based extraction system. Finally, data collection points were spaced at one-half mile upstream of the advance warning area to monitor average speed throughout the simulated period as a means for estimating queue length.

**Table 6-4: Data Collection Point Summary**

Data Collection Point IDs	Location	Purpose
1-2	200 feet downstream of full lane closure	Capacity Measurement
3-5	Beginning of Zone 1 (Transition Area)	
6-8	Beginning of Zone 2 (500 feet upstream of Transition Area)	Speed, Flow, and Lane Utilization Measurement
9-11	Beginning of Zone 3 (1000 feet upstream of Transition Area)	
12-14	Beginning of Zone 4 (1 mile upstream of Transition Area)	Queue Length Estimation
15-44	1/2 mile intervals upstream of Advance Warning Area	

While understanding capacity and mitigating queue length at freeway work zones may be of particular interest to agencies and practitioners, driver frustration and road user costs are primarily driven by travel delay. Therefore, travel time measurements were

coded at the entry point to the Vissim network and at the end of the transition area to estimate average travel time through the simulated six-mile work zone corridor.

#### 6.2.2.2 Vissim Input Volume Distributions

As emphasized previously, a critical objective of Task 1 is the development of generalized recommendations for modeling freeway lane closures across the southeastern United States. These recommendations are applied in Task 2 to draw conclusions on the impact of various geometric, traffic stream, environmental, and work zone-specific characteristics on MOEs of interest to agencies and practitioners. To maximize the transferability and validity of the findings associated with each task, volume inputs were coded based on a thorough data collection effort conducted via three primary sources: (1) publicly available traffic data from GDOT CCSs; (2) semi-automatically extracted traffic data from the AI-based system featured in Chapters 3-5 of this report; and (3) literature review. Given the broad purposes of Task 1 and Task 2, a range of model inputs were selected that capture the specific conditions observed at the study sites while producing sufficient variability in model outputs for drawing wide-ranging conclusions.

For the purposes of this research, Site A (summarized in Section 6.2.2) was assumed to be representative of rural, six-lane freeway facilities, which are likely to exhibit lower overall traffic volumes than their urban counterparts but a substantially higher proportion of heavy trucks. On the contrary, Site B (summarized in Section 6.2.2) was assumed to be representative of a typical urban, six-lane freeway in southeastern United States. As mentioned previously, trajectory data collected as part of this case study was limited to 12 five-minute intervals that comprise a single one-hour period at Site B on Wednesday, April 6, 2011. Since traffic flow is congested for all but three of the five-minute intervals that comprise the one-hour period, measured traffic volumes are not indicative of true demand.

The Traffic Analysis and Data Application maintained by GDOT (GDOT, 2021) includes data collected from thousands of short-term, weigh-in-motion, and CCSs throughout the state of Georgia and is publicly available through a dynamic web mapping interface. Given the limitations of the field data noted previously, two CCSs located near the study work zones were leveraged to develop Vissim model inputs, as each station provides vehicle count and classification by lane in one-hour intervals. Data from these two CCSs was assumed to be generally representative of Site A and Site B for the purposes of this research. Summary statistics from each location are provided below:

- Site A (GDOT CCS 191-0187, September 2019) – I-95 approximately 3.5 miles north of SR-57 in Townsend, GA
  - Average Northbound Peak Hour Volume (Weekday) = 1,480 vehicles/hour
  - Average Truck % (Weekday, 9AM – 9PM) = 30%
  - Average Northbound Peak Hour Volume (Weekend) = 1,739 vehicles/hour

- Average Truck % (Weekend, 9AM – 9PM) = 14%
- Site B (GDOT CCS 051-0383, September 2016) – I-95 approximately 1.5 miles north of I-16 in Pooler, GA
  - Average Northbound Peak Hour Volume (Weekday) = 2,706 vehicles/hour
  - Average Truck % (Weekday, 9AM – 9PM) = 16%
  - Average Northbound Peak Hour Volume (Weekend) = 2,842 vehicles/hour
  - Average Truck % (Weekend, 9AM – 9PM) = 8%

**Figure 6-2** shows the distribution of traffic volumes at each CCS by time of day and day of week.

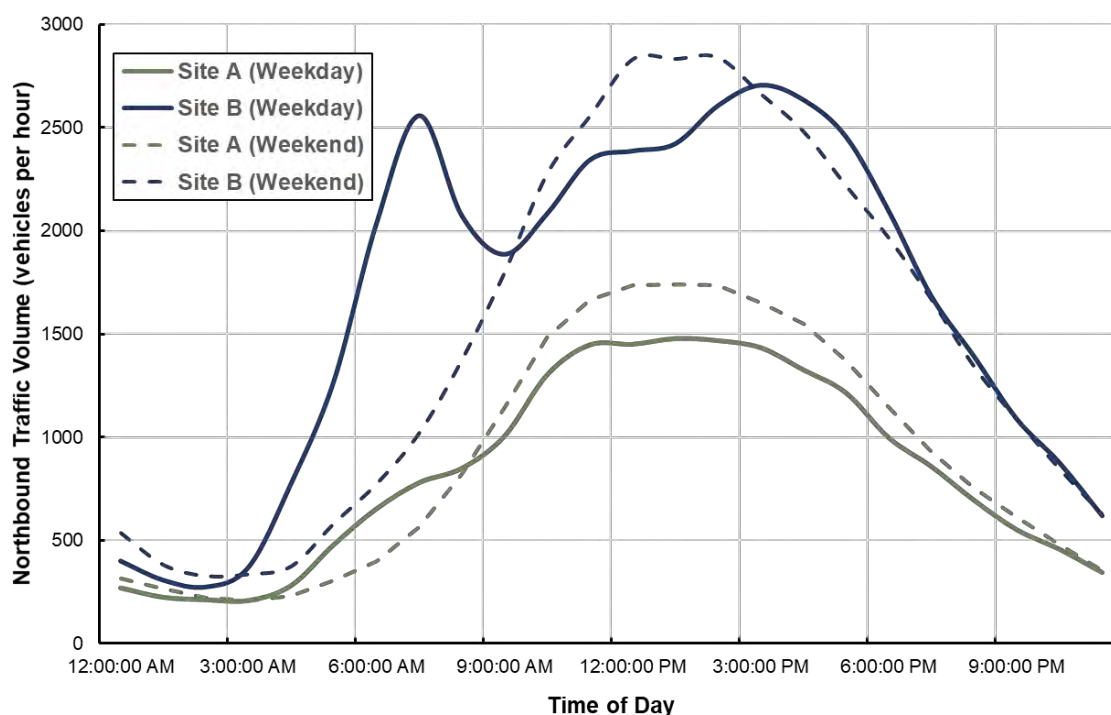


**FIGURE 6-2: NORTHBOUND I-95 GDOT CCS TRAFFIC VOLUME SUMMARY**

Based on the bulleted summary above and the traffic volume distributions illustrated in **Figure 6-2**, it was concluded that (1) the weekday data at Site B is suitable for use in developing Vissim model inputs for the sensitivity analysis conducted in Task 1, and (2) both weekday and weekend conditions should be analyzed as part of Task 2 to capture the full range of traffic characteristics that might be observed at rural and urban six-lane freeways across the southeastern United States.

#### Task 1 – Sensitivity Analysis Volume Inputs

Lane-based vehicle count and classification data from Site B collected during each weekday (excluding Labor Day) in September 2016 was used to develop the volume

inputs and vehicle compositions coded in Vissim for Task 1, as summarized in **Table 6-5**. To aid in the interpretation of **Table 6-5**, the following should be noted:

- Each Vissim model was coded to run for 43,200 simulation seconds (12 hours) to replicate the full rise and fall of traffic volumes from 9AM to 9PM, thereby allowing the opportunity for queues to form and dissipate upstream of the lane closure.
- A one hour seeding period (i.e., “warm-up” time, during which no outputs are collected from the model) was included in each model run.
- Three vehicle classes were modeled and deemed sufficient for capturing the range of vehicles included in the real-world traffic stream: passenger cars (average length = 18.5 feet), single-unit trucks (average length = 32.5 feet), and heavy trucks (average length = 73.5 feet).
- A single vehicle composition was coded for the entire simulation period, as the percentage of each vehicle class in the traffic stream did not vary substantially between 9AM and 9PM in the GDOT CCS data.

**TABLE 6-5: TASK 1 VISSIM VOLUME INPUTS AND VEHICLE COMPOSITIONS BY TIME PERIOD<sup>1,2</sup>**

Time of Day	Vissim Time Interval (s)	Volume (vph)			% Single Unit Trucks			% Heavy Trucks		
		Lane 1	Lane 2	Lane 3	Lane 1	Lane 2	Lane 3	Lane 1	Lane 2	Lane 3
9:00AM	0-3600	660	760	470						
10:00AM	3600-7200	760	860	540						
11:00AM	7200-10800	850	970	610						
12:00PM	10800-14400	850	970	610						
1:00PM	14400-18000	850	970	610						
2:00PM	18000-21600	900	1030	640	4%	3%	2%	24%	18%	0%
3:00PM	21600-25200	950	1080	670						
4:00PM	25200-28800	900	1030	640						
5:00PM	28800-32400	850	970	610						
6:00PM	32400-36000	760	860	540						
7:00PM	36000-39600	570	650	400						
8:00PM	39600-43200	470	540	340						

<sup>1</sup>Traffic volume and vehicle class percentages drawn directly from GDOT CCS data

<sup>2</sup>Lanes are numbered from right to left (i.e., “Lane 1” = right lane)

The input volume distribution summarized in **Table 6-5** was assumed representative of the overall rise and fall of traffic volumes that may have been observed at the study site the day the video data was collected. This relationship with the field data collected from the AI-based extraction system was critical to forming a basis for the model calibration

and validation effort described in Section 6.3. The use of CCS data from April 6, 2011 was explored, but only partial data was available in the GDOT TADA system for this date.

#### Task 2 – Factorial Experiment Volume Inputs

The traffic volumes used in support of Task 1 were meant to provide a reasonable match to those that may have been observed on the day field data was collected at Site B. On the contrary, those developed as part of Task 2 were intended to be coarser in nature, thereby capturing the full range of conditions that might be observed at typical rural and urban six-lane freeways in the southeastern United States. The range of typical conditions at Site A and Site B summarized in Section 6.2.2.2 were adapted to form the following three general scenarios:

- Scenario 1—Site A (Rural), Typical Weekday, 30% Trucks
- Scenario 2—Site B (Urban), Typical Weekday, 15% Trucks
- Scenario 3—Site B (Urban), Typical Weekend, 5% Trucks

Though initially considered as a fourth scenario, it was determined that typical weekend traffic volumes at Site A (Rural) were unlikely to produce congestion in Vissim or in the field. Furthermore, a similar proportion of heavy trucks was observed in the traffic stream under this scenario as that on a typical weekday at Site B (Urban). Therefore, the traffic volumes and truck percentages represented by the three scenarios listed above were considered sufficient for capturing the range of likely conditions observed on freeway facilities at a regional scale.

The full set of input volume distributions used as part of Task 2 were developed from raw field data through the following multi-step process:

1. The distribution of traffic volumes by hour of the day was tabulated as a percentage of the maximum observed hourly volume for Scenario 1, Scenario 2, and Scenario 3.
2. The pre-breakdown capacity (vehicles per hour) of Site B under Scenario 2 was determined during Task 1 (see Section 6.3).
3. Three input volume distributions were developed for Scenario 2
  - a. Low (Maximum Hourly Volume = Theoretical Capacity - 200 vehicles / hour)
  - b. Medium (Maximum Hourly Volume = Theoretical Capacity)
  - c. High (Maximum Hourly Volume = Theoretical Capacity + 200 vehicles / hour)
4. A passenger car equivalent (PCE) of 2.5 was assumed for heavy trucks based on past research (Sarasua et al., 2006) and used to convert each of these three maximum hourly volumes to units of passenger cars per hour.
5. The maximum hourly volumes applicable to the “Low”, “Medium”, and “High” cases for Scenario 1 and Scenario 3 (in vehicles per hour) were calculated from the passenger car equivalent flow rates calculated in Step 4.



The full input volume distributions coded for each of the 12 cases referenced above are omitted here for brevity. Maximum hourly volumes modeled as part of Task 2 are summarized in Table 6-6.

**TABLE 6-6: TASK 2 MAXIMUM HOURLY VISSIM INPUT VOLUME BY SCENARIO**

Scenario ID	% Trucks	Max Volume (vph)	Max Volume (pcph)
1 (Low)	30%	2,028	2,940
1 (Med)	30%	2,197	3,185
1 (High)	30%	2,366	3,430
2 (Low)	15%	2,400	2,940
2 (Med)	15%	2,600	3,185
2 (High)	15%	2,800	3,430
3 (Low)	5%	2,735	2,940
3 (Med)	5%	2,963	3,185
3 (High)	5%	3,191	3,430

Further discussion regarding the application of the input volume distributions summarized above is provided in Section 6.4.

### 6.2.3 Analysis Framework

As indicated previously, the traffic data obtained from the AI-based extraction system focused on too narrow a time period to justify its use in developing macroscopic model inputs such as traffic volume, vehicle compositions, and desired speed. However, the vehicle trajectory data obtained from even one hour of video provided enough insight into site traffic operations to establish a framework for model calibration and analysis conducted during Task 1 and Task 2. Most critically, detailed lane-changing observations under a variety of geometric and traffic conditions allowed for the development of scenario- and vehicle class-specific lane change distance distributions. To the authors' knowledge, this is the first study to apply this type of data in Vissim.

#### 6.2.3.1 Model Calibration Data and Car-Following Parameters

The video data described in Chapter 4 was used to measure flow rate, speed, and time gap at Site B (northbound I-95 in Pooler, GA) in 5-minute intervals during the one-hour period from 2:30PM – 3:30PM on April 6, 2011. While congestion persists throughout most of this one-hour period, the data summarized in **Table 6-7** shows that queues begin to dissipate from 3:00 – 3:30PM. As such, the calibration effort described in the next section was focused in part on replicating this pattern of congestion; however, simulated speed and flow rate were only qualitatively compared to that in the video data, as input demand flow rates were acquired from other sources.

**TABLE 6-7: SEMI-AUTOMATICALLY EXTRACTED TRAFFIC DATA SUMMARY**

Time	Mean Speed (mph)	Median Time Gap (s)
Oversaturated Conditions		

2:30 PM	16.9	1.94
2:35 PM	17.7	1.84
2:40 PM	31.8	1.69
2:45 PM	32.6	1.97
2:50 PM	34.1	1.67
2:55 PM	37.9	1.79
Average	29.2	1.80
<b>Undersaturated Conditions</b>		
3:00 PM	20.9	1.86
3:05 PM	23.7	1.71
3:10 PM	46.7	1.46
3:15 PM	55.0	1.47
3:20 PM	53.3	1.40
3:25 PM	55.1	1.53
Average	42.1	1.58

Given the lack of temporal breadth in the semi-automatically extracted traffic data and inherent error in vehicle counts obtained from the AI-based system during congested conditions, estimated equivalent hourly flow rates were not considered for use as a calibration metric. Furthermore, the traffic volumes developed from GDOT CCS data are intended to be representative of the study site but likely differ from those that would have been observed on the day the video was captured. In this way, modeling a broader range of input volumes was expected to minimize the chances of “over-calibrating” to a site-specific condition.

On the contrary, while not used as a direct input, time gap measurements motivated the range of values for the CC1 (gap time distribution) parameter coded in Vissim. The median values summarized in **Table 6-7** were obtained after screening trajectory data such that records for vehicle following pairs with a time headway greater than 4.0 seconds were excluded (Dong et al., 2015). Additionally, records collected under oversaturated conditions were deemed unrepresentative of the true desired time gap that defines car-following behavior in Vissim. Past literature indicates that vehicle acceleration and deceleration associated with late lane change maneuvers—particularly those of heavy vehicles—at locations upstream of the full lane closure may inflate time gap measurements (Jehn and Turochy, 2019). Therefore, a median time gap of approximately 1.6 seconds measured during undersaturated conditions was considered as a baseline input for the CC1 parameter in Vissim.

Recalling from earlier discussion that the CC0 (standstill distance) parameter is a component of the desired safety distance (i.e., desired time gap) in Vissim, the contribution of CC0 was subtracted from the median time gap calculation. Assuming a CC0 value of 10 feet per recommendations in the literature (Dong et al., 2015), this calculation becomes:

$$CC1 (s) = Median Time Gap (ft) - \frac{CC0 (ft)}{Median Speed (mph) * 1.47 \left( \frac{ft}{s} \right)}$$

$$CC1 = 1.6 - \frac{10}{42.1 * 1.47} = 1.4s$$

A range of candidate values for the CC1 parameter between 1.0s and 1.8s were ultimately selected for use in the subject sensitivity analysis to bracket the expected calibrated value. This range coincides with that prescribed by Yeom et al. in a 2016 study completed in support of NCHRP Project 03-107, which provided generalized simulation guidance based on nationwide field data (Yeom et al., 2016). Remaining car-following and lane-changing parameter ranges were selected based on the comprehensive literature search noted in Section 6.2 and are summarized in **Table 6-8**. Where multiple selected parameter values are listed, further discussion is provided later in this chapter.

**TABLE 6-8: CAR-FOLLOWING AND LANE CHANGING PARAMETER RANGE SUMMARY**

Parameter	Default Value	Selected Value(s)
<b>Car-Following</b>		
CC0 (ft)	4.92	10
CC1 (s)	0.9	1.0, 1.2, 1.4, 1.6, 1.8
CC2 (ft)	13.12	26.24
Other Car-Following Parameters		Default
<b>Lane-Changing</b>		
Safety Distance Reduction Factor	0.6	0.3, 0.45, 0.6
-1 ft/s <sup>2</sup> per distance	200	100
Maximum deceleration (own/trailing), Maximum Deceleration for Cooperative Braking	-9.84 ft/s <sup>2</sup>	-15 ft/s <sup>2</sup>
Cooperative Lane Change	Unchecked	Checked within 1/2 mile of transition area
Lane Change Distance	656.2 ft	Field data-based distribution
Other Lane-Changing Parameters		Default

Though not included in Table 6-8, the desired acceleration distribution for heavy trucks was also modified from its default based on past findings in the literature. Specifically, default Vissim parameters assume a mean standstill acceleration of 8.2 ft/s<sup>2</sup> for heavy trucks, whereas recent research suggests that a mean value of 2.2 ft/s<sup>2</sup> is more representative of the actual performance capabilities of Interstate semitrailers (Yang et al., 2016). This stark difference between the default and adjusted values for desired truck acceleration produces substantial variation in model outputs when the percentage of trucks in the traffic stream is not negligible (i.e., 5% or greater). Since the scenarios analyzed as part of this research consider up to 30% trucks in the traffic stream, this adjustment was deemed critical to the study outcomes.

### Lane Change Distance Distributions

Based on the lane change study presented in Chapter 4, lane change positions were extracted for the two sites, Site A and B, including set of lane-changing observations that vary by type of lane closure, upstream geometry, and traffic stream characteristics. A total of eight unique, vehicle class-specific lane change distance distributions—four each for passenger cars and heavy trucks—were developed for use in Vissim based on the extracted data. These distributions are summarized in **Table 6-9** and **Table 6-10**.

**TABLE 6-9: LANE CHANGE DISTANCE DISTRIBUTION SUMMARY (PASSENGER CARS)**

Distance Upstream of Full Lane Closure (ft)	Curved Upstream Geometry, Right-Side Closure	Straight Upstream Geometry, Right-Side Closure	Curved Upstream Geometry, Left-Side Closure	Straight Upstream Geometry, Left-Side Closure
	Cumulative % Merging After Distance			
840	5%	5%	15%	0%
1,340	25%	10%	30%	10%
1,840	65%	30%	50%	60%
6,120	100%	100%	100%	100%

**TABLE 6-10: LANE CHANGE DISTANCE DISTRIBUTION SUMMARY (HEAVY TRUCKS)**

Distance Upstream of Full Lane Closure (ft)	Curved Upstream Geometry, Right-Side Closure	Straight Upstream Geometry, Right-Side Closure	Curved Upstream Geometry, Left-Side Closure	Straight Upstream Geometry, Left-Side Closure
	Cumulative % Merging After Distance			
840	0%	0%	0%	0%
1,340	15%	20%	0%	10%
1,840	45%	40%	0%	25%
6,120	100%	100%	100%	100%

In each case above, the “distance” column represents the distance upstream of the full lane closure that vehicles in Vissim will begin to look for opportunities to merge from the closed lane to one of two remaining open lanes. The trajectory data used to develop the lane change distance distributions only included observations at up to approximately 1,840 feet upstream of the lane closure (i.e., 1,000 feet upstream of the beginning of the lane closure taper). Based on the typical applications presented in Part 6 of the *Manual on Uniform Traffic Control Devices (MUTCD)*, a “Road Work Ahead” sign should be placed at 5,140 feet upstream of the lane closure taper on freeway facilities. The MUTCD also prescribes a taper length of approximately 840 feet for a freeway facility with a speed limit of 70 mph and 12-foot travel lanes. As such, it was assumed that drivers are unlikely to begin searching for opportunities to merge (except for purposes of discretionary lane changes) further upstream than one mile from the beginning of the lane closure taper. Accordingly, a maximum lane change distance of 6,120 feet (840 feet + 5,280 feet) was coded in Vissim.

Lastly, lane changing observations were acquired under both undersaturated and oversaturated conditions as part of the case study detailed in Chapter 4. Since lane changes occurring under congested conditions are constrained by the cooperativeness of vehicles in adjacent lanes and available gaps under tighter vehicle spacing, only observations associated with undersaturated conditions were considered when developing the lane change distance distributions presented in **Table 6-9** and **Table 6-10**. That said, observations under oversaturated conditions were considered as a primary calibration metric, since the point at which lane changes are executed is influenced by the location where drivers first look for acceptable gaps to merge. Further discussion on this topic is provided in the next section.

## 6.3 Task 1 – Sensitivity Analysis

### 6.3.1 Introduction

As introduced in Section 6.1.2, the purpose of this initial task was twofold. First, the Vissim models developed as part of this study were calibrated using the lane change distance distributions obtained from the AI-based extraction system by exploring various combinations of the driving behavior parameter ranges identified earlier in the chapter. The methodologies and outcomes described herein may be used to inform future modeling efforts that make use of vehicle class-specific lane change distance distributions in Vissim. Second, the calibrated Vissim models were run with a literature-recommended static value for the lane change distance to highlight the disparity in resultant macroscopic model outputs. The reliability and utility of semi-automatically extracted traffic data and the potential future value of utilizing lane change distance distributions in Vissim are assessed based on the results of this exercise.

### 6.3.2 Sensitivity Analysis Experiment Design

Base Vissim model geometry, network objects, and input traffic volumes used as part of the subject sensitivity analysis were detailed earlier in the chapter. A six-mile freeway work zone corridor with a simulated 3-2 lane closure was coded in Vissim to run for a total of 12 hours (43,200 seconds) per random seed. The spatial and temporal extents of the model were intended to capture the propagation and dissipation of queues upstream of the simulated lane closure. Since data from the AI-based extraction system was unable to provide sufficient detail to motivate the development of input demand volumes, GDOT CCS data near Site B (Northbound I-95 milepost 97 in Pooler, GA) on a typical weekday in September 2016 was deemed sufficiently representative of study site conditions. Traffic characteristics at this CCS site were provided in detail in **Table 6-5**. Finally, baseline driving behavior parameters were selected based on recommendations in the literature, as summarized in **Table 6-8** in Section 6.2.3.1.

As alluded to throughout this chapter, the structure of the subject sensitivity analysis was formed by exploring various levels of the following parameters, each redefined here for clarity:



- CC1 (Gap Time Distribution, s) – This parameter represents the multiplicative component of the desired safety distance in Vissim. At higher speeds, this parameter has the greatest influence on the desired following headway between a lead and trailing vehicle. Consequently, literature has found this parameter to have the greatest influence on simulated throughput. In the context of 3-2 freeway lane closures, research conducted as part of NCHRP Project 03-107 recommended a minimum value of 1.0s and maximum value of 1.8s (Yeom et al., 2016).
- SDRF (Safety Distance Reduction Factor) – The SDRF parameter is unitless and defines the maximum reduction in the calculated safety distance that a vehicle will allow when searching for an acceptable gap to merge into an adjacent lane. The default value is 0.6, though the literature has indicated that smaller values may be necessary at merge, diverge, weaving, and work zone segments on freeways (FDOT, 2014).
- LCD (Lane Change Distance, ft) – For required lane changes (e.g., merges ahead of an off-ramp, turn bay, or lane closure), this parameter defines the distance upstream at which a driver will begin to look for acceptable gaps to merge. In legacy versions of PTV Vissim and in past literature, this parameter is modeled as a static value. This study is believed to be one of the first to leverage the capability of recent versions of Vissim (i.e., beginning with PTV Vissim 2020) to model the lane change distance as a vehicle class-specific distribution.

Though additional input parameters impact simulation outputs to varying degrees, these three parameters were deemed most influential in replicating the lane-changing behavior studied as part of the case study presented in Chapter 4 of this report.

Several key items are worth noting with regard to the specific ranges selected for each of these parameters. First, the CC1 parameter was varied between a mean value of 1.0s and 1.8s, but modeled based on a normal distribution with a standard deviation of 0.20s in each case. The standard deviation value was selected based on that required (to the nearest 0.1s) to yield a maximum possible gap time of 4.0s in Vissim when coding a mean gap time of 1.8s. Second, the SDRF parameter was varied at three levels—0.60 (default), 0.45 (75% of default) and 0.30 (50% of default). Based on recent guidance from PTV (VDOT, 2020), the need for substantial deviation from the default value of the SDRF parameter was not expected. As such, these three values of the SDRF parameter were deemed sufficient, and each fall within the literature-recommended range for freeway lane closures. Finally, the lane change distance distributions summarized in **Table 6-9** and **Table 6-10** required modification before application in Vissim. A 2007 study by Toledo and Zohar modeled the duration of lane changes on a freeway segment in California and observed a mean lane-changing duration of 4.6s (Toledo and Zohar, 2007). At an average speed of 70 mph, a vehicle will travel nearly 500 feet over this

period. Since the lane change distance parameter in Vissim defines the point upstream of a required lane change that a vehicle will *begin* to look for opportunities to merge, each of the distances that form the distributions summarized previously were increased by 300, 500, and 700 feet. These three values were intended to bracket the expected distance traveled by vehicles in Vissim prior to successfully completing a lane change under low-density conditions.

The full factorial sensitivity experiment conducted as part of Task 1 is outlined in **Table 6-11**. In the table, the term “RFD” refers to “raw field data”, and the three-character coding system (X-X-X) used to denote specific cases was developed as follows:

First Character (CC1 Parameter Value):

- A – mean = 1.0s, standard deviation = 0.2s
- B – mean = 1.2s, standard deviation = 0.2s
- C – mean = 1.4s, standard deviation = 0.2s
- D – mean = 1.6s, standard deviation = 0.2s
- E – mean = 1.8s, standard deviation = 0.2s

Second Character (Lane Change Distance Modifications)

- 1 – RFD
- 2 – RFD + 300 feet
- 3 – RFD + 500 feet
- 4 – RFD + 700 feet

Third Character (SDRF Parameter Value):

- A – Default (0.60)
- B – 75% of Default (0.45)
- C – 50% of Default (0.30)

In total, 45 unique cases were developed and run using the same 10 random seeds. The additional 15 cases that comprise combinations of scenarios using the RFD lane change distance distributions (i.e., “1” for the second character in the scenario ID) were eliminated from the experiment after initial simulation runs indicated these scenarios were unnecessary. The outputs from these initial runs deviated substantially from field-observed lane change distance distributions, so the size of the experiment was reduced accordingly.

**TABLE 6-11: SENSITIVITY ANALYSIS EXPERIMENT SCENARIOS**

Scenario	Mean CC1 (s)	Lane Change Distance Distribution	Safety Distance Reduction Factor
A-2-A	1	RFD + 300 feet	Default
A-3-A	1	RFD + 500 feet	Default
A-4-A	1	RFD + 700 feet	Default
B-2-A	1.2	RFD + 300 feet	Default
B-3-A	1.2	RFD + 500 feet	Default
B-4-A	1.2	RFD + 700 feet	Default
C-2-A	1.4	RFD + 300 feet	Default
C-3-A	1.4	RFD + 500 feet	Default
C-4-A	1.4	RFD + 700 feet	Default
D-2-A	1.6	RFD + 300 feet	Default
D-3-A	1.6	RFD + 500 feet	Default
D-4-A	1.6	RFD + 700 feet	Default
E-2-A	1.8	RFD + 300 feet	Default
E-3-A	1.8	RFD + 500 feet	Default
E-4-A	1.8	RFD + 700 feet	Default
A-2-B	1	RFD + 300 feet	0.45
A-3-B	1	RFD + 500 feet	0.45
A-4-B	1	RFD + 700 feet	0.45
B-2-B	1.2	RFD + 300 feet	0.45
B-3-B	1.2	RFD + 500 feet	0.45
B-4-B	1.2	RFD + 700 feet	0.45
C-2-B	1.4	RFD + 300 feet	0.45
C-3-B	1.4	RFD + 500 feet	0.45
C-4-B	1.4	RFD + 700 feet	0.45
D-2-B	1.6	RFD + 300 feet	0.45
D-3-B	1.6	RFD + 500 feet	0.45
D-4-B	1.6	RFD + 700 feet	0.45
E-2-B	1.8	RFD + 300 feet	0.45
E-3-B	1.8	RFD + 500 feet	0.45
E-4-B	1.8	RFD + 700 feet	0.45
A-2-C	1	RFD + 300 feet	0.30
A-3-C	1	RFD + 500 feet	0.30
A-4-C	1	RFD + 700 feet	0.30
B-2-C	1.2	RFD + 300 feet	0.30
B-3-C	1.2	RFD + 500 feet	0.30
B-4-C	1.2	RFD + 700 feet	0.30
C-2-C	1.4	RFD + 300 feet	0.30

Scenario	Mean CC1 (s)	Lane Change Distance Distribution	Safety Distance Reduction Factor
C-3-C	1.4	RFD + 500 feet	0.30
C-4-C	1.4	RFD + 700 feet	0.30
D-2-C	1.6	RFD + 300 feet	0.30
D-3-C	1.6	RFD + 500 feet	0.30
D-4-C	1.6	RFD + 700 feet	0.30
E-2-C	1.8	RFD + 300 feet	0.30
E-3-C	1.8	RFD + 500 feet	0.30
E-4-C	1.8	RFD + 700 feet	0.30

The lane change distance modifications applied in Vissim relative to the RFD scenario are summarized in **Table 6-12**. Users should be aware that Vissim currently requires distance distributions to be entered in metric units (i.e., meters), even if imperial units are selected as the universal default preference.

**Table 6-12: Lane Change Distance Modification Summary**

RFD		RFD + 500 feet	
Distance (ft)	Distance (m)	Distance (ft)	Distance (m)
840	256	1,340	408
1,340	408	1,840	561
1,840	561	2,340	713
6,120	1,865	6,620	2,018
RFD + 300 feet		RFD + 700 feet	
1,140	347	1,540	469
1,640	500	2,040	622
2,140	652	2,540	774
6,420	1,957	6,820	2,079

### 6.3.3 Sensitivity Analysis Results

This subsection demonstrates the sensitivity of simulation outputs under a single set of input traffic volumes and vehicle compositions to changes in the parameters summarized in **Table 6-11**. The form and outcomes of this experiment are consistent with those of a traditional model calibration effort. First, the parameters expected to have the greatest influence on simulation outputs of interest were varied to identify the parameter set that generates the best match to field conditions observed at the study freeway work zone. For traditional measures of effectiveness such as speed, travel time, and flow rate, this comparison was performed qualitatively due to the limitations in the field data discussed previously. However, this sensitivity analysis is unique in that the lane change distance distribution—a key *input* to the simulation—was validated against model outputs. Goodness-of-fit statistics were calculated to evaluate the relative match

of simulation lane changing outputs to field-observed lane changing behavior and select a preferred scenario for subsequent use in Task 2. Finally, model outputs under the calibrated parameter set were compared to those generated when using a literature-based default value for the lane change distance in Vissim. The results of this sensitivity analysis provide guidance for future modeling efforts and opportunities for further research.

#### Qualitative Evaluation of Traffic Measures of Effectiveness

Simulated average speed by time of day under each of the 45 studied scenarios is presented in **Figure 6-3**, **Figure 6-4**, and **Figure 6-5** as a series of speed “heat maps”. These heat maps use a green-to-red color scale coded based on the volume-weighted average speed across all travel lanes during each 15-minute interval from 10:00AM to 8:00PM. Since the video camera used to collect trajectory data at the study freeway work zone was mounted at the lane closure taper, the graphics focus on modeled conditions within the transition area. Beneath the speed heat maps, each figure also summarizes the maximum pre-breakdown flow rate, average queue discharge rate, and maximum corridor travel time observed in the model as an average of the 10 random seed runs conducted for each case. Based on guidance in the literature (Kondyli et al., 2013), the onset of breakdown is typically defined by a sudden drop in speed at the bottleneck in question that persists for multiple time periods and is accompanied by upstream queue formation. A breakdown identification algorithm was developed for classifying each time interval in Vissim as follows:

- The simulated free flow speed through the work zone was calculated as 59 mph based on model outputs from time periods with low flow rates
- Breakdown events were identified based on a sudden, sustained drop in speed of at least 25% below free flow speed ( $59 \text{ mph} \times 75\% = 44 \text{ mph}$ ), measured at the data collection point just downstream of the bottleneck location
  - A sudden drop in speed was defined as a decrease in average speed of at least 10% of the observed speed from the previous interval
  - A sustained drop in speed was defined as three consecutive five-minute intervals with observed speeds below the threshold
  - Data collection points placed one-quarter mile upstream of the lane closure were examined during each time interval to confirm queue propagation

This breakdown identification algorithm was also used to classify 15-minute intervals as congested or uncongested for the purposes of calculating measures of capacity and categorizing lane changing observations, as discussed later in this section.


As shown in **Figure 6-3**, **Figure 6-4**, and **Figure 6-5**, a wide range of traffic conditions were observed between scenarios—all of which utilized the same traffic volume inputs and vehicle compositions. At a value of 1.0s for the CC1 parameter (i.e., the nine



scenarios with an “A” as the first character in their respective ID), little to no congestion was observed throughout the simulation during any of the 10 random seed runs conducted. Conversely, congestion persisted throughout nearly the entire simulation period under scenarios coded with a value of 1.8s for the CC1 parameter (i.e., the nine scenarios with an “E” as the first character in their respective ID). Though the maximum pre-breakdown flow rate and average queue discharge rate associated with these relative decreases in capacity vary by only 100-200 vehicles per hour per open lane through the simulated work zone, corridor-wide impacts are more substantial. The trends shown in the figures foreshadow those discussed later as part of Task 2 and demonstrate that large increases in travel time and queue length may be observed as a result of seemingly slight changes in flow-based measures of capacity. Under scenarios A-2-A through A-4-A, maximum travel time through the simulated six-mile corridor is between seven and nine minutes per vehicle, on average. Under scenarios E-2-A through E-4-A, the maximum corridor travel time extends to nearly 40 minutes per vehicle, representing up to a 400% increase relative to that under scenarios A-2-A through A-4-A, despite only a 20% decrease in the maximum pre-breakdown flow rate and average queue discharge rates observed in model outputs. This underscores the outsized role that small changes in headway play in resulting travel time (and therefore congestion) and the value of field data for selecting a headway distribution.

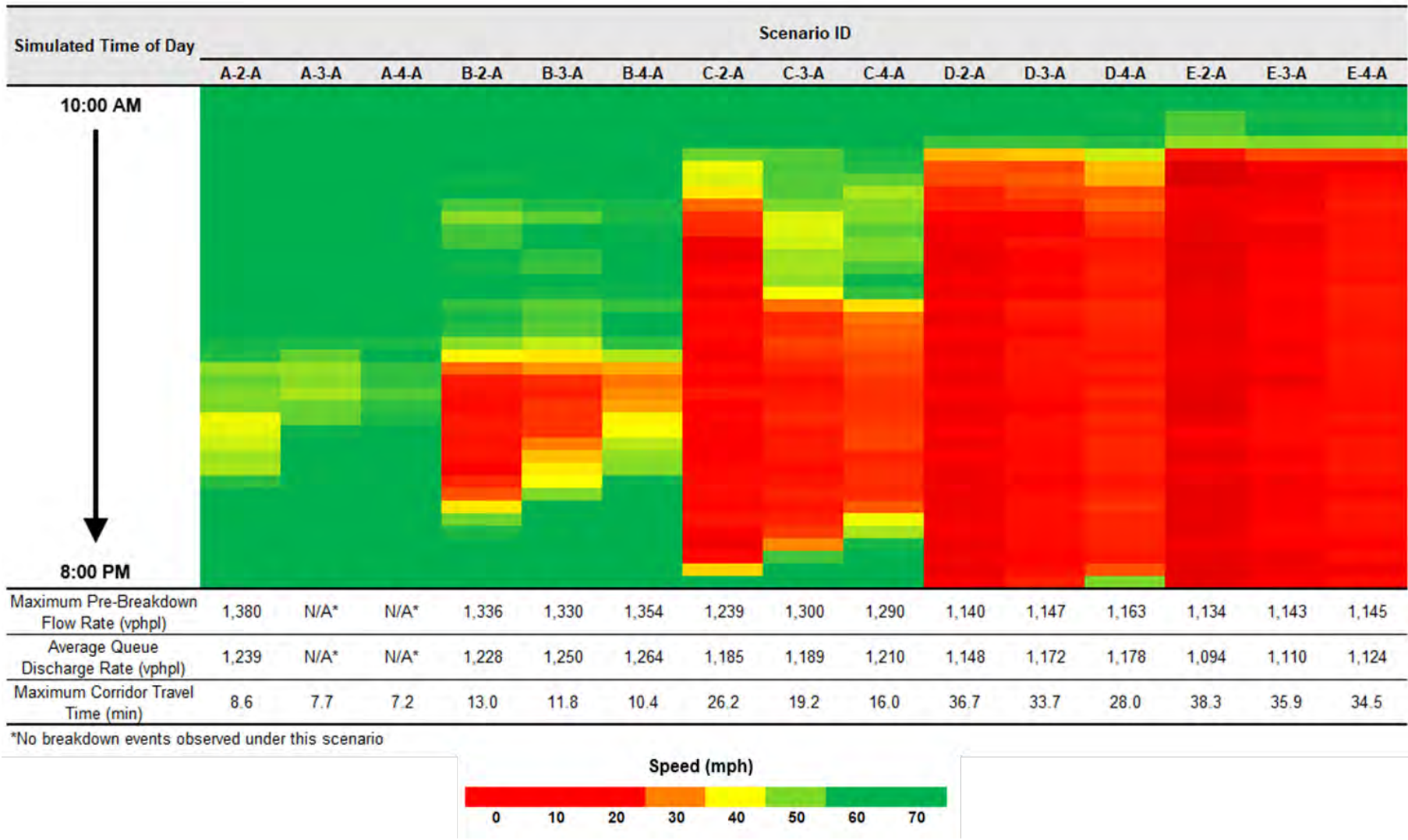


**FIGURE 6-3: SENSITIVITY ANALYSIS OUTPUTS SUMMARY AND ZONE 1/TRANSITION AREA SPEED HEAT MAP (SDRF = 0.60)**



Quantitatively Evaluate Work Zone Driver Behavior using 2D Imaging,  
3D LiDAR, & Artificial Intelligence in Support of Congestion Mitigation  
Model Calibration & Validation (Project G2)

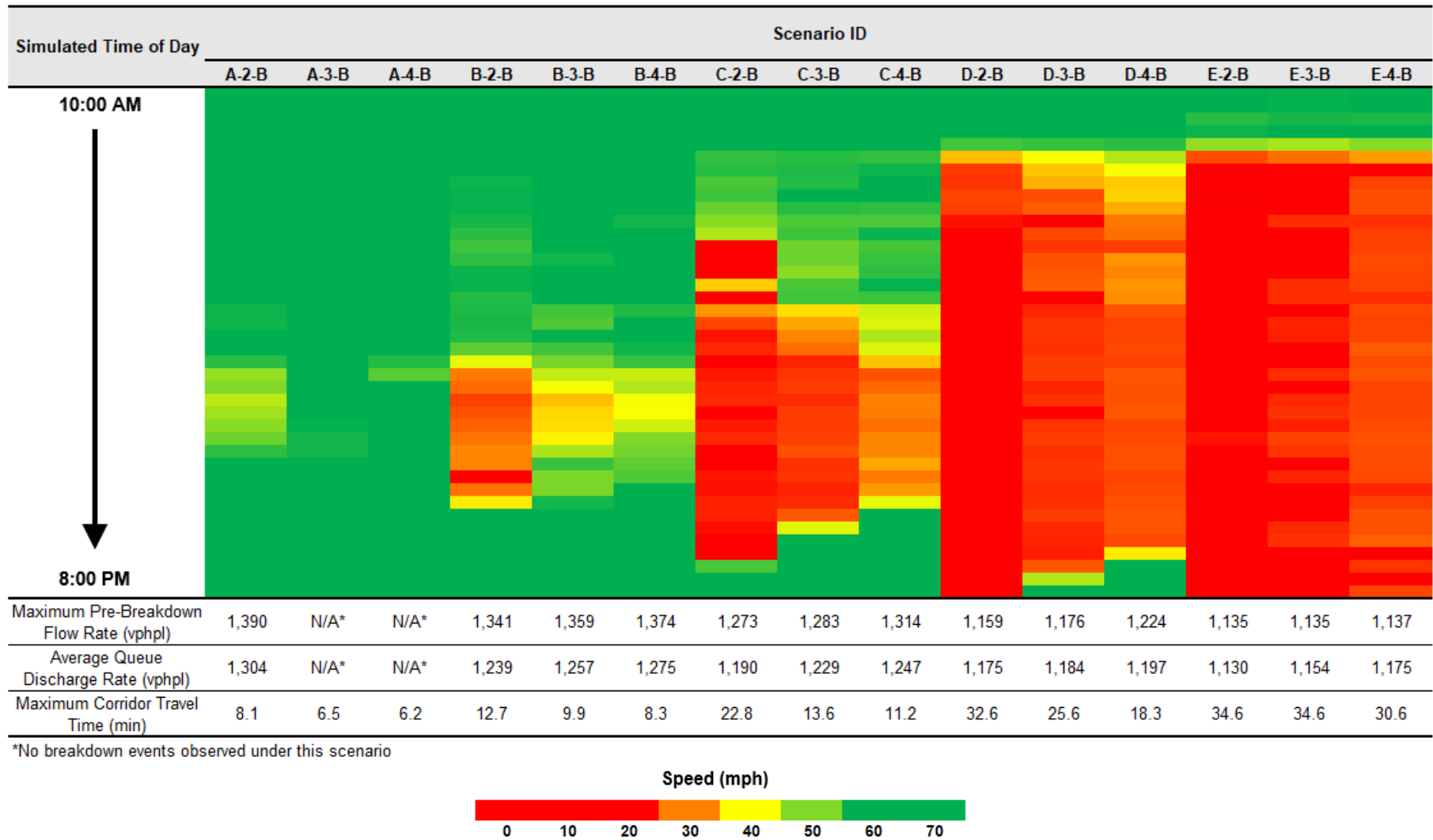


**FIGURE 6-4: SENSITIVITY ANALYSIS OUTPUTS SUMMARY AND ZONE 1/TRANSITION AREA SPEED HEAT MAP (SDRF = 0.45)**

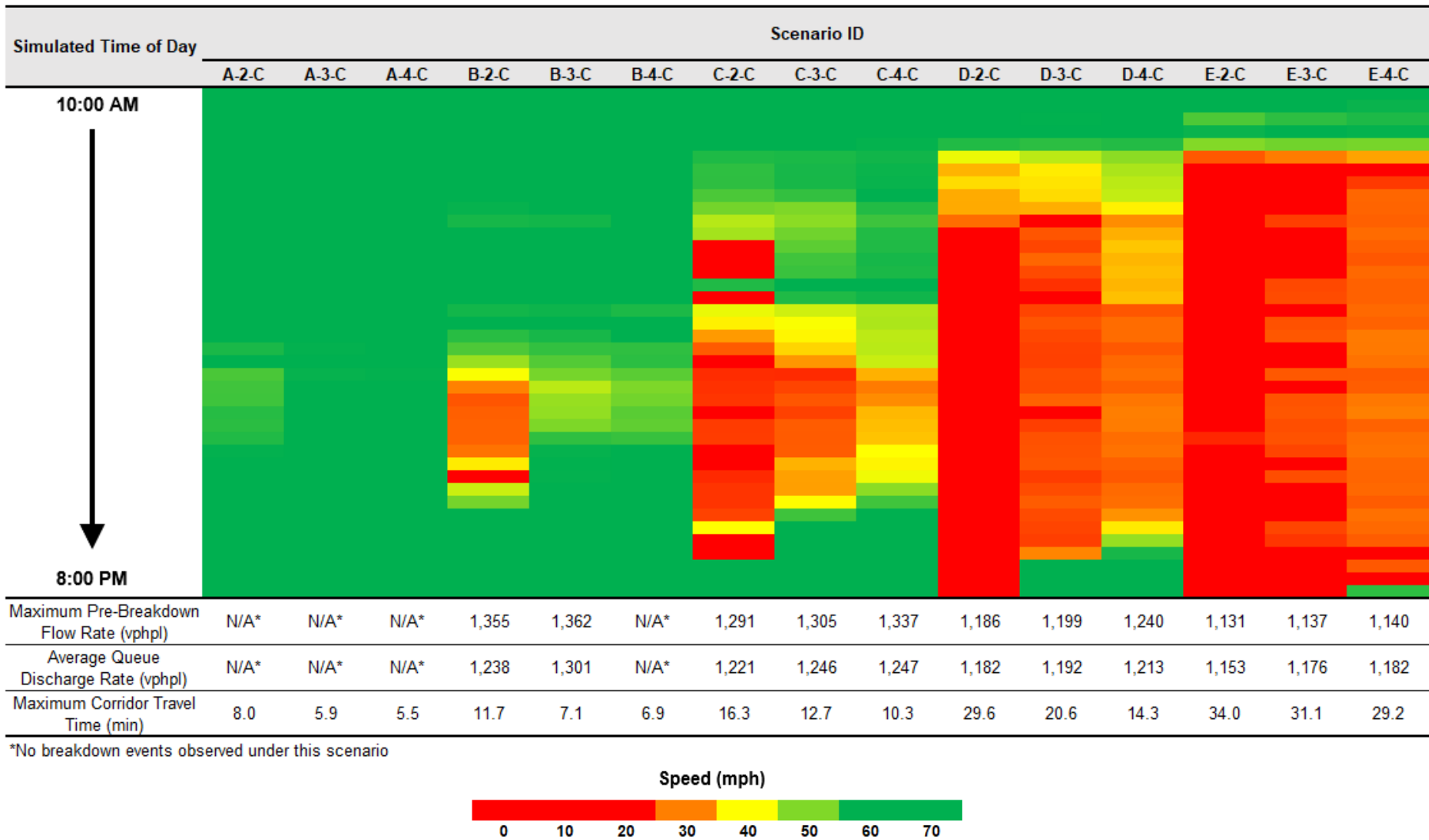


**FIGURE 6-5: SENSITIVITY ANALYSIS OUTPUTS SUMMARY AND ZONE 1/TRANSITION AREA SPEED HEAT MAP (SDRF = 0.30)**



Comparing Figures 6-3, 6-4, and 6-5, the amount of congestion observed in the 10 random seed runs conducted for each case diminishes markedly as the safety distance reduction factor is reduced below its default value of 0.60. From Case C-2-A (SDRF = 0.60) to Case C-2-C (SDRF = 0.30), the maximum corridor travel time decreases from over 26 minutes per vehicle to just over 16 minutes per vehicle. This 38% decrease in travel time occurs despite modest increases in measures of capacity; when averaged across the 10 random seed runs conducted for each scenario, the maximum pre-breakdown flow rate and average queue discharge rate increase by just 4% and 3%, respectively, under scenario C-2-C relative to scenario C-2-A.

Regardless, given that congestion was only observed over a short period in the field data, scenarios B-2-A through B-4-A, B-2-B through B-4-B, and B-2-C through B-4-C were deemed most capable of replicating the lane changing behavior observed in the field data. As such, these nine scenarios were carried forward for validation of Vissim lane change outputs against field observations.

#### Quantitative Evaluation of Lane Change Distance Distributions

The full set of 45 unique cases was narrowed to each of the nine scenarios coded with a CC1 value of 1.2s (i.e., scenarios with a “B” as the first character in their respective ID), as these scenarios best replicated field data collected as part of this study. Detailed lane changing observations were then extracted from Vissim and compared to the field distributions summarized earlier in the chapter. This exercise was completed through the use of two methodologies. First, given the ubiquity of discretionary lane changes occurring during undersaturated conditions—especially within Zone 4—mandatory lane changes occurring prior to the onset of congestion were evaluated using the Direct Output feature in Vissim. This feature allows the user to collect data from individual events (e.g., lane changes, signal changes, or signal detector records) or track vehicle trajectories throughout the simulation period and is infrequently used in practice due to the large output file sizes generated. In this case, individual lane change events were extracted from Vissim and filtered to only include mandatory lane changes occurring within one mile of the simulated lane closure. To limit run time and output file size while ensuring that only undersaturated conditions were modeled, the same 10 random seed runs conducted previously for cases B-2-A through B-4-A, B-2-B through B-4-B, and B-2-C through B-4-C were coded to terminate after two simulation hours (i.e., 7,200 seconds). Over the course of these two simulation hours, the following data was collected for each scenario:

##### *Lane Changes (file extension “.spw”)*

- Vehicle ID
- Time of Lane Change (simulation seconds)
- Location of Lane Change
  - Link Number
  - Original Lane
  - New Lane

*Vehicle Record (file extension “.fzp”)*

- Vehicle ID
- Time of Record (simulation seconds)
- Vehicle Class

Records within the .spw files were filtered to ensure that each represented a mandatory lane change associated with the modeled lane closure. An algorithm was coded in Microsoft Excel to classify a record as “eligible” for lane change distance distribution calculations only if the following conditions were met:

- The lane change represented the *last* lane change recorded for a given Vehicle ID upstream of the lane closure connector
- The lane change involved a merge from the rightmost lane to the adjacent center lane

Each “eligible” record was binned based on location (Zone 1, Zone 2, Zone 3, or Zone 4) and vehicle class (passenger car, heavy truck). The results of this exercise are presented in **Table 6-13** for a lane closure with straight upstream geometry and low traffic density.

**TABLE 6-13: OUTPUT LANE CHANGE DISTANCE DISTRIBUTION SUMMARY<sup>1</sup>**

Lane Change Distance Distribution (Straight Upstream Section, Passenger Cars)										
Scenario	B-2-A	B-3-A	B-4-A	B-2-B	B-3-B	B-4-B	B-2-C	B-3-C	B-4-C	Field Data
Zone 4	70%	75%	78%	72%	77%	80%	63%	69%	76%	70%
Zone 3	11%	9%	8%	13%	10%	8%	18%	18%	15%	20%
Zone 2	9%	7%	7%	8%	7%	6%	15%	8%	5%	5%
Zone 1	9%	8%	8%	8%	7%	7%	4%	5%	4%	5%
Lane Change Distance Distribution (Straight Upstream Section, Heavy Trucks)										
Scenario	B-2-A	B-3-A	B-4-A	B-2-B	B-3-B	B-4-B	B-2-C	B-3-C	B-4-C	Field Data
Zone 4	60%	65%	70%	62%	69%	74%	73%	79%	81%	60%
Zone 3	15%	17%	15%	17%	18%	15%	13%	9%	8%	20%
Zone 2	17%	13%	9%	15%	9%	6%	8%	6%	5%	20%
Zone 1	8%	5%	5%	7%	5%	4%	7%	7%	6%	0%

<sup>1</sup>All observations taken prior to the onset of breakdown to ensure lane changes were not constrained by oversaturated conditions

The results shown in **Table 6-13** highlight a few noteworthy trends. First, the number of vehicles completing mandatory lane changes within Zone 1 is overstated under all analyzed scenarios. This finding is especially evident for heavy trucks. Even under scenario B-4-C—which minimizes the likelihood of late merges occurring based on input parameter values (because this scenario employs the maximum lane change distance and minimum SDRF) —approximately 6% of all lane changes occur within Zone 1, despite the fact that no trucks were observed in the rightmost lane within Zone 1 in the field data. On the contrary, the proportion of vehicles changing lanes within Zone 4 was

generally greater in Vissim than in the field data. These findings underscore the challenges of calibrating a Vissim model to lane changing behavior. As mentioned earlier in this chapter, a vehicle traveling at 70 mph will traverse the 500-foot distance that comprises Zone 2 and Zone 3 within approximately five seconds. As a result, field-observed lane changing behavior may be more replicable at coarser levels (e.g., distance bins greater than 500 feet in length). Even so, **Table 6-13** suggests a fairly reasonable match to field-observed lane changing behavior across most of the nine scenarios considered.

The second of two methodologies utilized to evaluate modeled lane changing behavior focused on mandatory lane changes occurring *after* the onset of congestion. Though not all scenarios were presented in **Table 6-13** previously, the methodology for assessing lane changes occurring *prior* to the onset of congestion is biased towards cases with more aggressive driving behavior parameters. In other words, the cases with the smallest value for the CC1 and SDRF parameters are likely to produce the best fit to lane changes occurring under non-congested conditions, assuming that the lane change distance distribution itself is held constant. On the other hand, post-breakdown lane changing behavior is a more convoluted function of the variables studied as part of this sensitivity analysis. As such, calibration to lane changing behavior observed under congested conditions was deemed to contribute to the predictive robustness of the models carried forward to Task 2.

Accordingly, the proportion of lane changes occurring within each zone after the onset of breakdown was estimated and compared to the field data. This comparison is provided in **Figure 6-6**, where the goodness-of-fit of the model data to the field data was assessed using the root mean square normalized error (RMSNE). The RMSNE was not computed through direct comparison of the observed and expected lane change proportions for each zone. Rather, the total number of lane changes observed in Vissim across the 10 random seed runs conducted for each scenario (e.g., 5,647 lane changes by passenger cars under scenario B-3) was multiplied by the field-observed percentages associated with each zone in the field data. The resultant number of lane changes was then compared with the raw number of lane changes observed within each zone in Vissim to compute the RMSNE. As shown in the figure, the largest relative errors occur under scenarios coded with more aggressive lane changing behavior (e.g., smaller values of SDRF), particularly within Zone 4. Overall, scenario B-3-A minimized the RMSNE (at a value of 0.049, as shown in **Figure 6-6**). Therefore, the lane change distance distributions (RFD + 500 feet) and values of CC1 (1.2s) and SDRF (0.60) considered under case B-3-A were selected as the preferred parameter set for use during Task 2.

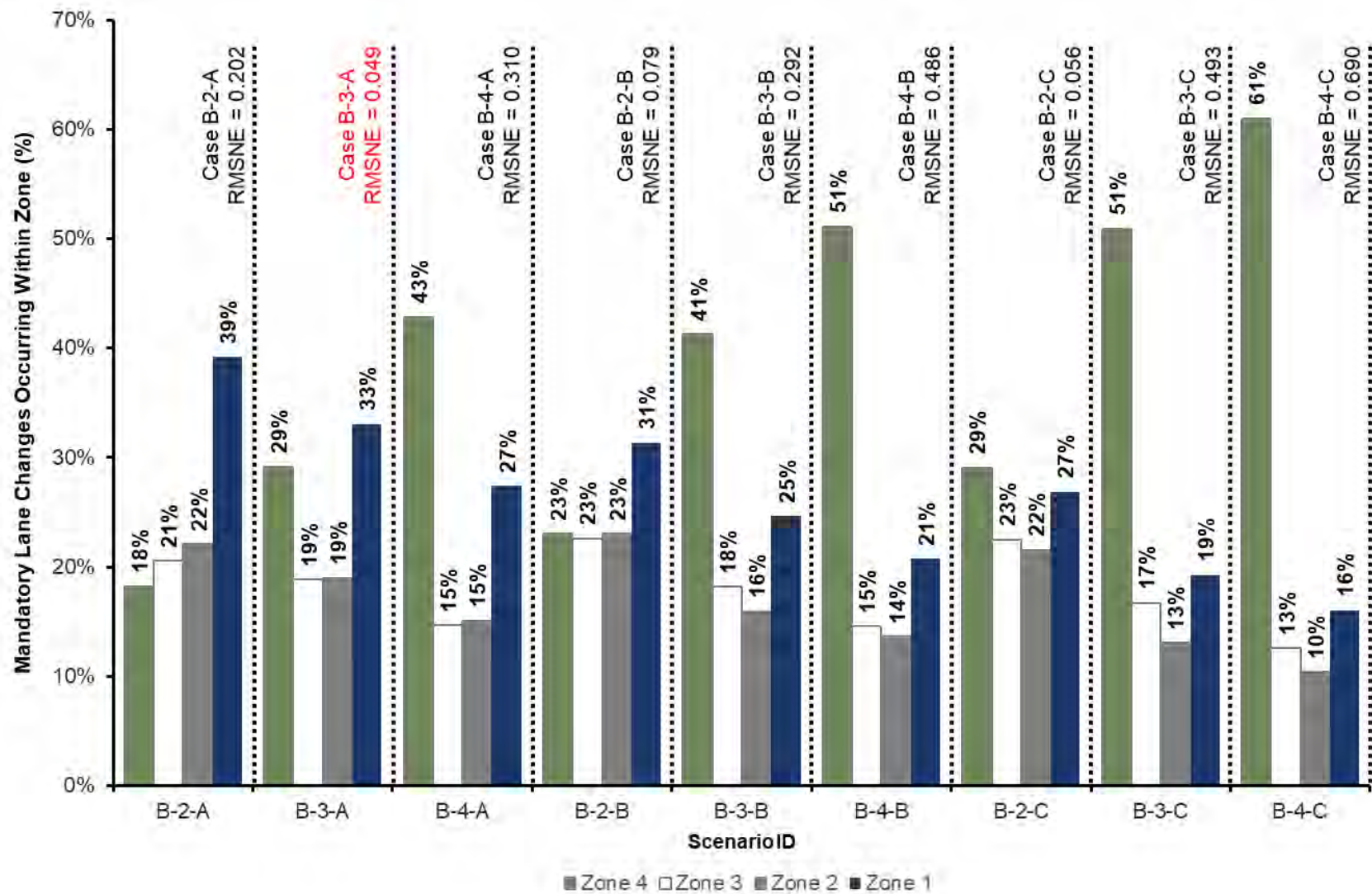


**FIGURE 6-6: OUTPUT LANE CHANGE DISTANCE EVALUATION (OVERSATURATED CONDITIONS)**

### Comparisons to Default Lane Change Distance

Finally, a copy of the scenario B-3 Vissim model was coded to run with the connector lane change distance set to a typical “default” value for freeway work zones. Based on guidance in the literature (Yeom et al., 2016; Jehn and Turochy, 2019), a static value of 3,000 feet was selected and applied in Vissim. Outputs under the calibrated and typical “default” lane change distances are compared in **Figure 6-7** and **Figure 6-8**.

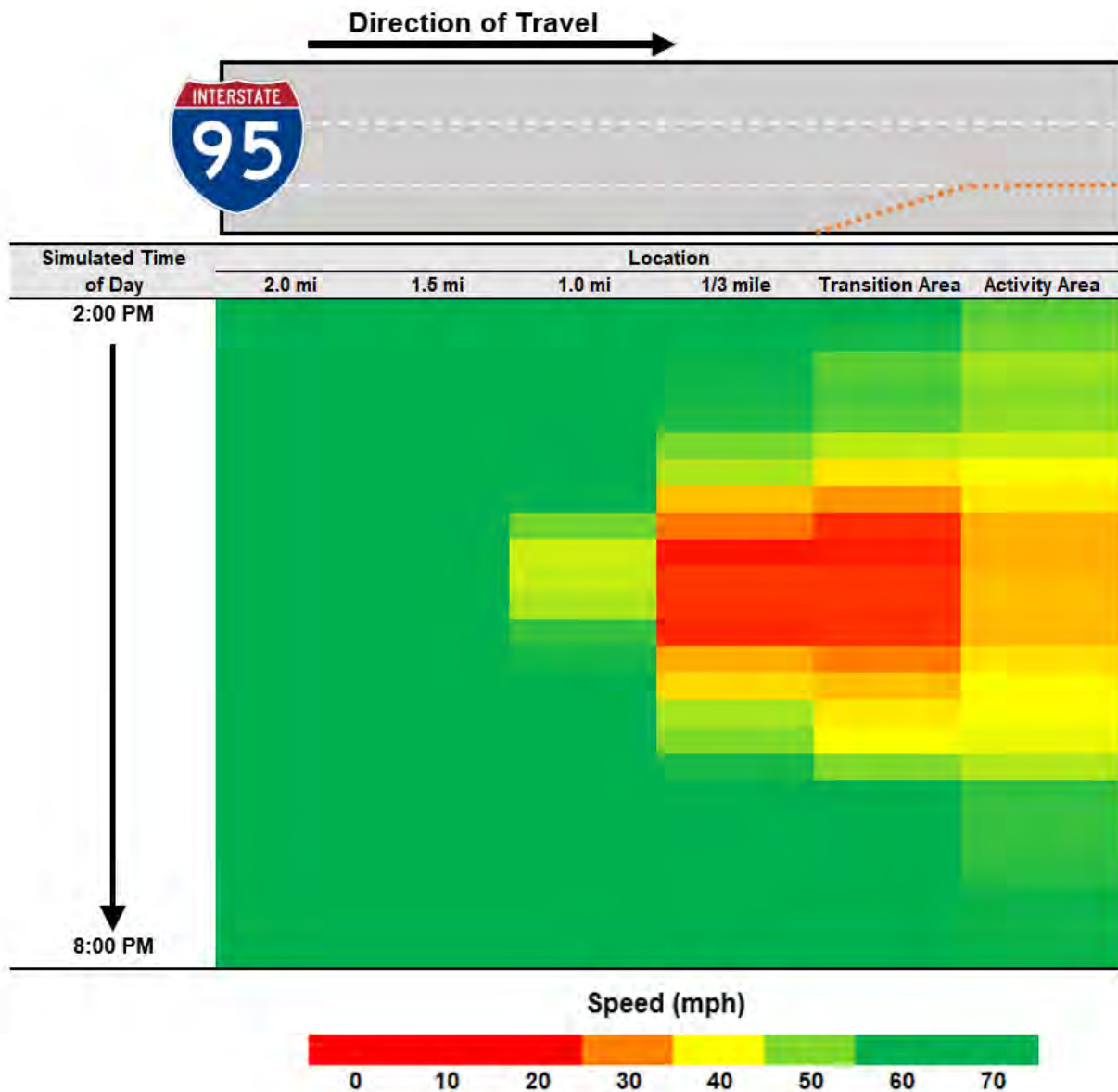


**FIGURE 6-7: CORRIDOR SPEED HEAT MAP (SCENARIO B-3—CALIBRATED LANE CHANGE DISTANCE DISTRIBUTION)**



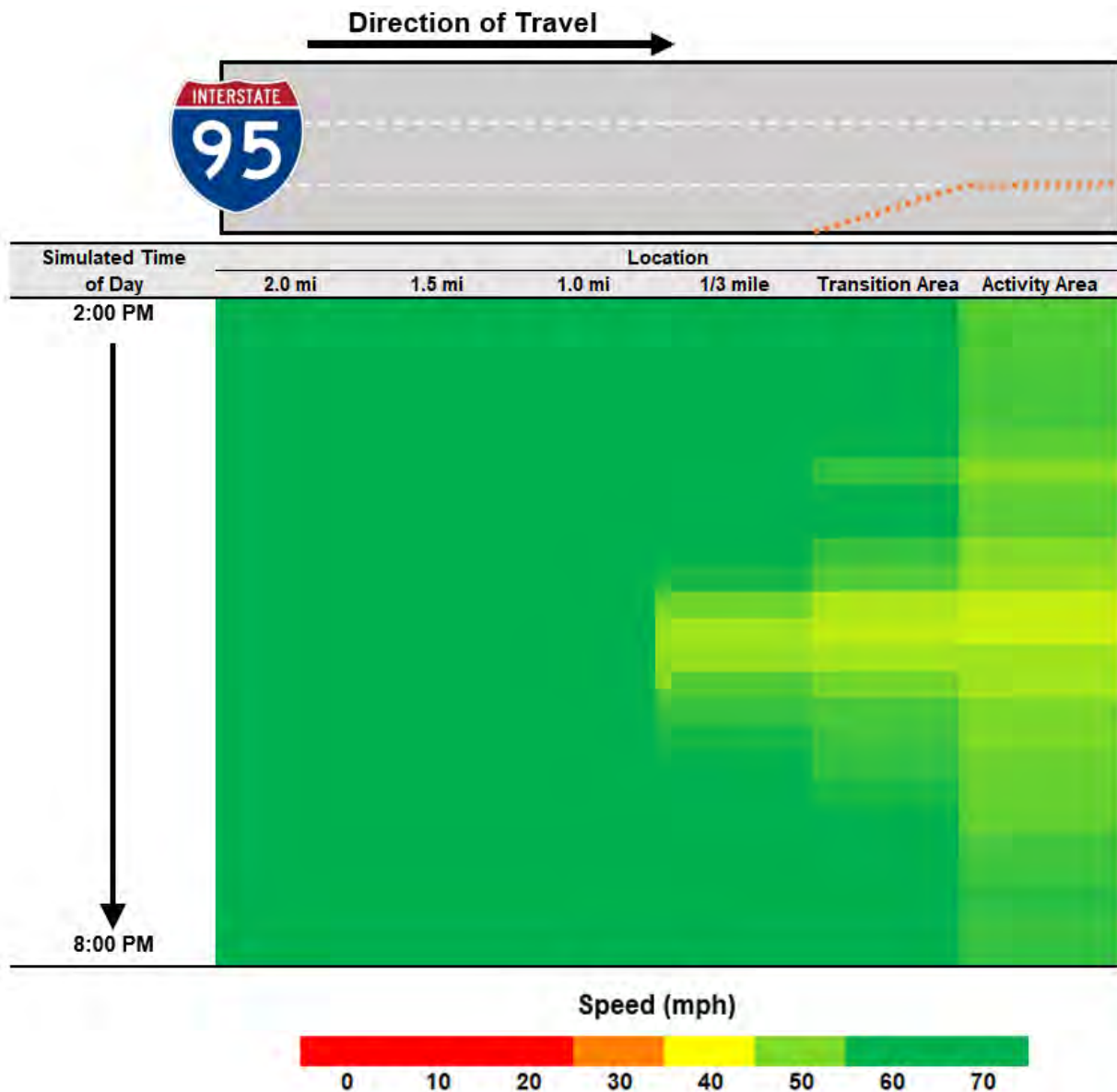


**FIGURE 6-8: CORRIDOR SPEED HEAT MAP (SCENARIO B-3—DEFAULT LANE CHANGE DISTANCE)**

The qualitative differences in modeled speeds demonstrated in the figures is backed quantitatively by output measures of effectiveness. Under the calibrated parameter set, a maximum pre-breakdown flow rate of 1,330 vehicles per hour per open lane through the work zone was observed, with a maximum corridor travel time of approximately 9.3 minutes. On the contrary, no breakdown events were observed under the typical “default” lane change distance, and the maximum corridor travel time during a given random seed run was 6.4 minutes (-31%), on average. Given that the weighted average lane change distance represented by the distribution coded in Vissim under the calibrated scenario is approximately 4,000 feet for passenger cars and 3,800 feet for trucks, this finding is somewhat counterintuitive. In other words, larger values of the

lane change distance are generally associated with “smoother” operations in practice and are less likely to produce congestion in Vissim (VDOT, 2020). These results highlight the disruptions to traffic operations possible when even a small number of vehicles initiate lane changes near or downstream of the beginning of the transition area.

Moreover, the results of Task 1 expose a gap in the existing body of research relative to freeway work zone simulation model calibration in Vissim. Specifically, if one desired to replicate the congestion pattern shown in **Figure 6-7** while assuming a static value for the lane change distance, other parameters—such as CC1 and SDRF—would require further modification. As noted in Section 6.2.1, model calibration is a cumbersome process often handled differently from modeler to modeler. These differences lead to inconsistencies in practice, and more importantly, differences in the results and conclusions associated with a given analysis. Consequently, there exists a critical need to continue to narrow the number of “unknowns” in calibrating Vissim models, especially those used to study freeway work zones. The lane change distance distributions collected at the study 3-2 lane closures serve as a starting point for future modeling efforts, at a minimum. Future research should extend application of these distributions or consider additional field data collected at other lane closure configurations (e.g., 2-1 freeway lane closures) to build upon the findings presented here.

## 6.4 Task 2 – Modeling Freeway Work Zone Traffic Operations at Sites With Varying Characteristics

### 6.4.1 Introduction

The calibrated model developed as part of Task 1 was intended to be representative of conditions observed under a single case captured by the field data summarized in Section 6.2.3. The purpose of this second task was to extend the preferred parameter set identified during Task 1 to theoretical three-to-two freeway lane closures exhibiting the remaining geometric and traffic stream characteristics represented by the field data. A full factorial experiment was conducted to determine how traffic measures of effectiveness vary as a function of demand-to-capacity ratio, truck percentage, upstream geometry, and lane closure side. The outcomes of this task support agency work zone scheduling and traffic control decisions by demonstrating the sensitivity of critical variables such as travel time and queue length to seemingly minor changes in measures of capacity. The findings of this work allude to opportunities for future research utilizing freeway work zone lane changing behavior data to further current understanding of the range of conditions possible under various geometric configurations and traffic stream characteristics.

### 6.4.2 Experiment Design and Refinement

Vissim input geometry, network objects, and driving behavior parameters coded in the calibrated scenario B-3 model were used as the basis for generating a total of 36 additional cases to be studied. Each of these cases are listed in **Table 6-14**, where the “low”, “medium”, and “high” traffic volume input categories were developed as summarized in Section 6.2.2.

As was done for Task 1, a three-character coding system (X-X-X) was used to denote the specific cases that comprise the full factorial experiment conducted here. This coding system was developed as follows:

First Character (Upstream Geometry):

- C – Curved Upstream Geometry
- S – Straight Upstream Geometry

Second Character (Maximum Input Volume/Truck Percentage)

- 1 – 2,940 pcph/5%
- 2 – 3,185 pcph/5%
- 3 – 3,430 pcph/5%
- 4 – 2,940 pcph/15%
- 5 – 3,185 pcph/15%
- 6 – 3,430 pcph/15%
- 7 – 2,940 pcph/30%
- 8 – 3,185 pcph/30%
- 9 – 3,430 pcph/30%

Third Character (Lane Closure Side):

- R – Right-Side Closure
- L – Left-Side Closure

The following should be noted relative to the list of scenarios described above and in **Table 6-14**. First, the curved and straight upstream geometry scenarios were coded with different lane change distance distributions based on the observed field data; all other components of the model were left identical to the baseline calibrated scenario identified as part of Task 1. This calibrated scenario included a lane change distance coded with a distance offset of 500 feet relative to the raw field data, a CC1 value of 1.2s, and the default value of the SDRF. Second, the range of input volume distributions selected was intended to account for the influence of demand-to-capacity ratio (d/c) on pre- and post-breakdown operations through the simulated work zone. As noted in Section 6.2.2, these input volume distributions were selected to bracket the theoretical pre-breakdown capacity of the simulated work zone, as measured through pilot simulation runs. When using a passenger car equivalent of 2.5 for heavy trucks, variation in the input volume distributions from the “low” to “high” scenarios results in a d/c ratio between 0.92 and 1.08. Finally, right-side and left-side lane closures were coded in Vissim by varying the orientation of the lane closure connector and replicating the lane change distance distributions observed in the field data.

**TABLE 6-14: FACTORIAL EXPERIMENT ANALYSIS SCENARIOS**

Scenario	% Trucks	Upstream Geometry	Lane Closure Side	Input Volume Distribution
C-1-R	5%	Curved	Right	Low
C-2-R	5%	Curved	Right	Medium
C-3-R	5%	Curved	Right	High
C-4-R	15%	Curved	Right	Low
C-5-R	15%	Curved	Right	Medium
C-6-R	15%	Curved	Right	High
C-7-R	30%	Curved	Right	Low
C-8-R	30%	Curved	Right	Medium
C-9-R	30%	Curved	Right	High
C-1-L	5%	Curved	Left	Low
C-2-L	5%	Curved	Left	Medium
C-3-L	5%	Curved	Left	High
C-4-L	15%	Curved	Left	Low
C-5-L	15%	Curved	Left	Medium
C-6-L	15%	Curved	Left	High
C-7-L	30%	Curved	Left	Low
C-8-L	30%	Curved	Left	Medium
C-9-L	30%	Curved	Left	High
S-1-R	5%	Straight	Right	Low
S-2-R	5%	Straight	Right	Medium
S-3-R	5%	Straight	Right	High
S-4-R	15%	Straight	Right	Low
S-5-R	15%	Straight	Right	Medium
S-6-R	15%	Straight	Right	High
S-7-R	30%	Straight	Right	Low
S-8-R	30%	Straight	Right	Medium
S-9-R	30%	Straight	Right	High
S-1-L	5%	Straight	Left	Low
S-2-L	5%	Straight	Left	Medium
S-3-L	5%	Straight	Left	High
S-4-L	15%	Straight	Left	Low
S-5-L	15%	Straight	Left	Medium
S-6-L	15%	Straight	Left	High
S-7-L	30%	Straight	Left	Low
S-8-L	30%	Straight	Left	Medium
S-9-L	30%	Straight	Left	High

### 6.4.3 Factorial Experiment Results

The findings of Task 1 validate the utility of semi-automatically extracted traffic data in mitigating the complexity of the calibration process and providing a basis for future modeling efforts utilizing lane change distance distributions in Vissim. One practical application of these field-measured lane change distance distributions to developing robust Vissim models is presented as part of Task 2. The results summarized in this subsection first explore traditional output measures of capacity at freeway lane closures, such as the maximum pre-breakdown flow rate and average queue discharge flow rate, as a function of independent variables listed in **Table 6-14**. These trends are then compared against measures of corridor performance typically analyzed by practitioners and of critical importance to agencies and road users, such as speed, travel time, and queue length. The outcomes of this exercise support those from past studies of freeway bottlenecks but add to the body of freeway work zone simulation literature by supporting a methodology for replicating real-world driving behavior and traffic flow in microsimulation models.

Prior to assessing model outputs, the minimum number of runs required for establishing statistical confidence in the results was computed. Corridor travel time exhibited the greatest standard deviation when comparing the 10 random seed runs conducted for scenario B-3 as part of Task 1. As such, the following equation was evaluated for the maximum corridor travel time assuming a tolerable error of 15%, 95% confidence level, and 10 random seed runs.

$$n = \left( \frac{s * t_{\frac{\alpha}{2}}}{\mu * \varepsilon} \right)^2$$

*Where:*

*n = required number of simulation runs*

*s = standard deviation of the maximum corridor travel time, in minutes*

*$t_{\frac{\alpha}{2}}$  = critical value of a two-sided t-statistic at a confidence level of  $\alpha$  and  $n-1$  degrees of freedom*

The results of this computation are shown in **Table 6-15** and yield a minimum requirement of five simulation runs. As such, 10 random seed runs were deemed sufficient for conducting the remainder of the experiment.



**TABLE 6-15: DETERMINATION OF REQUIRED NUMBER OF SIMULATION RUNS**

Random Seed Run	Maximum Corridor Travel Time (minutes)
1	8.9
2	11.8
3	7.3
4	9.6
5	8.7
6	9.9
7	8.1
8	8.2
9	9.1
10	11.3
Maximum (minutes)	11.8
Minimum (minutes)	7.3
Standard Deviation (minutes)	1.4
Average (minutes)	9.3
Tolerable Error (minutes)	1.4
Required Number of Runs <sup>1</sup>	4.9

<sup>1</sup>Calculation for required number of runs assumes  $n - 1 = 9$  degrees of freedom

### Freeway Capacity Measurements

The maximum pre-breakdown flow rate, average queue discharge flow rate, and demand-to-capacity ratio associated with each of the modeled scenarios are summarized in **Table 6-16** and **Table 6-17** for right- and left-side closures, respectively. As shown in the tables, only 23 scenarios yielded a breakdown event during at least one random seed run. For scenarios modeled with 5% trucks in the traffic stream (i.e., those with a “1”, “2”, or “3” as the second character in their respective ID), neither the “low” nor “medium” input volume distributions led to congestion during any of the 10 random seed runs conducted for those cases. For consistency with the original experiment design—that is, to ensure that the modeled input volume distributions bracket theoretical capacity and capture an adequate range of demand-to-capacity ratios—two additional scenarios were developed. Denoted as scenario “C-33-L” and “C-33-R”, these scenarios were coded with an input volume distribution approximately 100 vehicles per hour greater than that coded for scenarios “C-3-L” and “C-3-R”.

**TABLE 6-16: SUMMARY OF CAPACITY MEASUREMENTS (RIGHT-SIDE LANE CLOSURE)**

Measure of Effectiveness	Scenario ID									
	C-1-R	C-2-R	C-3-R	C-33-R	C-4-R	C-5-R	C-6-R	C-7-R	C-8-R	C-9-R
Maximum Pre-Breakdown Flow Rate (vphpl) <sup>1,2</sup>	-	-	1,517	1,582	-	1,317	1,291	-	1,107	1,080
Average Queue Discharge Rate (vphpl) <sup>1,2</sup>	-	-	1,558	1,586	-	1,219	1,238	-	955	985
Maximum Input Volume (vphpl) <sup>2</sup>	1,368	1,482	1,596	1,710	1,200	1,300	1,400	1,014	1,099	1,183
Estimated Demand-to-Capacity Ratio (D/C) <sup>3</sup>	-	-	1.05	1.08	-	0.99	1.08	-	0.99	1.10
Measure of Effectiveness	Scenario ID									
	S-1-R	S-2-R	S-3-R	S-33-R	S-4-R	S-5-R	S-6-R	S-7-R	S-8-R	S-9-R
Maximum Pre-Breakdown Flow Rate (vphpl) <sup>1,2</sup>	-	-	1,566	1,582	-	1,325	1,330	-	1,100	1,088
Average Queue Discharge Rate (vphpl) <sup>1,2</sup>	-	-	1,572	1,602	-	1,222	1,253	-	955	975
Maximum Input Volume (vphpl) <sup>2</sup>	1,368	1,482	1,596	1,710	1,200	1,300	1,400	1,014	1,099	1,183
Estimated Demand-to-Capacity Ratio (D/C) <sup>3</sup>	-	-	1.02	1.08	-	0.98	1.05	-	1.00	1.09

<sup>1</sup>Capacity measurements shown represent an average of the 10 random seed runs conducted for a given scenario

<sup>2</sup>Vissim input volume distributions were coded in one-hour intervals; capacity measurements are shown as 15-minute equivalent hourly flow rates

<sup>3</sup>Demand-to-capacity ratio calculated by comparing the maximum pre-breakdown flow rate to the maximum input volume

**TABLE 6-17: SUMMARY OF CAPACITY MEASUREMENTS (LEFT-SIDE LANE CLOSURE)**

Measure of Effectiveness	Scenario ID									
	C-1-L	C-2-L	C-3-L	C-33-L	C-4-L	C-5-L	C-6-L	C-7-L	C-8-L	C-9-L
Maximum Pre-Breakdown Flow Rate (vphpl) <sup>1,2</sup>	-	-	1,492	1,553	-	1,290	1,291	-	1,121	1,117
Average Queue Discharge Rate (vphpl) <sup>1,2</sup>	-	-	1,506	1,548	-	1,191	1,266	-	965	1,021
Maximum Input Volume (vphpl) <sup>2</sup>	1,368	1,482	1,596	1,710	1,200	1,300	1,400	1,014	1,099	1,183
Estimated Demand-to-Capacity Ratio (D/C) <sup>3</sup>	-	-	1.07	1.10	-	1.01	1.08	-	0.98	1.06
Measure of Effectiveness	Scenario ID									
	S-1-L	S-2-L	S-3-L	S-33-L	S-4-L	S-5-L	S-6-L	S-7-L	S-8-L	S-9-L
Maximum Pre-Breakdown Flow Rate (vphpl) <sup>1,2</sup>	-	-	1,530	1,551	-	-	1,311	-	1,139	1,102
Average Queue Discharge Rate (vphpl) <sup>1,2</sup>	-	-	1,541	1,606	-	-	1,283	-	958	1,004
Maximum Input Volume (vphpl) <sup>2</sup>	1,368	1,482	1,596	1,710	1,200	1,300	1,400	1,014	1,099	1,183
Estimated Demand-to-Capacity Ratio (D/C) <sup>3</sup>	-	-	1.04	1.10	-	-	1.07	-	0.96	1.07

<sup>1</sup>Capacity measurements shown represent an average of the 10 random seed runs conducted for a given scenario

<sup>2</sup>Vissim input volume distributions were coded in one-hour intervals; capacity measurements are shown as 15-minute equivalent hourly flow rates

<sup>3</sup>Demand-to-capacity ratio calculated by comparing the maximum pre-breakdown flow rate to the maximum input volume

The results summarized in **Table 6-16** and **Table 6-17** should be interpreted with the following in mind. First, though the *Highway Capacity Manual* recommends default passenger car equivalent flow rates for heavy trucks and suggested values for freeway work zones are provided in the literature (TRB, 2016; Sarasua et al., 2006; Jehn and Turochy, 2020), capacity measurements are presented in units of vehicles per hour per lane to provide for easier interpretation across input truck percentages. Second, demand-to-capacity ratios were calculated by comparing *one-hour* input volume distributions to *15-minute* equivalent hourly flow rates at capacity in Vissim. As such, the maximum of the *15-minute* equivalent hourly input flow rates at the entry point to the Vissim network are likely higher than that shown. Lastly, the maximum pre-breakdown flow rates and average queue discharge flow rates shown in the tables represent an average over the individual breakdown events observed during each of the 10 random seed runs conducted for a given scenario. Though the queue discharge rate did not vary substantially from run-to-run, the maximum pre-breakdown flow rate differed by up to 140 vehicles per hour per lane between random seed runs for a given scenario. Therefore, the demand-to-capacity ratio shown is intended to represent the “average” case, but higher or lower values may be calculated when considering individual runs or by converting input flow rates to their 15-minute equivalents.

Regardless, the results highlight that capacity measurements do not vary substantially at the same input truck percentage when comparing right- and left-side lane closures or those with curved and straight upstream geometry. Considering the results under right-side lane closures versus those under left-side lane closures, the maximum observed difference in the pre-breakdown capacity occurred between scenarios S-8-L and S-8-R, where scenario S-8-L exhibited a maximum pre-breakdown flow rate 39 vehicles per hour per lane greater than that under scenario S-8-R (+4%). Similarly, when considering the results under curved upstream geometry versus those under straight upstream geometry, the maximum observed difference in pre-breakdown capacity occurred between scenarios C-3-R and S-3-R. Under scenario S-3-R, the average of the maximum pre-breakdown flow rate was 48 vehicles per hour per lane greater than that under scenario C-3-R (+3%). When the input truck percentage is held constant, no pair of scenarios yielded differences in the maximum pre-breakdown flow rate or average queue discharge rate of greater than 4%.

On the contrary, the capacity measurements in the tables underscore the noteworthy impact that heavy trucks have on traffic flow, particularly at freeway lane closures. The best-performing scenario (S-33-R) from a capacity standpoint exhibited a maximum pre-breakdown flow rate of 1,582 vehicles per hour per lane, approximately 500 vehicles per hour per lane greater than the worst-performing scenario (C-9-R). Likewise, the best-performing scenario (S-33-L) produced an average queue discharge rate approximately 650 vehicles per hour per lane greater than the worst-performing scenario (S-8-R). The larger spread in the queue discharge rate data supports findings from past literature (Sarasua et al., 2006; Jehn and Turochy, 2020) that the impact of heavy trucks is magnified after the onset of congestion due to differences in vehicle size and performance capabilities. To provide a tangible measure of the impact of heavy trucks

on capacity measurements for comparative purposes, a passenger car equivalent (PCE) factor was calculated based on the methodology applied by Jehn and Turochy (2020). The average of the maximum pre-breakdown flow rates observed under each truck percentage were converted to units of passenger cars per hour per lane by varying the PCE factor until the standard deviation of the calculated PCE flow rates was minimized. Using an Excel-based optimization tool, an optimum PCE of 2.7 was calculated, resulting in an average flow rate of approximately 1,660 passenger cars per hour per lane.

### Corridor Performance Measures

Taken at face value, the differences among capacity measurements between lane closure side and upstream segment geometry presented in the previous subsection have little practical significance. However, as alluded to earlier in this chapter and discussed in this subsection, even minor fluctuations in capacity can have a substantial impact on corridor performance. The minimum, maximum, and average travel time through the six-mile simulated work zone corridor is summarized in **Table 6-18** and **Table 6-19** for each of the 40 analyzed scenarios.

**TABLE 6-18: SUMMARY OF CORRIDOR TRAVEL TIME MEASUREMENTS (RIGHT-SIDE LANE CLOSURE)**

Maximum Corridor Travel Time Statistics <sup>1</sup>	Scenario ID									
	C-1-R	C-2-R	C-3-R	C-33-R	C-4-R	C-5-R	C-6-R	C-7-R	C-8-R	C-9-R
Minimum (min)	5.2	5.3	6.7	13.8	5.3	5.4	13.0	5.3	5.5	37.9
Maximum (min)	5.4	5.9	7.9	17.9	5.4	9.3	22.6	11.2	35.7	39.0
Average (min)	5.3	5.5	7.2	16.1	5.3	7.3	17.1	6.1	20.8	38.3

Maximum Corridor Travel Time Statistics <sup>1</sup>	Scenario ID									
	S-1-R	S-2-R	S-3-R	S-33-R	S-4-R	S-5-R	S-6-R	S-7-R	S-8-R	S-9-R
Minimum (min)	5.2	5.3	6.4	12.9	5.3	5.4	11.6	5.3	5.4	38.5
Maximum (min)	5.5	6.2	7.9	16.6	5.9	7.7	15.5	14.2	39.2	39.8
Average (min)	5.3	5.5	7.0	14.5	5.4	6.3	13.2	6.7	23.1	39.1

<sup>1</sup>Values displayed in the table are all relative to the maximum travel time observed during a given random seed run



**TABLE 6-19: SUMMARY OF CORRIDOR TRAVEL TIME MEASUREMENTS (LEFT-SIDE LANE CLOSURE)**

Maximum Corridor Travel Time Statistics <sup>1</sup>	Scenario ID									
	C-1-L	C-2-L	C-3-L	C-33-L	C-4-L	C-5-L	C-6-L	C-7-L	C-8-L	C-9-L
Minimum (min)	5.2	5.2	6.9	15.7	5.3	5.4	10.5	5.3	5.6	29.7
Maximum (min)	5.3	5.4	8.6	18.8	5.7	8.1	12.8	5.5	19.2	36.1
Average (min)	5.3	5.3	7.5	17.6	5.4	6.3	11.3	5.4	10.2	34.0

Maximum Corridor Travel Time Statistics <sup>1</sup>	Scenario ID									
	S-1-L	S-2-L	S-3-L	S-33-L	S-4-L	S-5-L	S-6-L	S-7-L	S-8-L	S-9-L
Minimum (min)	5.2	5.2	6.3	10.8	5.3	5.4	8.5	5.4	5.9	36.2
Maximum (min)	5.5	5.5	6.9	15.3	6.1	7.2	12.3	12.3	28.1	38.3
Average (min)	5.3	5.3	6.6	12.2	5.4	6.1	9.9	6.4	15.0	37.3

<sup>1</sup>Values displayed in the table are all relative to the maximum travel time observed during a given random seed run

The results presented in the tables support previous findings in the literature by demonstrating that maximum corridor travel time—and by association, maximum queue length—increases rapidly as the gap between pre- and post-breakdown capacity increases. A 2012 study by Hu, Schroeder, and Rouphail explored the “two-capacity” phenomenon documented by numerous others (Hu et al., 2012). Through a comprehensive literature search and theoretical experiment conducted using FREEVAL software, the authors compared output measures of effectiveness for a six-mile, three-lane freeway section coded with a single lane closure under two scenarios. Under the first scenario, the capacity of the freeway facility in question was assumed the same before and after the onset of congestion, whereas a 5% “capacity drop” after the onset of breakdown was assumed under the second scenario. The results of this experiment showed that a 5% decrease in the queue discharge rate relative to the pre-breakdown flow rate at capacity yielded a 41% increase in corridor travel time and 78% increase in maximum queue length. These findings were used as rationale for incorporating queue discharge flow in the Freeway Facilities methodology in the *Highway Capacity Manual*. Moreover, the authors of this study concluded that corridor performance measures of effectiveness were most sensitive to slight deviations in this capacity drop at demand-to-capacity ratios near 1.0.

As noted previously, Vissim input traffic volumes developed for the current experiment were coded to yield demand-to-capacity ratios no greater than 1.1. In this way, the results of the experiment are most useful for understanding traffic operations at three-to-two freeway lane closures where scheduling decisions are most difficult for agencies. That is, when typical freeway demand is well in excess of theoretical capacity (e.g., on a major urban freeway corridor between 7:00AM and 7:00PM), lane closures are likely to be restricted during these periods of the day. However, when expected freeway demand is near capacity (e.g.,  $d/c \leq 1.1$ ), such decisions become more difficult and

impactful. A few key trends highlighted in the tables are discussed in the subsections that follow.

#### Left- vs. Right-Side Lane Closures

When input truck percentage and upstream geometry (e.g., curved vs. straight horizontal alignment) are held constant, the results summarized in **Table 6-17** and **Table 6-18** generally indicate that the simulated work zone corridor exhibits less delay under left-side lane closures than right-side lane closures. At an input truck percentage of 5%, the difference in maximum corridor travel time is less striking, increasing or decreasing by an average of no more than 1.5 minutes per vehicle. However, it is worth noting that the maximum corridor travel time *increases* by nearly 10% under scenario C-33-L relative to scenario C-33-R. A similar trend is not observed under scenarios S-33-L and S-33-R, suggesting that a slight increase in corridor travel time is possible under low truck traffic volumes when curved geometry exists upstream of the lane closure. This finding may be attributable to the increase in late lane changes observed in the field data and coded in Vissim under curved upstream geometry relative to that under straight upstream geometry.

However, as the percentage of trucks increases in the traffic stream, this trend is reversed. Given that most heavy trucks utilize the right two lanes on six-lane freeway facilities, it is intuitive that corridor travel time and queue length increase under right-side lane closures relative to left-side lane closures, with the largest differences observed under scenarios with 30% trucks in the traffic stream. As depicted visually in **Figure 6-9**, maximum corridor travel time increases by upwards of 50% under scenario S-8-R relative to scenario S-8-L, from an average of 15 minutes per vehicle to more than 23 minutes per vehicle. Queues persist for approximately 1.5 hours longer and reduced speeds extend nearly two miles farther upstream of the modeled lane closure under scenario S-8-R than under scenario S-8-L. These findings align with the discussion in the previous subsection; despite substantial differences in corridor measures of effectiveness, the maximum pre-breakdown flow rate, average queue discharge rate, and corresponding “capacity” drop observed after breakdown differed by no more than 4% between scenarios in each case.

A more subtle trend in the data also highlights the sensitivity of corridor operations to stochastic variation in the simulation outputs when a greater percentage of trucks are included in the traffic stream. Namely, the range of the maximum corridor travel time in the 10 random seed runs conducted for scenarios S-8-L and S-8-R included measurements as low as 5.4 minutes per vehicle and as high as 39.2 minutes per vehicle. Given that the only differences among these simulation runs are the random seeds (all traffic and geometric characteristics are constant among them), this finding underscores both how variable traffic conditions are as demand nears capacity and the appropriateness of characterizing the appearance of breakdown conditions (as a measure of capacity) as probabilistic, rather than deterministic. Informed agency scheduling and traffic control layout decisions are especially impactful in such cases.

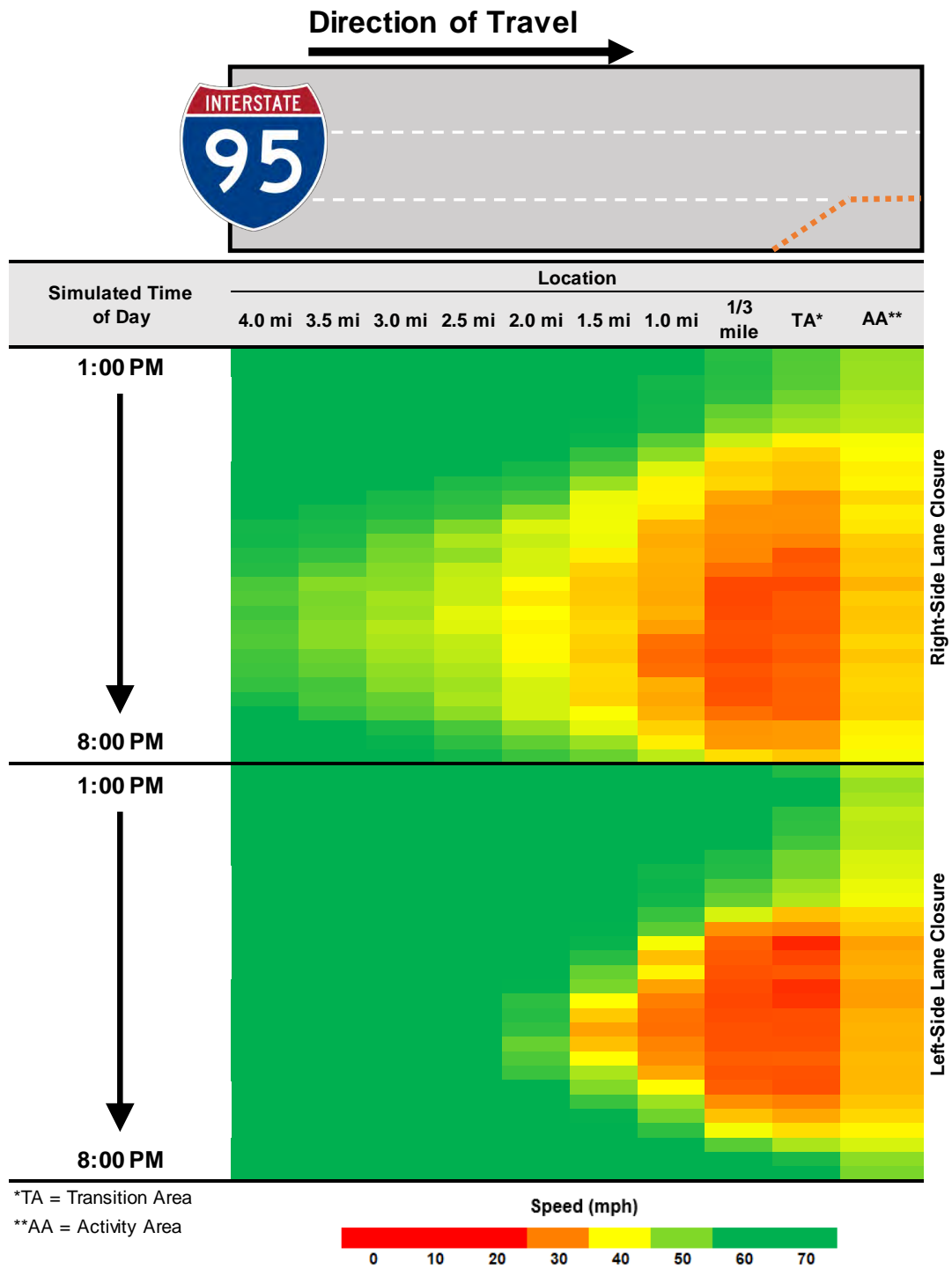


**FIGURE 6-9: CORRIDOR SPEED HEAT MAP (SCENARIO S-8-R vs. SCENARIO S-8-L)**

### Curved vs. Straight Upstream Geometry

With input truck percentage and lane closure side held constant, the results summarized in **Table 6-17** and **Table 6-18** are mixed relative to the comparisons presented for left- and right-side lane closures previously. Specifically, when fewer trucks are present in the traffic stream, the results generally indicate that the simulated work zone corridor exhibits less delay under straight upstream geometry than curved upstream geometry. At an input truck percentage of 5%, the maximum corridor travel time increases by 5.4 minutes for a left-side closure (+44%) and 1.6 minutes for a right-side closure (+11%) under curved upstream geometry relative to that under straight upstream geometry. As described in the previous subsection, this finding may be attributable to the increased number of lane changes observed within Zone 1 and Zone 2 (i.e., closest to the transition area) in the field data and coded in the Vissim models under curved upstream geometry. When drivers have less time to visualize a downstream lane closure, late lane changes become more likely and required braking maneuvers become more aggressive. These trends are depicted visually in **Figure 6-10**.

Conversely, as the percentage of trucks in the traffic stream increases, corridor performance generally improves under curved upstream geometry relative to that under straight upstream geometry. Under scenario C-8-L, maximum corridor travel time is 4.8 minutes less (-32%) than that under scenario S-8-L. Though an increase in the lane change distance coded in Vissim has typically been associated with an increase in modeled capacity and related measures of corridor performance, this finding may be attributable to less efficient use of available lane capacity in the closed lane when lane changes occur farther upstream of the transition area. Differences in maximum corridor travel time are less pronounced or inverted when drawing the same comparisons under right-side lane closures. A 10% decrease in maximum corridor travel time was observed under scenario C-8-R relative to scenario S-8-R; however, under scenario C-6-R, maximum corridor travel time and queue duration are 3.9 minutes and 2.4 hours longer, respectively, than those under scenario S-6-R.

These mixed results highlight caveats in the field data and Vissim models and allude to opportunities for further research. First, no trucks were observed in the leftmost lane in the field data under curved upstream geometry. The number of trucks observed in the leftmost lane on a six-lane, suburban freeway is likely practically insignificant in any context, and the Vissim models run as part of this experiment were coded such that more than 90% of all heavy trucks enter the network in the right two lanes. However, the results suggest that Vissim model outputs are sensitive to coding the lane change distance distributions to allow for mandatory lane changes by heavy trucks to occur within  $\frac{1}{2}$  mile of the transition area under a left-side closure. As discussed in the next section, future field data collection and Vissim modeling efforts should examine truck lane changing behavior further given the apparent sensitivity of model outputs to related input parameters.

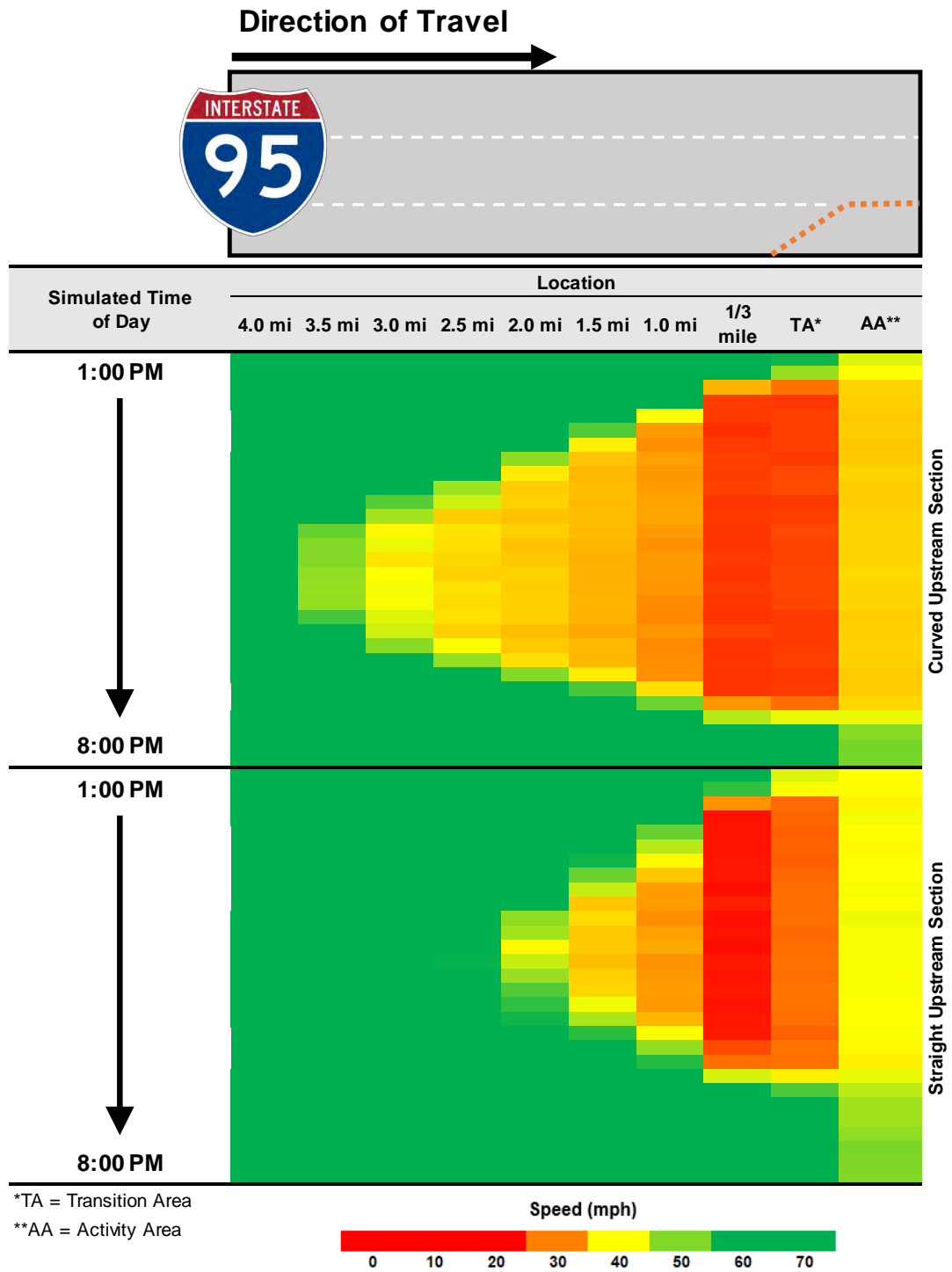


**FIGURE 6-10: CORRIDOR SPEED HEAT MAP (SCENARIO C-33-L vs. SCENARIO S-33-L)**



## 6.5 Summary

As emphasized at the beginning of this chapter, freeway work zones have a profound impact on the safety and mobility of the traveling public. Recent surveys of state departments of transportation have revealed inconsistencies in work zone scheduling and traffic control decisions (Ramadan and Sisiopiku, 2016). Similarly, there exists a need to limit ambiguity and maximize consistency in microsimulation model development and calibration (VDOT, 2020), particularly when analyzing freeway work zones. Recent advances in technology because of the AI-based semi-automatic traffic data extraction system summarized in this report facilitate initiatives that address these issues but also necessitate advances in supporting research efforts.

This chapter represents a significant contribution to the body of literature and summarizes two primary tasks. First, Task 1 explored the sensitivity of Vissim model outputs to changes in key input parameters. Of the parameters found to have the greatest influence on simulated capacity and most critical to calibrating freeway work zone simulation models, the lane change distance has been least studied. As such, this is believed to be the first study of its kind to leverage lane change distance distributions built from field data as inputs in Vissim. The outcomes of this task validated the utility of semi-automatically extracted traffic data by demonstrating the disparity in model outputs under the field data-based lane change distance distributions studied here and the typical “default” value found in the literature. A calibrated parameter set was vetted and carried forward as part of this project but may also be used as a starting point for future modeling efforts.

Second, Task 2 applied the calibrated parameter set developed as part of Task 1 to a full factorial experiment examining the impact of various geometric and traffic stream characteristics on traffic measures of effectiveness such as flow rate, speed, travel time, and queue length. The results of this effort suggest that typical measures of pre- and post-breakdown freeway capacity are not sensitive to changes in lane closure side or upstream geometry at three-to-two lane closures but vary substantially based on the percentage of trucks in the traffic stream. More critically, substantial deterioration in corridor performance measures such as travel time and queue length are possible even under fluctuations in pre- and post-breakdown capacity of less than 5%. The findings presented in this chapter generally suggest that maximum corridor travel time and queue length are greater under right-side lane closures and curved upstream geometry. Additionally, for some specific combinations of input traffic volume distribution and truck percentage when demand approaches capacity, the model output corridor travel time varied by as much as 30 minutes per vehicle under a single scenario, underscoring the sensitivity of freeway work zone traffic operations—and the fragility of traffic flow stability—at demand-to-capacity ratios near 1.0.

The methodologies and findings presented in this chapter fill existing gaps in the body of freeway work zone capacity and simulation literature and allude to significant opportunities for future research. Subsequent studies should focus on reducing ambiguity in Vissim model development and calibration and facilitating understanding

of the sensitivity of corridor measures of effectiveness—those of most concern to agencies and road users—to changes in the prevailing characteristics at a given freeway work zone.

## Chapter 7: CONCLUSIONS AND RECOMMENDATIONS

This chapter presents conclusions and recommendations. In this research project, a preliminary version of an AI-based work zone traffic and driver behavior information extraction system using widely available 2D camera images, machine learning, and computer vision has been proposed and developed to extract real-world traffic and driver behavior information, including vehicle count, vehicle classification, vehicle speed, time headway, and lane change location.

A case study involving two 30-minute work zone videos collected on an I-95 work zone near Savannah, Georgia, was used to 1) demonstrate the use of the proposed AI-system to extract traffic and driver behavior information, 2) present the benefits of analyzing the extracted information to obtain accurate and refined traffic and driver behavior information (called analyzed information) including traffic counts, traffic speeds, traffic headway, and work zone driver merge behaviors. This research focuses on studying the feasibility of using AI technology to extract traffic information to enhance traffic simulation. A separate effort with a pilot study with a large diverse data set is recommended in the future to further validate, refine and implement the proposed method. The preliminary findings of analyzing the extracted information are as follows:

- 1) For the traffic speed study, in low traffic speed conditions (high traffic density), the average traffic speed was 22MPH with a standard deviation of 7 MPH. An average traffic speed of 53 MPH with a standard deviation of 10 MPH in high traffic speed conditions (low traffic density).
- 2) For aggregation time interval study, in uniform traffic speed conditions (low speed or high-speed traffic), it was found that the variability/standard deviation of aggregated traffic speed distribution does not vary significantly based on different aggregation time intervals. Therefore, using 15-minute time intervals is acceptable to support subsequent traffic simulation. However, to provide the simulation model with more accurate/consistent speed distribution inputs, it is recommended that a small aggregation interval, such as 5-minutes, be used during the speed transition periods with significant speed changes, like from free flow to saturated flow (such as from 7AM – 8AM or 4PM to 5PM), so insight behaviors could be observed.
- 3) For driver following behavior study, the measurement of the time-gap between vehicles in the inner traffic lane was found to be shorter in high traffic speed conditions than in low traffic speed conditions, while the time-gap between vehicles in the outer traffic lane did not show a noticeable difference in different traffic speeds. The average time-gap in high traffic speed conditions was 1.5 seconds compared to 1.9 seconds in low traffic speed conditions. The standard deviation of the time-gap was also found to be slightly larger in high traffic speed conditions. The standard deviation of time headway in high traffic speed conditions is 0.95 seconds compared to 0.8 seconds in low traffic speed conditions.
- 4) For the work zone driver merge behavior study that analyzed the lane change locations, the following are the preliminary findings:
  - a. A majority of cars (53%) merge late (close to the work zone taper) in low traffic speed conditions (high traffic density), compared to only 12% in high traffic speed conditions (low traffic density).

- b. Among the 53% late merges in high traffic density conditions, 28% of the cars merge dangerously late inside the work zone transition areas.
- c. A majority of truck drivers typically merge earlier than car drivers (more than 50% of trucks merge 1000 feet in front of the work zone taper).

An error analysis was performed to assess the accuracy of the proposed AI-system and identify the factors contributing to the errors. The following is the summary of the error analysis and findings.

- 1) An error analysis methodology is established by comparing the extracted data with manually collected ground reference data (real-world data), and it involved:
  - a. Analyzing the outliers of aggregated speed distribution in different time intervals, and
  - b. Identifying the factors impacting the accuracy based on three categories of error sources, including a) sensor-related factors, b) traffic and environment-related factors, c) algorithm-related factors.
- 2) The findings from the error analysis reveal that,
  - a. In traffic count error analysis,
    - i. Traffic count results show overcounting of the vehicles under high traffic speed conditions. Errors in the short-term vehicle tracking and re-identification algorithm were identified as possibly contributing to overcounting, which is an algorithm-related error factor.
    - ii. Traffic count results show undercounting of the vehicles under low traffic speed conditions. The occlusion of vehicles (vehicles in the lane closer to the camera blocking the view of vehicles in the lane further from the camera) was identified as a factor potentially contributing to undercounting the traffic, which is a combined impact of both traffic and environment-related and sensor-related error factors.
  - b. In traffic speed error analysis,
    - i. The traffic speed was underestimated (by 6 MPH) at higher traffic speeds (greater than 85 km/h). The low video frame rate, an algorithm-related error factor, contributed to the traffic speed underestimation.

Based on the error analysis findings, it is recommended that the camera be set at a high location (over 50 ft) so that vehicles in all lanes can be captured without occlusion. It is also recommended that a high video frame rate be used, and that the vehicle detection and re-identification algorithm be refined to improve the vehicle count and traffic speed accuracy in the preliminary version of the proposed AI-system.

A case study was conducted using the real-world data collected on I-95 and it demonstrated the preliminary version of AI-based work zone traffic and driver information extraction system (using widely available 2D camera images) is promising for the study of real-world work zone traffic and driver data. It can provide valuable input that has previously not existed, and it can greatly help develop accurate and reliable traffic simulation models.

A work zone simulation model was developed to perform a study that explored the sensitivity of Vissim model outputs to changes in key input parameters, especially lane change distance leveraging the extracted real-world traffic and driver behavior information instead of using typical “default” value found in the literature. The outcomes of this study highlighted the disparity in model outputs under the field data-based lane change distance distributions extracted from the AI-system and the typical “default” value, thereby confirming the utility of the extracted real-world traffic and driver behavior information. The applications using the enhanced work zone traffic simulation models are also presented to provide guidance for transportation agencies for improving their work zone traffic management.

Further, the calibrated parameter set developed using the real-world traffic data was applied to a full factorial experiment examining the impact of various geometric and traffic stream characteristics on traffic measures of effectiveness such as flow rate, speed, travel time, and queue length. The results of this effort suggest that typical measures of pre- and post-breakdown freeway capacity are not sensitive to changes in lane closure side or upstream geometry at three-to-two lane closures but vary substantially based on the percentage of trucks in the traffic stream. However, substantial deterioration in corridor performance measures such as travel time and queue length are possible even under fluctuations in pre- and post-breakdown capacity of less than 5%. The findings presented in this chapter generally suggest that maximum corridor travel time and queue length are greater under right-side lane closures and curved upstream geometry. Additionally, for some specific combinations of input traffic volume distribution and truck percentage when demand approaches capacity, the model output corridor travel time varied by as much as 30 minutes per vehicle indicating significant delays and queues are possible at a given freeway lane closure, even when typical freeway demand is near capacity (i.e.,  $d/c \leq 1.1$ ).

The following are the recommendations for future research to refine the AI-based work zone traffic and driver information extraction system for full-scale implementation:

- 1) A large dataset with diverse conditions (including different traffic saturation levels, lighting, weather conditions, and different roadway geometries, such as curved roadways, camera viewing angles, etc.) and longer duration is recommended to further validate and improve the preliminary version of the AI-based work zone traffic and driver behavior data extraction system.
- 2) Develop a method to further enhance the accuracy of the vehicle count and speed computation method to remove outliers and noises by applying enhanced data analysis (including multi-interval data aggregation and statistical analysis, etc.).
- 3) Perform assessment of the camera image quality (including resolution, distance- to-camera position, lighting conditions, blurriness in various conditions (such as in fog, cases of occlusion, etc.) and its impact on vehicle detection and classification.
- 4) Implement camera calibration based on real-world vehicle positions along with current vehicle tracking and re-identification methods to enhance the current vehicle count and speed computation.

The following are the recommendations for further enhancing the driver behavior study using the widely available read-world camera images:

- 1) Study real-world work zone traffic and driver merge behaviors in diverse conditions (including different traffic saturation levels, lighting, and weather conditions, and different roadway geometries, such as curved roadways, camera angles, etc.).
- 2) Establish a performance measure to determine the adequate time interval for traffic information and driver behavior analysis. This performance measure could be the variability, like the standard deviation, in a one-time interval. A finer time interval would be needed if the variability is too large so we could produce accurate simulation outcomes.
- 3) Develop a quantitative method with a confidence level indicator to differentiate the extracted traffic and driver behavior information with good and bad quality. The transportation agencies' willingness to adopt automatically and semi-automatically extracted vehicle count and speed information using widely available camera images has been significantly hindered by the lack of a viable method to separate the extracted traffic and driver behavior data, such as vehicle counts and speed information, with good and bad data quality. Developing this quantitative method must enable transportation agencies to use the extracted information with good quality and have a confidence level for taking full advantage of their widely available cameras (such as the 5000 cameras in Metro Atlanta, Georgia). This method should include but not be limited to issues such as a) image quality from camera sensors, b) traffic and environment conditions, c) AI and computer vision computation methods, and d) multi-interval data aggregation and its statistical analysis to remove the outliers and noises.

The following are the recommendations for further extending the Vissim traffic simulation study performed in Chapter 6:

- 1) Extend the calibrated parameter set developed as part of the simulation study presented in this report to future study of three-to-two lane closures in lieu of typical default values found in the literature and consider the calibrated parameter set developed when modeling other lane closure configurations (e.g., two-to-one) in the absence of site-specific data.
- 2) Collect more field data related to truck lane changing behavior and perform detailed analysis on truck lane change phenomenon, as Vissim model outputs were found to be highly sensitive to slight changes in related inputs. The field data collected as part of this study indicated that truck lane changing behavior differs before and after the onset of breakdown (i.e., trucks begin to change lanes further upstream of the transition area after queues have formed and propagated upstream).

The following are the recommendations for improving the work zone safety and mobility based on the outcomes of the traffic simulation study:



- 1) Schedule lane closures when demand is less than 90% of theoretical capacity, when possible. This is because significant delays and queues are possible at a given freeway lane closure, even when typical freeway demand is near capacity (i.e.,  $d/c \leq 1.1$ ).
- 2) Do not configure work zone traffic control such that the transition area begins within  $\frac{1}{2}$  mile downstream of a horizontal curve. Field data collected as part of this project suggests that drivers will wait longer to change lanes without visual confirmation of the downstream lane closure.

## REFERENCE LIST

1. Acunzo D, Zhu Y, Xie B, Barattoff G. Context-adaptive approach for vehicle detection under varying lighting conditions. In 2007 IEEE Intelligent Transportation Systems Conference 2007 Sep 30 (pp. 654-660). IEEE.
2. Alkherret AA, Al-sayed A, Mousa RM. Determining Microscopic Traffic Variables using Video Image Processing. International Journal of Computer Applications. 2014 Jan 1;104(6).
3. Arróspide J, Salgado L, Nieto M, Jaureguizar F. On-board robust vehicle detection and tracking using adaptive quality evaluation. In 2008 15th IEEE International Conference on Image Processing 2008 Oct 12. IEEE.
4. Aytakin B, Altuğ E. Increasing driving safety with a multiple vehicle detection and tracking system using ongoing vehicle shadow information. In 2010 IEEE International Conference on Systems, Man and Cybernetics 2010 Oct 10 (pp. 3650-3656). IEEE.
5. Bay H, Tuytelaars T, Van Gool L. Surf: Speeded up robust features. In European conference on computer vision 2006 May 7 (pp. 404-417). Springer, Berlin, Heidelberg.
6. Bharadwaj N, Kumar P, Arkatkar S, Maurya A, Joshi G. Traffic data analysis using image processing technique on Delhi–Gurgaon expressway. Current Science. 2016 Mar 10;808-22.
7. Bharadwaj, N., P. Edara, C. Sun, H. Brown, and Y. Chang. Traffic Flow Modeling of Diverse Work Zone Activities. Transportation Research Record, Journal of the Transportation Research Board, Vol. 2672(16), pp. 23-34. (2018).
8. Blanc N, Steux B, Hinz T. LaRASideCam: A fast and robust vision-based blindspot detection system. In 2007 IEEE intelligent vehicles symposium 2007 Jun 13 (pp. 480-485). IEEE.
9. Boora A, Ghosh I, Chandra S. Identification of free flow condition on two-lane intercity highways under heterogeneous traffic condition. In 27th ARRB Conference, Linking people, places and opportunities, Melbourne, Australia 2016 Nov.
10. Boulton TE, Micheals R, Gao X, Lewis P, Power C, Yin W, Erkan A. Frame-rate omnidirectional surveillance and tracking of camouflaged and occluded targets. In Proceedings Second IEEE Workshop on Visual Surveillance (VS'99)(Cat. No. 98-89223) 1999 Jun 26 (pp. 48-55). IEEE.
11. Broggi A, Cappalunga A, Cattani S, Zani P. Lateral vehicles detection using monocular high resolution cameras on TerraMax™. In 2008 IEEE Intelligent Vehicles Symposium 2008 Jun 4 (pp. 1143-1148). IEEE.
12. Buch N, Velastin SA, Orwell J. A review of computer vision techniques for the analysis of urban traffic. IEEE Transactions on Intelligent Transportation Systems. 2011 Mar 17;12(3):920-39.
13. Burnos P, Gajda J, Piwowar P, Sroka R, Stencel M, Zeglen T. Measurements of road traffic parameters using inductive loops and piezoelectric sensors. 2007.
14. CDOT Traffic Analysis and Forecasting Guidelines:  
<https://www.codot.gov/library/traffic/traffic-manuals->

guidelines/traffic\_analysis\_forecasting\_guidelines/cdot\_traffic-analysis-and-forecasting-guidelines\_v01-072018.pdf

15. Chan YM, Huang SS, Fu LC, Hsiao PY. Vehicle detection under various lighting conditions by incorporating particle filter. In 2007 IEEE Intelligent Transportation Systems Conference 2007 Sep 30 (pp. 534-539). IEEE.
16. Chang HY, Fu CM, Huang CL. Real-time vision-based preceding vehicle tracking and recognition. In IEEE Proceedings. Intelligent Vehicles Symposium, 2005. 2005 Jun 6 (pp. 514-519). IEEE.
17. Chang WC, Cho CW. Real-time side vehicle tracking using parts-based boosting. In 2008 IEEE International Conference on Systems, Man and Cybernetics 2008 Oct 12 (pp. 3370-3375). IEEE.
18. Chang J, Wang L, Meng G, Xiang S, Pan C. Vision-based occlusion handling and vehicle classification for traffic surveillance systems. IEEE Intelligent Transportation Systems Magazine. 2018 Apr 23;10(2):80-92.
19. Chatterjee I, Edara P, Menneni S, Sun C. Replication of work zone capacity values in a simulation model. Transportation research record. 2009;2130(1):138-48.
20. Chin SM, Franzese O, Greene DL, Hwang HL, Gibson RC. Temporary losses of highway capacity and impacts on performance. Oak Ridge National Laboratory. 2002 May.
21. Chung J, Sohn K. Image-based learning to measure traffic density using a deep convolutional neural network. IEEE Transactions on Intelligent Transportation Systems. 2017 Aug 16;19(5):1670-5.
22. Cui J, Liu F, Li Z, Jia Z. Vehicle localisation using a single camera. In 2010 IEEE Intelligent Vehicles Symposium 2010 Jun 21 (pp. 871-876). IEEE.
23. Dalal N, Triggs B. Histograms of oriented gradients for human detection. In 2005 IEEE computer society conference on computer vision and pattern recognition (CVPR'05) 2005 Jun 20 (Vol. 1, pp. 886-893). IEEE.
24. Daniel, Janice, Karen Dixon, and David Jared. "Analysis of fatal crashes in Georgia work zones." Transportation Research Record 1715.1 (2000): 18-23.
25. Dey PP, Chandra S, Gangopadhaya S. Speed distribution curves under mixed traffic conditions. Journal of transportation engineering. 2006 Jun;132(6):475-81.
26. Dong J, Houchin AJ, Shafieirad N, Lu C, Hawkins NR, Knickerbocker S. Vissim calibration for urban freeways.
27. Edara, P. K., & Cottrell, B. H. (2007). Estimation of traffic mobility impacts at work zones: state of the practice. In Proceedings of the Transportation Research Board 2007 Annual Meeting.

28. Edara P, Chatterjee I. Multivariate regression for estimating driving behavior parameters in work zone simulation to replicate field capacities. *Transportation Letters*. 2010 Jul 1;2(3):175-86.
29. Elefteriadou LA. The highway capacity manual 6th edition: A guide for multimodal mobility analysis. *Ite journal*. 2016 Apr;86(4).
30. Fang W, Zhao Y, Yuan Y, Liu K. Real-time multiple vehicles tracking with occlusion handling. In 2011 Sixth International Conference on Image and Graphics 2011 Aug 12 (pp. 667-672). IEEE.
31. Fatality Analysis Reporting System (FARS). 2016 Final and 2017 Annual Report File, National Highway Traffic Safety Administration (NHTSA). FARS data shown here are from the 50 States, District of Columbia, and Puerto Rico. Accessible at: <https://www.workzonesafety.org/crash-information/work-zone-fatal-crashes-fatalities/#national>
32. FHWA. Manual on Uniform Traffic Control Devices. 2012.
33. FHWA work zone facts and statistics [Internet]. Dot.gov. [cited 2021 Aug 11]. Available from: [https://ops.fhwa.dot.gov/wz/resources/facts\\_stats.htm](https://ops.fhwa.dot.gov/wz/resources/facts_stats.htm)
34. Fitzsimmons EJ, Souleyrette RR, Nambisan SS. Measuring horizontal curve vehicle trajectories and speed profiles: pneumatic road tube and video methods. *Journal of transportation engineering*. 2013 Mar 1;139(3):255-65.
35. Florida Department of Transportation, Traffic Analysis Handbook: A Reference 118 for Planning and Operations. Tallahassee, FL. 2014.
36. Freund Y, Schapire R, Abe N. A short introduction to boosting. *Journal-Japanese Society For Artificial Intelligence*. 1999 Sep 1;14(771-780):1612.
37. Gao X, Boult TE, Coetzee F, Ramesh V. Error analysis of background adaption. In Proceedings IEEE Conference on Computer Vision and Pattern Recognition. CVPR 2000 (Cat. No. PR00662) 2000 Jun 15 (Vol. 1, pp. 503-510). IEEE.
38. GDOT Traffic Analysis & Data Application webpage: <https://gdottrafficdata.drakewell.com/publicmultinodemap.asp>. 2021.
39. Ghasemzadeh, A., & Ahmed, M. M. (2019). Exploring factors contributing to injury severity at work zones considering adverse weather conditions. *IATSS research*, 43(3), 131-138.
40. Sil G, Maji A. Video based data collection process for geometric design consistency evaluation of four-lane median divided horizontal curves. *Transportation Research Procedia*. 2017 Jan 1;27:672-9.
41. Hall DL, McMullen SA. Mathematical techniques in multisensor data fusion. Artech House; 2004.
42. Hang, J., Yan, X., Ma, L., Duan, K., & Zhang, Y. (2018). Exploring the effects of the location of the lane-end sign and traffic volume on multistage lane-changing behaviors in work zone

areas: A driving simulator-based study. *Transportation research part F: traffic psychology and behaviour*, 58, 980-993.

43. Haselhoff A, Schauland S, Kummert A. A signal theoretic approach to measure the influence of image resolution for appearance-based vehicle detection. In 2008 IEEE Intelligent Vehicles Symposium 2008 Jun 4 (pp. 822-827). IEEE.
44. Haselhoff A, Kummert A. A vehicle detection system based on haar and triangle features. In 2009 IEEE Intelligent Vehicles Symposium 2009 Jun 3 (pp. 261-266). IEEE.
45. Hadi RA, Sulong G, George LE. Vehicle detection and tracking techniques: a concise review. *arXiv preprint arXiv:1410.5894*. 2014 Oct 22.
46. Haselhoff A, Kummert A. An evolutionary optimized vehicle tracker in collaboration with a detection system. In 2009 12th International IEEE Conference on Intelligent Transportation Systems 2009 Oct 4 (pp. 1-6). IEEE.
47. Haritaoglu I, Harwood D, Davis LS. W/sup 4: real-time surveillance of people and their activities. *IEEE Transactions on pattern analysis and machine intelligence*. 2000 Aug;22(8):809-30.
48. He, Y., Shu, Z., Ge, Y., & Daniel, J. (2016). Drivers' Lane Change Maneuver and Speed Behavior in Freeway Work Zones. In *Proceedings of SAE-China Congress 2015: Selected Papers* (pp. 229-241). Springer, Singapore.
49. Heaslip K, Kondyli A, Arguea D, Elefteriadou L, Sullivan F. Estimation of freeway work zone capacity through simulation and field data. *Transp Res Rec*. 2009;2130(1):16–24.
50. Hilario CH, Collado JM, Armingol JM, De La Escalera A. Pyramidal image analysis for vehicle detection. In *IEEE Proceedings. Intelligent Vehicles Symposium*, 2005. 2005 Jun 6 (pp. 88-93). IEEE.
51. Ho TJ, Chung MJ. An approach to traffic flow detection improvements of non-contact microwave radar detectors. In 2016 International Conference on Applied System Innovation (ICASI) 2016 May 26 (pp. 1-4). IEEE.
52. Hoffmann C. Fusing multiple 2D visual features for vehicle detection. In 2006 IEEE Intelligent Vehicles Symposium 2006 Jun 13 (pp. 406-411). IEEE.
53. Hu X, Xu X, Xiao Y, Chen H, He S, Qin J, Heng PA. SINet: A scale-insensitive convolutional neural network for fast vehicle detection. *IEEE transactions on intelligent transportation systems*. 2018 Oct 1;20(3):1010-9.
54. Hu J, Schroeder BJ, Roupail NM. Rationale for incorporating queue discharge flow into Highway Capacity Manual procedure for analysis of freeway facilities. *Transportation research record*. 2012 Jan;2286(1):76-83.
55. Idler C, Schweiger R, Paulus D, Mdhlich M, Ritter W. Realtime vision based multi-target-tracking with particle filters in automotive applications. In 2006 IEEE Intelligent Vehicles Symposium 2006 Jun 13 (pp. 188-193). IEEE.

56. Iowa DOT Microsimulation Guidance:  
<https://iowadot.gov/ijr/docs/MicrosimulationGuidance.pdf>
57. Ito, T., & Kaneyasu, R. (2017). Predicting traffic congestion using driver behavior. *Procedia computer science*, 112, 1288-1297.
58. Jacob A, Anjaneyulu MV. Operating speed of different classes of vehicles at horizontal curves on two-lane rural highways. *Journal of Transportation Engineering*. 2013 Mar 1;139(3):287-94.
59. Jehn NL, Turochy RE. Calibration of Vissim Models for Rural Freeway Lane Closures: Novel Approach to the Modification of Key Parameters. *Transportation Research Record*. 2019 May;2673(5):574-83.
60. Jehn NL, Turochy RE. Development of breakdown probability models and heavy vehicle passenger car equivalents for rural freeway work zones. *Transp Res Rec*. 2020;2674(12):144–54.
61. Jehn NL, Turochy RE. Calibration of Vissim models for rural freeway Lane closures: Novel approach to the modification of key parameters. *Transp Res Rec*. 2019;2673(5):574–83.
62. Kallenbach I, Schweiger R, Palm G, Lohlein O. Multi-class object detection in vision systems using a hierarchy of cascaded classifiers. In *2006 IEEE Intelligent Vehicles Symposium 2006 Jun 13* (pp. 383-387). IEEE.
63. Kämpchen N. Feature-level fusion of laser scanner and video data for advanced driver assistance systems (Doctoral dissertation, Universität Ulm).
64. Kan XD, Ramezani H, Benekohal RF. Calibration of VISSIM for freeway work zones with time-varying capacity. 2014.
65. Ke R, Li Z, Kim S, Ash J, Cui Z, Wang Y. Real-time bidirectional traffic flow parameter estimation from aerial videos. *IEEE Transactions on Intelligent Transportation Systems*. 2016 Aug 17;18(4):890-901.
66. Khammari A, Nashashibi F, Abramson Y, Laurgeau C. Vehicle detection combining gradient analysis and AdaBoost classification. In *Proceedings. 2005 IEEE Intelligent Transportation Systems, 2005*. 2005 Sep 16 (pp. 66-71). IEEE.
67. Khammari A, Nashashibi F, Abramson Y, Laurgeau C. Vehicle detection combining gradient analysis and AdaBoost classification. In *Proceedings. 2005 IEEE Intelligent Transportation Systems, 2005*. 2005 Sep 16 (pp. 66-71). IEEE.
68. Kockelman, K. M., & Ma, J. (2007). Freeway speeds and speed variations preceding crashes, within and across lanes. In *Journal of the Transportation Research Forum* (Vol. 46, No. 1424-2016-117787, pp. 43-61).
69. Kondyli A, Elefteriadou L, Brilon W, Hall FL, Persaud B, Washburn S. Development and evaluation of methods for constructing breakdown probability models. *Journal of Transportation Engineering*. 2013 Sep 1;139(9):931-40.



70. Lam WW, Pang CC, Yung NH. Highly accurate texture-based vehicle segmentation method. OPTICAL ENGINEERING-BELLINGHAM-INTERNATIONAL SOCIETY FOR OPTICAL ENGINEERING-. 2004 Mar 1;43(3):591-603.
71. Li, Y., & Bai, Y. (2009). Highway work zone risk factors and their impact on crash severity. Journal of Transportation engineering, 135(10), 694-701.
72. Li S, Yu H, Zhang J, Yang K, Bin R. Video-based traffic data collection system for multiple vehicle types. IET Intelligent Transport Systems. 2013 Aug 16;8(2):164-74.
73. Li C, Dobler G, Feng X, Wang Y. TrackNet: Simultaneous Object Detection and Tracking and Its Application in Traffic Video Analysis. arXiv preprint arXiv:1902.01466. 2019 Feb 4.
74. Lin BF, Chan YM, Fu LC, Hsiao PY, Chuang LA, Huang SS, Lo MF. Integrating appearance and edge features for sedan vehicle detection in the blind-spot area. IEEE Transactions on Intelligent Transportation Systems. 2012 Feb 3;13(2):737-47.
75. Liu T, Zheng N, Zhao L, Cheng H. Learning based symmetric features selection for vehicle detection. InIEEE Proceedings. Intelligent Vehicles Symposium, 2005. 2005 Jun 6 (pp. 124-129). IEEE.
76. Liu W, Wen X, Duan B, Yuan H, Wang N. Rear vehicle detection and tracking for lane change assist. In2007 IEEE intelligent vehicles symposium 2007 Jun 13 (pp. 252-257). IEEE.
77. Liu C, Huynh DQ, Sun Y, Reynolds M, Atkinson S. A Vision-Based Pipeline for Vehicle Counting, Speed Estimation, and Classification. IEEE Transactions on Intelligent Transportation Systems. 2020 Jul 1.
78. Lowe DG. Object recognition from local scale-invariant features. InProceedings of the seventh IEEE international conference on computer vision 1999 Sep 20 (Vol. 2, pp. 1150-1157). IEEE.
79. Lownes N, Machemehl R. Sensitivity of simulated capacity to modification of VISSIM driver behavior parameters. Transp Res Rec. 2006;1988:102–10.
80. Luo, Y., Jia, B., Liu, J., Lam, W. H., Li, X., & Gao, Z. (2015). Modeling the interactions between car and bicycle in heterogeneous traffic. Journal of advanced transportation, 49(1), 29-47.
81. Maryland DOT Vissim Modeling Guidance: <https://www.roads.maryland.gov/OPPEN/MDOT%20SHA%20TFAD%20VISSIM%20Modeling%20Guidance%2011-21-2016.pdf>
82. Machida T, Naito T. GPU & CPU cooperative accelerated pedestrian and vehicle detection. In2011 IEEE international conference on computer vision workshops (ICCV workshops) 2011 Nov 6 (pp. 506-513). IEEE.
83. Mashhadi, A., M. Farhadmanesh, A. Rashidi, and N. Markovic. Review of Methods for Estimating Construction Work Zone Capacity. Transportation Research Record, Journal of the Transportation Research Board, Vol. 2675(??) (2021).

84. Mekker, M., Y. Lin, M. Elbahnasaway, T. Shamseldin, H. Li, A. Habib, and D. Bullock. Application of LiDAR and Connected Vehicle Data to Evaluate the Impact of Work Zone Geometry on Freeway Traffic Operations. *Transportation Research Record, Journal of the Transportation Research Board*, Vol. 2672(16), pp. 1-13. (2018).
85. National Highway Traffic Safety Administ. Fatality Analysis Reporting System (Fars): Analytical Users Manual, 1975-2010. North Charleston, SC: Createspace Independent Publishing Platform; 2013.
86. Negri P, Clady X, Hanif SM, Prevost L. A cascade of boosted generative and discriminative classifiers for vehicle detection. *EURASIP Journal on Advances in Signal Processing*. 2008 Dec;2008:1-2.
87. Niknejad HT, Mita S, McAllester D, Naito T. Vision-based vehicle detection for nighttime with discriminately trained mixture of weighted deformable part models. In 2011 14th International IEEE Conference on Intelligent Transportation Systems (ITSC) 2011 Oct 5 (pp. 1560-1565). IEEE.
88. Niknejad HT, Takeuchi A, Mita S, McAllester D. On-road multivehicle tracking using deformable object model and particle filter with improved likelihood estimation. *IEEE Transactions on Intelligent Transportation Systems*. 2012 Mar 22;13(2):748-58.
89. Nuevo J, Parra I, Sjöberg J, Bergasa LM. Estimating surrounding vehicles' pose using computer vision. In 13th International IEEE Conference on Intelligent Transportation Systems 2010 Sep 19 (pp. 1863-1868). IEEE.
90. Pang CC, Lam WW, Yung NH. A novel method for resolving vehicle occlusion in a monocular traffic-image sequence. *IEEE Transactions on Intelligent Transportation Systems*. 2004 Sep 3;5(3):129-41.
91. Pang CC, Lam WW, Yung NH. A method for vehicle count in the presence of multiple-vehicle occlusions in traffic images. *IEEE Transactions on Intelligent Transportation Systems*. 2007 Sep 4;8(3):441-59.
92. Ponsa D, López A, Lumbreras F, Serrat J, Graf T. 3D vehicle sensor based on monocular vision. In *Proceedings. 2005 IEEE Intelligent Transportation Systems, 2005*. 2005 Sep 16 (pp. 1096-1101). IEEE.
93. Ponsa D, López A, Serrat J, Lumbreras F, Graf T. Multiple vehicle 3D tracking using an unscented Kalman. In *Proceedings. 2005 IEEE Intelligent Transportation Systems, 2005*. 2005 Sep 16 (pp. 1108-1113). IEEE.
94. PTV Vissim 2021 User Manual: "PTV Vissim 2021 User Manual." (2020). PTV Group, Karlsruhe, Germany.
95. Rad R, Jamzad M. Real time classification and tracking of multiple vehicles in highways. *Pattern Recognition Letters*. 2005 Jul 15;26(10):1597-607.

96. Ramachandran RP, Arr G, Sun C, Ritchie SG. A pattern recognition and feature fusion formulation for vehicle reidentification in intelligent transportation systems. In 2002 IEEE International Conference on Acoustics, Speech, and Signal Processing 2002 May 13 (Vol. 4, pp. IV-3840). IEEE.
97. Redmon J, Farhadi A. YOLO9000: better, faster, stronger. In Proceedings of the IEEE conference on computer vision and pattern recognition 2017 (pp. 7263-7271).
98. Robert K. Video-based traffic monitoring at day and night vehicle features detection tracking. In 2009 12th International IEEE Conference on Intelligent Transportation Systems 2009 Oct 4 (pp. 1-6). IEEE.
99. Sarasua, W. A., Davis, W. J., Clarke, D. B., Kottapally, J., & Mulukutla, P. (2004). Evaluation of interstate highway capacity for short-term work zone lane closures. *Transportation Research Record*, 1877(1), 85-94.
100. Sarasua W, Davis W, Chowdhury M, Ogle J. Estimating interstate highway capacity for short-term work zone Lane closures: Development of methodology. *Transp Res Rec*. 2006;1948:45-57.
101. Sil G, Maji A. Video based data collection process for geometric design consistency evaluation of four-lane median divided horizontal curves. *Transportation Research Procedia*. 2017 Jan 1;27:672-9.
102. Sivaraman S, Trivedi MM. A general active-learning framework for on-road vehicle recognition and tracking. *IEEE Transactions on Intelligent Transportation Systems*. 2010 Feb 17;11(2):267-76.
103. Sivaraman S, Trivedi MM. Active learning for on-road vehicle detection: A comparative study. *Machine vision and applications*. 2014 Apr 1;25(3):599-611.
104. Sivaraman S, Trivedi MM. Real-time vehicle detection using parts at intersections. In 2012 15th international IEEE conference on intelligent transportation systems 2012 Sep 16 (pp. 1519-1524). IEEE.
105. Sivaraman S, Trivedi MM. Looking at vehicles on the road: A survey of vision-based vehicle detection, tracking, and behavior analysis. *IEEE transactions on intelligent transportation systems*. 2013 Jul 18;14(4):1773-95.
106. Sivaraman S, Trivedi MM. Vehicle detection by independent parts for urban driver assistance. *IEEE Transactions on Intelligent Transportation Systems*. 2013 Jun 14;14(4):1597-608.
107. Son TT, Mita S. Car detection using multi-feature selection for varying poses. In 2009 IEEE Intelligent Vehicles Symposium 2009 Jun 3 (pp. 507-512). IEEE.
108. Song GY, Lee KY, Lee JW. Vehicle detection by edge-based candidate generation and appearance-based classification. In 2008 IEEE Intelligent Vehicles Symposium 2008 Jun 4 (pp. 428-433). IEEE.

109. Song H, Liang H, Li H, Dai Z, Yun X. Vision-based vehicle detection and counting system using deep learning in highway scenes. *European Transport Research Review*. 2019 Dec 1;11(1):51.
110. Steux B, Lurgeau C, Salesse L, Wautier D. Fade: A vehicle detection and tracking system featuring monocular color vision and radar data fusion. In *Intelligent Vehicle Symposium*, 2002. IEEE 2002 Jun 17 (Vol. 2, pp. 632-639). IEEE.
111. Sun Z, Bebis G, Miller R. Monocular precrash vehicle detection: features and classifiers. *IEEE transactions on image processing*. 2006 Jun 19;15(7):2019-34.
112. Sun D, Elefteriadou L. Research and implementation of lane-changing model based on driver behavior. *Transportation Research Record*. 2010 Jan;2161(1):1-0.
113. Takeuchi A, Mita S, McAllester D. On-road vehicle tracking using deformable object model and particle filter with integrated likelihoods. In *2010 IEEE Intelligent Vehicles Symposium 2010 Jun 21* (pp. 1014-1021). IEEE.
114. Teoh SS, Bräunl T. Symmetry-based monocular vehicle detection system. *Machine Vision and Applications*. 2012 Sep 1;23(5):831-42.
115. Texas A&M Transportation Institute, TTI Urban Mobility Report: <https://static.tti.tamu.edu/tti.tamu.edu/documents/mobility-report-2019.pdf>, 2019
116. Toledo T, Zohar D. Modeling duration of Lane changes. *Transp Res Rec*. 2007.
117. Toyama K, Krumm J, Brumitt B, Meyers B. Wallflower: Principles and practice of background maintenance. In *Proceedings of the seventh IEEE international conference on computer vision 1999 Sep 20* (Vol. 1, pp. 255-261). IEEE.
118. Tsai, Y. J., Wang, C. R., & Wu, Y. (2011). A vision-based approach to study driver behavior in work zone areas. In *3rd International Conference on Road Safety and Simulation*.
119. VDOT TOSAM: <http://www.virginiadot.org/business/resources/TOSAM.pdf>
120. VDOT Vissim User Guide: [http://www.virginiadot.org/business/resources/VDOT\\_Vissim\\_UserGuide\\_Version2.0\\_Final\\_2020-01-10.pdf](http://www.virginiadot.org/business/resources/VDOT_Vissim_UserGuide_Version2.0_Final_2020-01-10.pdf). 2020.
121. Viola P, Jones M. Rapid object detection using a boosted cascade of simple features. In *Proceedings of the 2001 IEEE computer society conference on computer vision and pattern recognition*. CVPR 2001 2001 Dec 8 (Vol. 1, pp. I-I). IEEE.
122. Viola P, Jones MJ. Robust real-time face detection. *International journal of computer vision*. 2004 May 1;57(2):137-54.
123. Wang J, Bebis G, Miller R. Overtaking vehicle detection using dynamic and quasi-static background modeling. In *2005 IEEE Computer Society Conference on Computer Vision and Pattern Recognition (CVPR'05)-Workshops 2005 Sep 21* (pp. 64-64). IEEE.

124. Wang CC, Lien JJ. Automatic vehicle detection using local features—A statistical approach. *IEEE Transactions on Intelligent Transportation Systems*. 2008 Feb 26;9(1):83-96.
125. Washington DOT Protocol for Vissim Simulation: Washington State Department of Transportation. (2014). Protocol for VISSIM Simulation.
126. Weng, J., & Meng, Q. (2015). Incorporating work zone configuration factors into speed-flow and capacity models. *Journal of advanced transportation*, 49(3), 371-384.
127. Wijnhoven RG, de With PH. Unsupervised sub-categorization for object detection: Finding cars from a driving vehicle. In 2011 IEEE International Conference on Computer Vision Workshops (ICCV Workshops) 2011 Nov 6 (pp. 2077-2083). IEEE.
128. Withopf D, Jahne B. Learning algorithm for real-time vehicle tracking. In 2006 IEEE Intelligent Transportation Systems Conference 2006 Sep 17 (pp. 516-521). IEEE.
129. Wren CR, Azarbayejani A, Darrell T, Pentland AP. Pfinder: Real-time tracking of the human body. *IEEE Transactions on pattern analysis and machine intelligence*. 1997 Jul;19(7):780-5.
130. Yang G, Xu H, Wang Z, Tian Z. Truck acceleration behavior study and acceleration lane length recommendations for metered on-ramps. *International journal of transportation science and technology*. 2016 Oct 1;5(2):93-102.
131. Yeom C, Hajbabaie A, Schroeder BJ, Vaughan C, Xuan X, Roupail NM. Innovative work zone capacity models from nationwide field and archival sources. *Transportation Research Record*. 2015 Jan;2485(1):51-60.
132. Yeom C, Roupail NM, Rasdorf W, Schroeder BJ. Simulation guidance for calibration of freeway lane closure capacity. *Transportation Research Record*. 2016;2553(1):82-9.
133. Yuan Q, Thangali A, Ablavsky V, Sclaroff S. Learning a family of detectors via multiplicative kernels. *IEEE transactions on pattern analysis and machine intelligence*. 2010 Jun 17;33(3):514-30.
134. Zhang Y, Kiselewich SJ, Bauson WA. Legendre and Gabor moments for vehicle recognition in forward collision warning. In 2006 IEEE Intelligent Transportation Systems Conference 2006 Sep 17 (pp. 1185-1190). IEEE.
135. Zhang J, Chen D, Kruger U. Adaptive constraint K-segment principal curves for intelligent transportation systems. *IEEE transactions on intelligent transportation systems*. 2008 Nov 7;9(4):666-77.
136. Zhang X, Zheng N, He Y, Wang F. Vehicle detection using an extended hidden random field model. In 2011 14th International IEEE Conference on Intelligent Transportation Systems (ITSC) 2011 Oct 5 (pp. 1555-1559). IEEE.
137. Zhou J, Gao D, Zhang D. Moving vehicle detection for automatic traffic monitoring. *IEEE transactions on vehicular technology*. 2007 Jan 22;56(1):51-9.

138. Zhu, J., & Saccomanno, F. F. (2004). Safety Implications of Freeway Work Zone Lane Closures. *Transportation Research Record*, 1877(1), 53–61.